THE EFFECTS OF MAGNETIC FIELD ERRORS ON REVERSED FIELD PINCH PLASMA

by

ABDULGADER FETURI ALMAGRI

A thesis submitted in partial fulfillment of the
requirements for the degree of

Doctor of Philosophy
(Nuclear Engineering and Engineering Physics)

at the
UNIVERSITY OF WISCONSIN-MADISON
1990

THE EFFECTS OF MAGNETIC FIELD ERRORS ON REVERSED FIELD PINCH PLASMA

Under the supervision of Professor Julien Clinton Sprott (Physics)
and Professor Gilbert A. Emmert (Nuclear Engineering and Engineering Physics)
at the University of Wisconsin-Madison

ABSTRACT

Studies of magnetic field error effects on Reversed Field Pinch plasma were carried out on the Madison Symmetric Torus. Magnetic field errors at the poloidal gap were reduced by 18% in rms value. This modest reduction of field errors resulted in improved plasma discharges. The plasma loop voltage was reduced by about 31%, and the plasma resistivity was reduced by 36%. Reversal duration increased by 16%. The character of the sawtooth activity as seen on the toroidal field at the wall changed considerably when field errors were reduced. These results suggest improved plasma confinement. Field errors were reduced further by a factor of six in rms value. With this reduction of field errors, plasma loop voltage was reduced by about a factor of two. The discharge duration doubled. At this low level of field errors, the plasma exhibited coherent magnetic fluctuations. These fluctuations have a poloidal mode number $m = 1$ and toroidal mode number $n = 5 - 10$. These modes are typically

phase-locked to one another to form a localized perturbation. This perturbation rotates toroidally in the ion-diamagnetic drift direction with a speed of about 10^6 cm/sec. Occasionally these modes are observed to lock to the conducting wall. This locking is believed to be caused by the poloidal gap field errors. These locked discharges tend to be much shorter in duration and to have larger loop voltage. The behavior of locked discharges can be explained by a field-error instability. Some estimates of the internal radial magnetic fields and the resulting magnetic islands are calculted. These calculations show that the field errors need to be reduced to less than 2% of the poloidal field at the wall to reduce islands overlap.

ACKNOWLEDGMENTS

I would like to thank my advisor Professor J. C. Sprott for his support, helpful comments and suggestions during the course of this research. I would also like to thank Professor S. C. Prager for his suggestions, insight, and continued interest in field error studies. I would like to thank Professor G. A. Emmert for his interest in my welfare and my work. Thanks are also due to Professor R. N. Dexter and Professor S. Hokin for their suggestions and support.

This work would have been impossible without the efforts of John Laufenberg, Jim Morin, and the master of all trades Tom lovell. Also the invisible army of hourly workers who provided vital support for this work and in the general maintenance of MST. I would like to thank Glenn Fleet and his computer staff, Paul, Brent, Paul, and Larry for their endless patience and dedication.

I especially would like to thank Roch Kendrick for his help and for all the neat mechining tricks he showed me.

I am also grateful to all my fellow graduate students and postdocs who often provided their time, effort, and many useful discussions. I am especially indebted to Saeed Assdi and John Sarff for their unlimited assistance and support throughout these five years.

I would like to express my appreciation to my familly, Sheila, Omar and Tariq for their love and patience.

Finally, the most important people responsible for my persevering through the years of schooling are my parents. Dad if you can hear me from up there "SHOKRUN".

This work is supported by the U. S. Department of Energy.

TABLE OF CONTENTS

1. INTRODUCTION

1.1 TOROIDAL CONFINEMENT AND FIELD ERRORS

An axisymmetric toroidal magnetic field configuration is one in which most field lines continue indefinitely covering a set of nested toroidal surfaces. Some close upon themselves after making n number of transits the long way around the torus for every m number of transits the short way around forming magnetic surfaces. These surfaces, for which the ratio of m over n is a rational number, are called rational surfaces. These axisymmetric magnetic flux surfaces are what confine the hot plasma.

Unfortunately no actual magnetic field configuration is ideal. Magnetic field errors are those that would cause any deviation from the ideal axisymmetric configuration. There are many sources that can produce field errors. These can be local effects such as those produced by diagnostic portholes, or non-axisymmetric perturbations such as those produced by the voltage gaps in the conducting shell that surrounds the plasma, or by non-uniformities in the field windings. Also a rotating helical mode (m′, n′) will cause perturbations in the wall current thereby producing an m = m′ field error at a voltage gap. This type of field error has been observed in experiment in MST.

Magnetic field errors that are produced by voltage gaps can cause some of the field lines, which form the flux surfaces, to intersect the wall

of the device. Errors that are produced by portholes can cause localized bumps in the outer flux surfaces. All these errors will lead to increased plasma-wall interaction. Another effect of field errors is the production of magnetic islands. The Fourier component of the perturbation, $B_r(m,n)$, will be resonant at a rational surface whose safety factor q, where q is defined by $q=\frac{rB\phi}{RB\theta}$, the ratio of toroidal to poloidal field line transits, is equale to

$$q=\frac{m}{n},$$

leading to the formation of magnetic islands. A field error at the voltage gap in the shell may initiate an instability in an otherwise stable plasma. There are some experimental observations that suggest that such instability accure in experiment.

Field error degradation of plasma confinement is especially severe in reversed field pinch (RFP) plasmas because, first, RFP confinement is thought to be determined mainly by the outer region of the plasma and, second, RFP stability requires a conducting shell very close to the plasma. Field errors associated with the shell voltage gaps and holes are very near the region that determines the plasma confinement.

1.2 MAGNETIC FIELD ERROR EFFECTS ON THE RFP

Good plasma equilibrium and low transport rates require the existence of well defined magnetic flux surfaces. It has been recognized for

some time that magnetic field errors can cause loss of equilibrium and enhanced transport.[1] The presence of non-axisymmetric radial magnetic fields within the plasma has two well recognized effects harmful to magnetic confinement.

Radial magnetic fields can deform the outermost magnetic surface causing field lines to intercept the wall and magnetic flux to leave the plasma volume giving the possibility of particle and heat flow parallel to the magnetic field out of the plasma to the wall. This plasma-wall interaction can result in impurity release into the plasma which will further degrade its performance.

Radial magnetic fields can also break internal magnetic surfaces into islands. For low-q toroidal devices, such as an RFP, a field error component $B_r(m,n)$ will produce a magnetic island at the $q=\frac{m}{n}$ rational surface (r_s); the radial width of such an island is given by

$$w(m,n) = 4\sqrt{\frac{r_s B_r(m,n)}{n B_\theta \left|\frac{dq}{dr}\right|_{r_s}}}$$

where $B_r(m,n)$ is the amplitude of the radial field Fourier component with an n toroidal mode number and m poloidal mode number, B_θ and q are the poloidal field and safety factor, respectively, at the resonance surface $r=r_s$. The island width $w(m,n)$ will increase with the radial field amplitude and since $w \sim \frac{1}{\sqrt{n}}$, low-n errors are the most dangerous.

A particular concern for an RFP is its vulnerability to field errors having m = 0 poloidal mode number. Perturbations having m = 0 and arbitrary toroidal mode number n will resonate with RFP fields at the reversal surface (q = 0). This field error will produce an island at the reversal surface.

A potentially important source of m = 0 perturbations is the nonlinear interaction of unstable m = 1 modes that are driven unstable by field errors of m = 1 poloidal mode number. It has been shown that a large m = 0 island can be produced by unstable m = 1 modes.[2]

A nonlinear MHD code[3] has been employed to evaluate plasma equilibria in the presence of field errors. Results indicate that the response of the plasma can be either to amplify or attenuate the error magnetic field in the plasma region.[4, 24]

It has been shown experimentally that toroidal field ripples and other field errors degrade confinement.[5] The plasma resistance R_p was experimentally observed to be smaller when field errors are reduced.[5] Also, the presence of an m = 0 field error will require operation at higher θ values[4] or deeper reversal to keep the m = 0 island width at a small fraction of the reversal layer, which is consistent with the experimental observation.[6]

As field errors are reduced and the plasma is centered in the liner in HBTX1B, the plasma resistance R_p is reduced by a factor of about two, and the energy confinement time is increased by a factor of two or three.[5] The overall reduction in R_p is more than would be expected from the changes

in the cross-sectional area and current profiles of the plasma. However, poloidal beta was found to be independent of field errors on HBTX1B and on ETA-BETA when large toroidal field errors were introduced.[8]

On HBTX1A with a vertical field applied to center the plasma and with gap field error correction, the pulse length was increased from 5 to 14 msec.[9] For RFP devices such as HBTX1 that uses a liner, a vertical field is required to reduce the Shafranov displacement. The displacement decreases the cross-sectional area of the plasma. This would increase the plasma resistance and increase the average width of the vacuum region between the plasma and the conducting shell, which is of importance for MHD instabilities and fluctuation.[10, 11]

On TPE-1RM15 similar results of lower plasma resistance, higher electron temperature, longer pulse duration and increased energy confinement time were achieved when gap field errors were reduced and a vertical field was used to center the plasma inside the linear.[12]

On REPUTE-1, error field reduction experiments used toroidal field trimming coils to reduce the toroidal field ripples. This led to a reduction of the plasma loop voltage and to some improvement in the energy confinement time. However this decrease in the loop voltage due to ripple reduction was not so large because the device had other sources of field errors such as shell gaps and portholes.[13]

STP-3(M) also has shown that plasma loop voltage and pulse duration improves with the reduction of gap errors and with improved plasma positioning.[14]

OHTE's plasma pulse duration was increased by using saddle correction coils at the poloidal gap.[15]

Measurements on ZT-40M showed a large departure from the ideal magnetic field geometry. When these gross errors were corrected the plasma pulse duration was extended from 8 to 20 msec.[16]

1.3 RFP EQUILIBRIUM AND STABILITY

The reversed-field-pinch (RFP) is an axisymmetric toroidal configuration with two distinct features. First, the poloidal magnetic field (B_θ) and toroidal magnetic field (B_ϕ) are both of the same magnitude. Second, the toroidal field reverses direction near the outside of the plasma with respect to its direction on the magnetic axis. An RFP plasma is stable at high values of beta, β , due to high shear, S , where

$$\beta = \frac{2\mu_0 < p >}{B^2} \quad \text{and} \quad S = \frac{r}{q}\frac{dq}{dr}.$$

The plasma in an RFP is confined by a combination of a poloidal magnetic field due to a toroidal current flowing within the plasma and a toroidal magnetic field generated in part by external coils. The RFP configuration can be generated by the plasma itself by a process known as "self reversal".

For a perfectly conducting plasma bounded by a perfectly conducting wall, Woltjer[17] has shown that magnetic helicity, defined by

$$K = \int_V \mathbf{A} \cdot (\nabla \times \mathbf{A})\, dv$$

where A is the magnetic vector potential, is invariant for any flux tube. This leads to a pressureless minimum magnetic energy state configuration given by

$$\nabla \times \mathbf{B} = \lambda \mathbf{B}$$

with $\lambda =$ constant.

Taylor[18,19,20,21] conjectured that the total magnetic helicity is invariant for plasma with small but finite resistivity, at least for times shorter than the resistive diffusion time given by

$$\tau_d = \frac{a^2 \mu_o}{\eta}$$

where a is the plasma radius and η is the plasma resistivity. The finite resistivity allows the needed magnetic reconnection for relaxation to the minimum energy state.

In cylindrical geometry, this configuration is given by Bessel functions (figure 1.1), hence named the Bessel function model (BFM)

$$B_\phi = B_o J_o(\lambda r) \ , \ B_\theta = B_o J_1(\lambda r)$$

which gives a reversed toroidal field when $\lambda r \geq 2.405$.

The RFP plasma can be characterized by two parameters, the pinch parameter θ, and field reversal parameter F are defined by

$$F = \frac{B\phi(a)}{<B\phi>} \quad \text{and} \quad \theta = \frac{B\theta(a)}{<B\phi>}$$

where a is the plasma minor radius and $< >$ denotes the average over the plasma cross section. In the BFM model the pinch parameter θ is related to λ by $\theta = 0.5\lambda a$ and field reversal occurs when $\lambda r > 2.405$ or $\theta > 1.2$. The field reversal parameter F is related to θ by

$$F = \frac{\theta J_o(2\theta)}{J_1(2\theta)}$$

The F-θ diagram (figure 1.2) that shows F as a function of θ, is an instructive way to compare experiment with models. Experiments have confirmed that sustained RFP plasma do lie on such a curve in F-θ space, but a little to the right of the minimum energy curve. This is believed to be a finite β effect.

This BFM Model, where λ = constant, does not exist in practice since the plasma current density , j(r), is experimentally found to fall smoothly to zero in the outer regions of the plasma.[22,23] To fit the experimental data, the λ profile is often taken as constant out to a radius r_c (cut off radius), and beyond that, λ decreases linearly to zero at the plasma edge. This is referred to as the modified bessel function model[22,23] (MBFM).

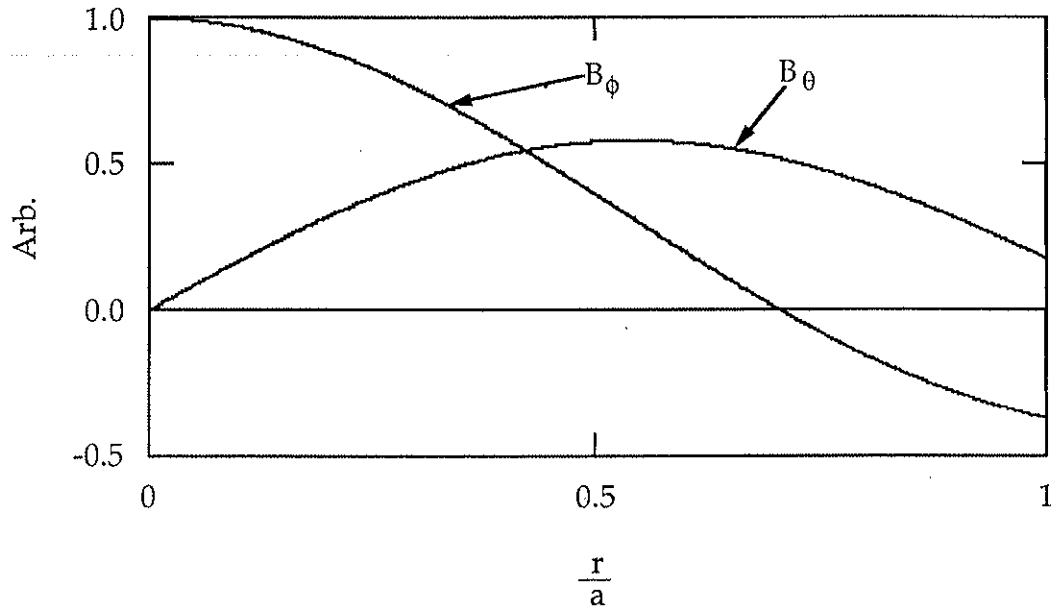

Figure 1.1 The poloidal and toroidal magnetic field spatial profiles for the BFM model at $\theta = 1.7$.

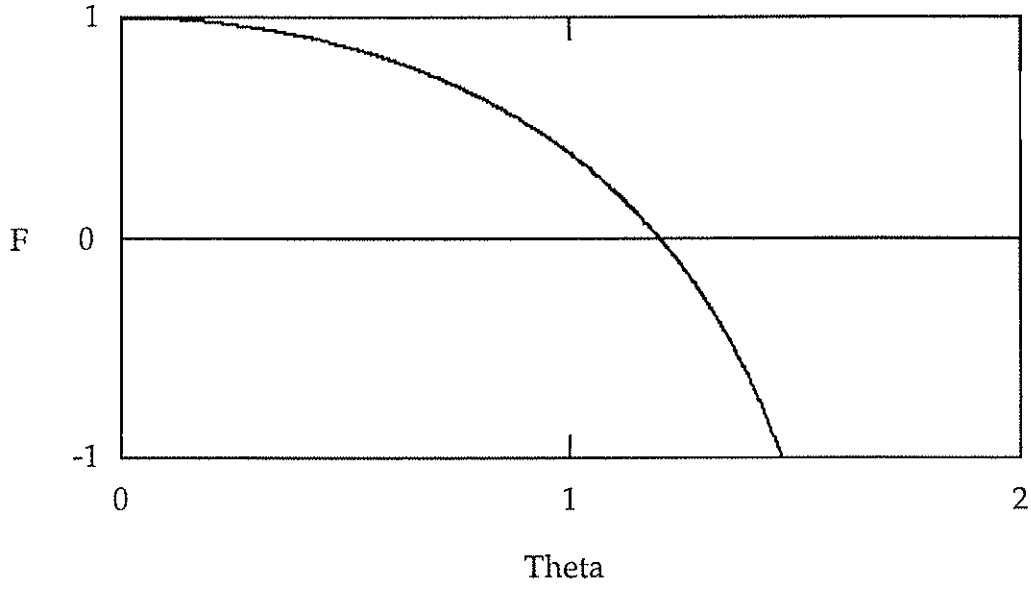

Figure 1.2 The F-θ curve for the BFM model.

Experimental data can be accommodated equally well by the polynomial function model[25] (PFM) which is used to model the MST plasma.

1.4 MOTIVATION AND OUTLINE

This thesis work is carried out on the new large RFP device, the Madison Symmetric Tours (MST), at the University of Wisconsin-Madison. The purpose of this work is to understand how field errors due to shell gaps and portholes affect RFP confinement in general and how the different modes of these perturbations interact with the plasma. And last but not least, the goal of this work is to improve MST plasma performance by eliminating field errors.

MST is designed with special attention paid to the minimization of magnetic field errors due to shell gaps, primary windings and portholes. The resulting machine design incorporates several unconventional features such as flanged gaps, continuity windings, small pumping and diagnostic holes and the use of the vacuum vessel as a single-turn toroidal field coil. However, MST was run during its first year of operation with the bias winding as an ohmic heating winding that does not match the plasma current distribution. This resulted in large non-axisymmetric magnetic field errors at the poloidal gap that are not part of the ideal RFP configuration.

There are many other sources of magnetic field errors, but the highly localized errors that occur at the poloidal gap are the most

dangerous because they produce a broad toroidal mode number spectrum (all n's) and thereby tend to cause the appearance of chains of magnetic islands. The net radial flux (m = 0 component) through the poloidal gap will resonate with the plasma at the reversal surface creating chains of magnetic islands that can destroy the reversal layer. For large field errors, the m = 0 islands could be large enough to connect the plasma core, which may be stochastic from plasma fluctuations, with the conducting wall. This would result in a complete loss of confinement.

The poloidal and toroidal gaps in MST are instrumented with a large set of magnetic pickup coils to measure the local radial magnetic fields at the gaps. A set of saddle correction coils, placed at the poloidal gap and driven by the primary current, is used to reduce the radial field and to change its poloidal mode spectrum.

The spatial structure of the field error was measured with the set of magnetic pickup coils permitting Fourier decomposition to find the dominant modes. Some modes have the same time dependence as the plasma and some have a more complicated time waveform, perhaps from effects of finite shell resistivity. The dominant modes of field error at the poloidal gap are m = 1, 2, and 4, which is consistent with the geometry of the MST poloidal gap system and the initial poloidal field system, the bias winding. The dominant mode of vacuum field error at the toroidal gap is n = 4, which is also consistent with the geometry of the MST toroidal gap system where the poloidal current is fed via four transmission lines. However, the toroidal mode spectrum changes in the presence of plasma.

Also, measurement of field errors associated with holes in the conducting shell were made on the old octupole. Measurements on MST showed that there is no significant coupling between holes in vacuum.

The dominant source of field errors in MST is the poloidal gap where a highly localized error occurs. By using the saddle like correction coils we were able to reduce some of the errors which have similar time dependence as the plasma current. Correcting these errors at the poloidal gap also reduced the error fields at the toroidal gap.

The gap error corrections had significant effects on the plasma; reducing the radial magnetic field resulted in lower plasma loop voltage, increased plasma duration and increased reversal duration. The electron temperature of the plasma, as measured by Thomson-scattering, also increased. Soft x-ray and other magnetic measurements showed that profiles are broader and the plasma outer region may have smaller islands.

The field error correction also had some effects on plasma fluctuations. With correction we have observed the presence of rotating plasma modes that are phase locked to each other forming a localized perturbation. Without correction, these modes were phase locked to the conducting wall. The most dramatic effect is seen on the behavior of the sawtooth oscillations which can be seen in the toroidal field at the wall and soft x-ray signals. With correction of field errors, these sawtooth oscillations have a period of about 0.5 msec or longer. However, without correction they occur very frequently and with a much shorter period.

These effects can also be seen on soft x-ray signals, but without correction the soft x-ray signals are very small. The nonlinear coupling of plasma modes is thought to be the cause of these oscillations.

Stationary toroidal modes have been measured in MST. Due to coil misalignment we can only put an upper bound on the amplitude of these modes of about 4% of the axisymmetric component. Experimental measurements suggest that these modes play an important role in the field error instability suggested by Kerst.[26]

Some estimate of the magnetic island widths that result from the measured radial fields at the poloidal gap are made. These estimates indicate that one should reduce field errors to 2% of the poloidal field at the wall to prevent islands overlap.

The machine description, diagnostics, and the sources of field errors in MST will be taken up in Chapter 2. Experimental results will be described in Chapter 3. Chapter 4 summarizes the results and conclusions.

REFERENCES

1 D. W. Kerst, J. Plasma Phys. **4**, 253 (1962).

2 D. D. Schnack, E. J. Caramana, and R. A. Nebel, Phys. Fluids **28**, 321 (1985).

3 K. L. Sidikman, J. D. Callen, and R. A. Nebel, Bull. Am. Phys. Soc. **32** , 1830 (1987).

4 R. I. Pinsker and A. H. Reiman, Phys. Fluids **29**, 782 (1986).

5 B. Alper, D. E. Evans, D. P. Storey, and H. Tsui, Bull. Am. Phys. Soc. **30**, 1406 (1985).

6 H. A. Bodin and A. A. Newton, Nucl. Fusion **20**, 1255 (1980).

8 B. Alper, P. G. Carolan, S. Martini, S. Ortolani, 12th Euro. Conf. on Cont. Fus. and Plasma Physics (Budapest 1985) Vol. 1 Page 638.

9 P. G. Carolan, B. Alber, M. K. Bevir, H. A. B. Bodin, C. A. Bunting, D. R. Brotherton_Ratcliffe, H. Ahmed, D. E. Evans, D. Evans, A. R. Field, L. Firth, M. J. Forrest, C. G. Gimblett, N. C. Hawkes, P. G. Hutchinson, M. Malacarne, A. Manley, A. A. Newton, P. G. Noonan, A. Patel, N. J. Peacock, D. P. Storey, H. Tsui, P. D. Wilcock, Plasma Physics and Controlled Nuclear Fusion Research (1984) Proc. 10th IAEA conference London, Vol. 2 Page 446. IAEA Vienna

10 P. G. Noonan, H. Tsui, A. A. Newton (1985), Plasma Physics and Controlled Fusion Vol. 27 No. 11 Page 1307.

11 Y. L. Ho, S. C. Prager, D. D. schnack, Phys. Rev. Lett. **62**, 1504 (1989).

12 T. Shimada, Y. Hirano, Y. Yagi, A. A. Newton, K. Ogawa, Plasma Physics and Controlled Nuclear Fusion Research (1986) Proc. 12th Int. Conf. Kyoto, 1986, Paper CN-47/K-1-3.

13 K. Hattori, K. Itami, Fujita, J. Morikawa, H. Nihei, Z. Yoshida, N. Inone, H. Ji, A. Fujisawa, N. Asakura, K. Yamagishi, T. Shinohara, Y. Nagayama, H. Toyama, K. Miyamoto, Nuclear Fusion **28**, 311 (1988).

14 S. Yamadas, S. Masamune, A. Nagata, H. Arimoto, H. Oshiyama, K. I. Sato. Proceedings of the Japan-US Workshop on RFP Data Base Evaluation, Tokyo 1989.

15 R. J. LaHaye, R. R. Goforth, G. L. Jackson, M. J. Shaffer, P. L. Taylor, Bull. Am. Phys. Soc. **26**, 1056 (1981).

16 R. S. Massey, C. J. Buchenauer, L. C. Burkhardt, A. R. Jacobson, J. G. Melton, G. Miller, R. W. Moses, K. F. Schoenberg, R. G. Watt, Los Alamos National Laboratory Report LA-9567-MS

17 L. Woltjer, Proc. National Academy of Sciences **44**, 489 (1958).

18 J. B. Taylor, Phys. Rev. Lett. **33**, 1139 (1974).

19 J. B. Taylor, Rev. Mod. phys. **58**, 741 (1986).

20 H. A. B. Bodin and A. A. Newton, Nuclear Fusion **20**, 1255 (1982).

21 J. P. Freidberg, Rev. Mod. Phys. **54**, 801 (1982).

22 K. F. Schoenberg, Nuclear Fusion **22**, 1433 (1982).

23 R. B. Howell, Bull. Am. Phys. Soc. **31**, 1547 (1986).

24 K. Hattori, K. Hirano, Y. Yagi, T. Shimada, Y. Maejima, I. Hirota, K. Ogawa, Plasma Physics and Controlled Fusion Vol. 31 No.14 (1989).

25 J. C. Sprott, Phys. Fluids **31**, 2266 (1988).

26 D. W. Kerst, Several shield, Shell and gap problems-method for rough estimation, Universty of Wisconsin-Madison, Report PLP # 909 (1983).

2. EXPERIMENTAL APPARATUS AND DIAGNOSTICS

The Madison Symmetric Torus (MST) is a toroidal reversed field pinch device for plasma physics and fusion research. A brief description of the unique design features of this device and the inherent sources of magnetic field errors associated with it will be the topic of this chapter.

2.1 MACHINE DESCRIPTION

The MST is a reversed field pinch device which was designed with special attention paid to the minimization of magnetic field errors associated with the shell gaps, portholes and field winding.[1, 2, 3]

MST has a large conducting toroidal shell that serves as the vacuum vessel, the toroidal field winding and the conducting shell for equilibrium and stability. The shell is made from 5 cm thick aluminum with a major radius of 150 cm and a minor radius of 52 cm (figure 2.1). This shell thickness corresponds to a poloidal magnetic field soak-in time, defined by $\tau = 2\mu_o d^2/\eta$, of about 60 msec. Since the discharge duration is approximately 50 to 80 msec, the shell will contain the magnetic flux and provide the equilibrium on the time scale of the experiment.

The conducting shell has two voltage gaps, toroidal and poloidal. The toroidal gap is a cut in the conducting shell the long way around to allow the toroidal magnetic field to enter the shell. The poloidal gap is a cut in the conducting shell the short way around to allow the poloidal magnetic to enter

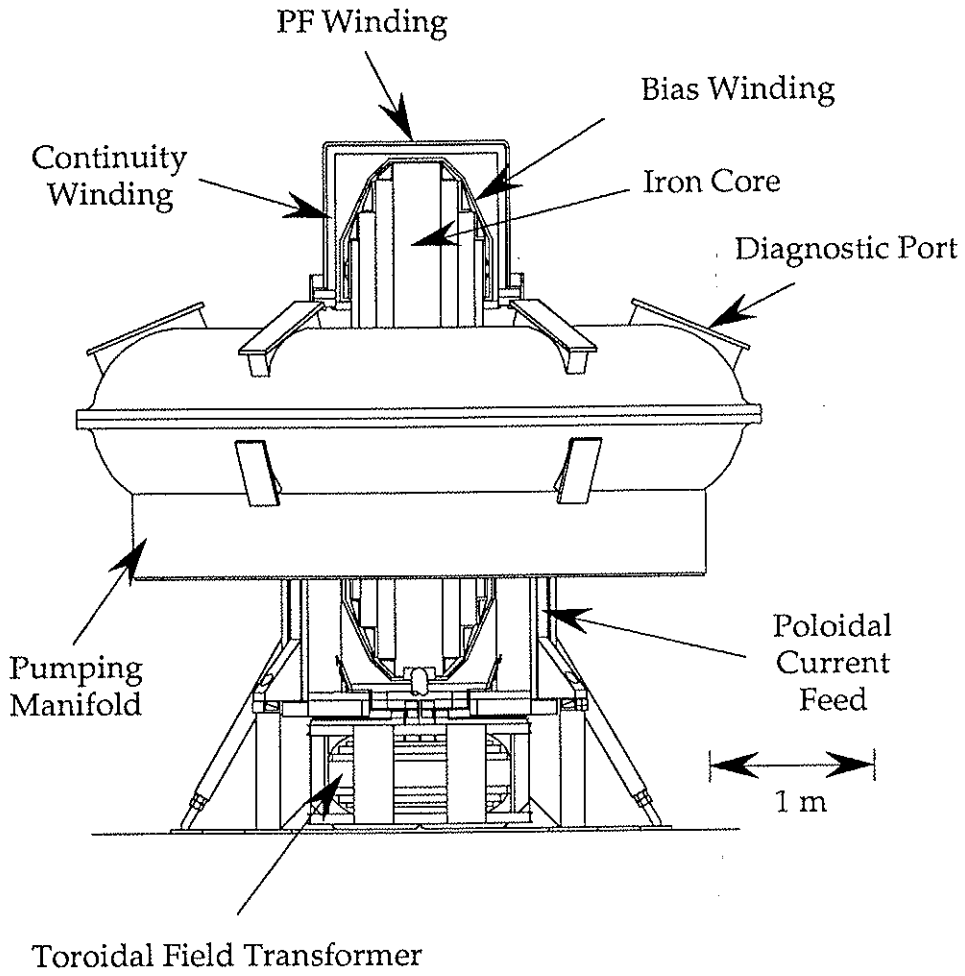

Figure 2.1 The Madison Symmetric Torus (MST).

the shell.

Ohmic heating and field generation are provided by a 2.0 Volt-second laminated iron core transformer, which links the plasma to the 20 turn primary winding (variable from 5 to 40 turns). The pulsed current to this winding is supplied by discharging a high voltage capacitor bank (5 kV maximum).

To maintain a small value of field error at the poloidal gap, the poloidal field system [1, 2, 3, 4, 5] is divided into three separate sets of windings around the iron core. A schematic of the layout of these windings, the currents associated with them and how the windings control the shell current as it reaches the poloidal gap is shown in figure 2.2.

The first winding is called the continuity winding. It is connected to the poloidal gap through an extended flange. This winding provides a low impedance path for the surface currents flowing on the inside surface of the shell, from one side of the gap to the other around the core. Without the continuity winding these currents would have to flow on the outside surface of the shell. Since the outside surface current distribution differs from that on the inside surface, a poloidal component to the current would have to exist along the gap edge and the poloidal flange to connect the two distributions. This poloidal current will produce a large radial magnetic field in the gap. However, forcing the surface currents to flow in the continuity winding does not eliminate all field errors in the gap, but rather only the errors associated with the currents flowing on the outside surface of the shell. The rest of field errors are reduced by using the second winding and the poloidal flange.

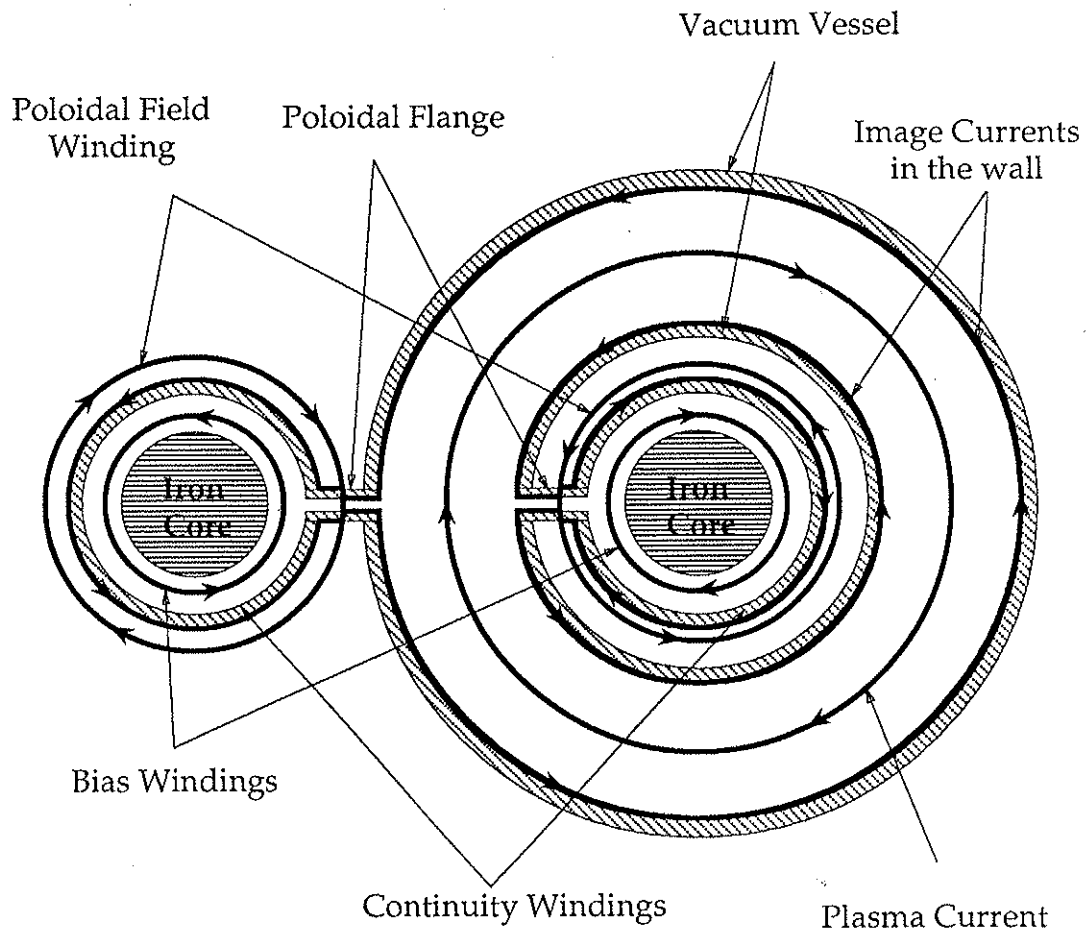

Figure 2.2 The MST poloidal field system.

The second winding is called the poloidal field (PF) winding. The PF winding consists of forty turns tightly wrapped around the outside of the continuity winding and piercing the poloidal flange through the holes depicted in figure 2.3. These holes are distributed around the gap to approximate the plasma image current distribution. This PF winding is designed to force the surface currents to flow from the inside surface of the poloidal flange, through the holes, to the outside surface of the flange and the continuity winding where any pulsed field error will be shielded from the plasma by the 5-cm-thick wall of the shell. The desired hole placement in the flange is determined by the plasma equilibrium, where the holes are chosen to lie on a magnetic flux surface within the flange with the appropriate spacing of turns to allow all turns to carry the same current. This distribution will be imperfect for plasma current and pressure profiles which differ from those assumed in the equilibrium code. Deviations from the design case are expected to produce a radial magnetic field with a dominant m=1 poloidal mode number which can be seen in the formation stage of the discharge. The poloidal flange will reduce errors associated with the discreteness of the PF winding.

The third winding is called the bias winding. It is used to reverse bias the iron core in order to achieve a flux swing of up to 2 Volt-seconds. This 40 turn winding is connected in a 20:1 ratio and carries 8000 Ampere-turns of dc current for 3 to 10 seconds. This winding prevents core saturation which would produce a pulsed field error at the gap. More importantly, it is critical that the bias winding be distributed along the iron core in such a way to trap

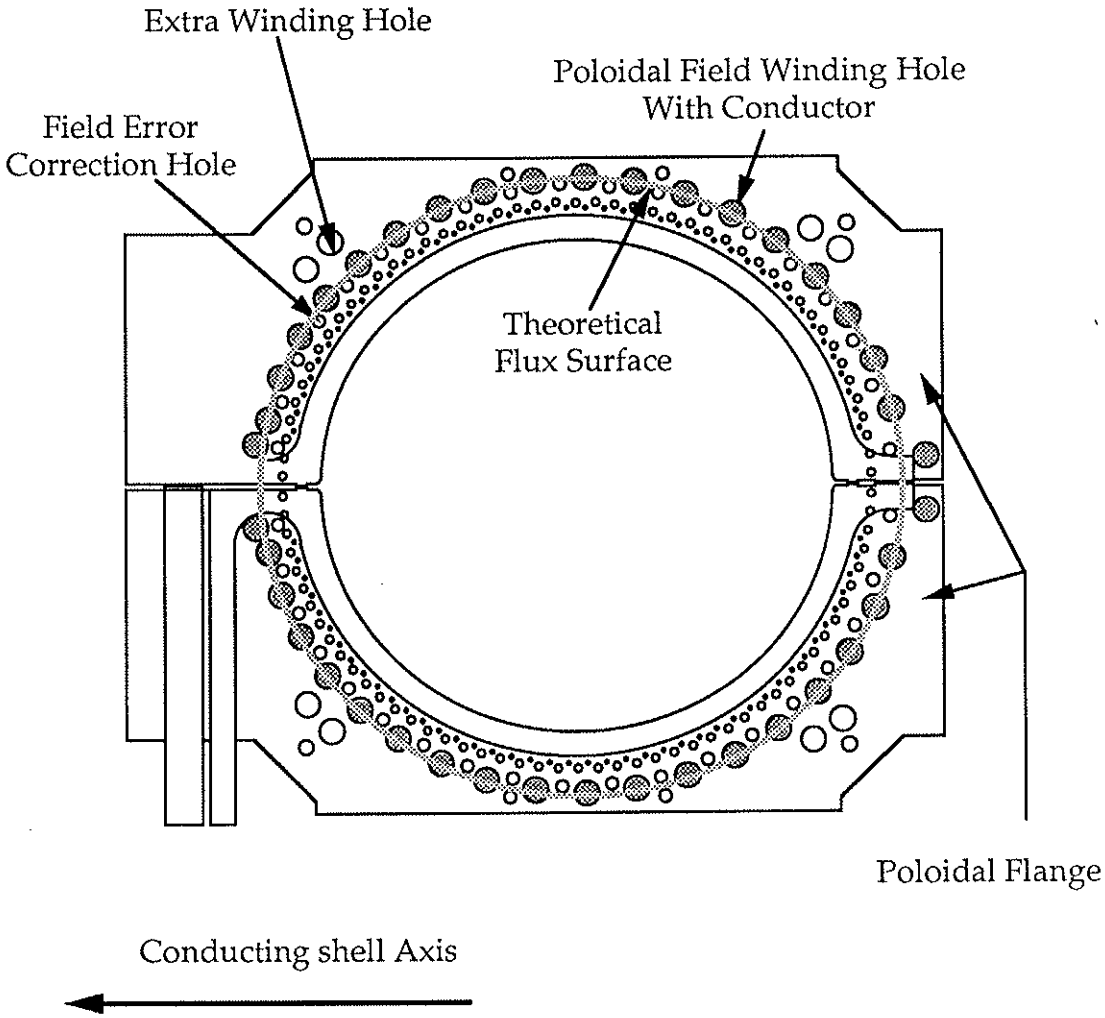

Figure 2.3 The MST poloidal Flange.

most of the magnetic flux inside the core and not allow it to leak into the plasma volume. Since it carries a dc current, the resultant error flux would enter the plasma though the entire shell surface, not just at the gap as for a pulsed error. Thus, the desired distribution of the bias winding around the core was determined empirically.

The toroidal field is produced by running a poloidal current in the conducting shell, shown in figure 2.4. The shell is used as a one-turn secondary winding of a 0.5 volt-second transformer.[1,2,3] This results in easy diagnostic and maintenance access. The primary of this transformer is supplied by an electrolytic capacitor bank (450 V, 0.5 F). The poloidal current is fed to the shell from the transformer via a long axisymmetric flange system to symmetrize the wall currents. The flange consists of an annular disk which connects the conducting shell to a cylindrical section. Four transmission lines from the toroidal field transformer connect to the bottom of the cylindrical section at four locations. As will be seen later in this chapter, this has resulted in a vacuum field with a dominant n = 4 field error. This n = 4 ripple in the toroidal field is minimized by a long cylindrical section. The maximum average vacuum toroidal magnetic field is about 600 Gauss. This transformer can also be drivenn by discharging a high voltage capacitor bank for the aided-reversal mode of operation.

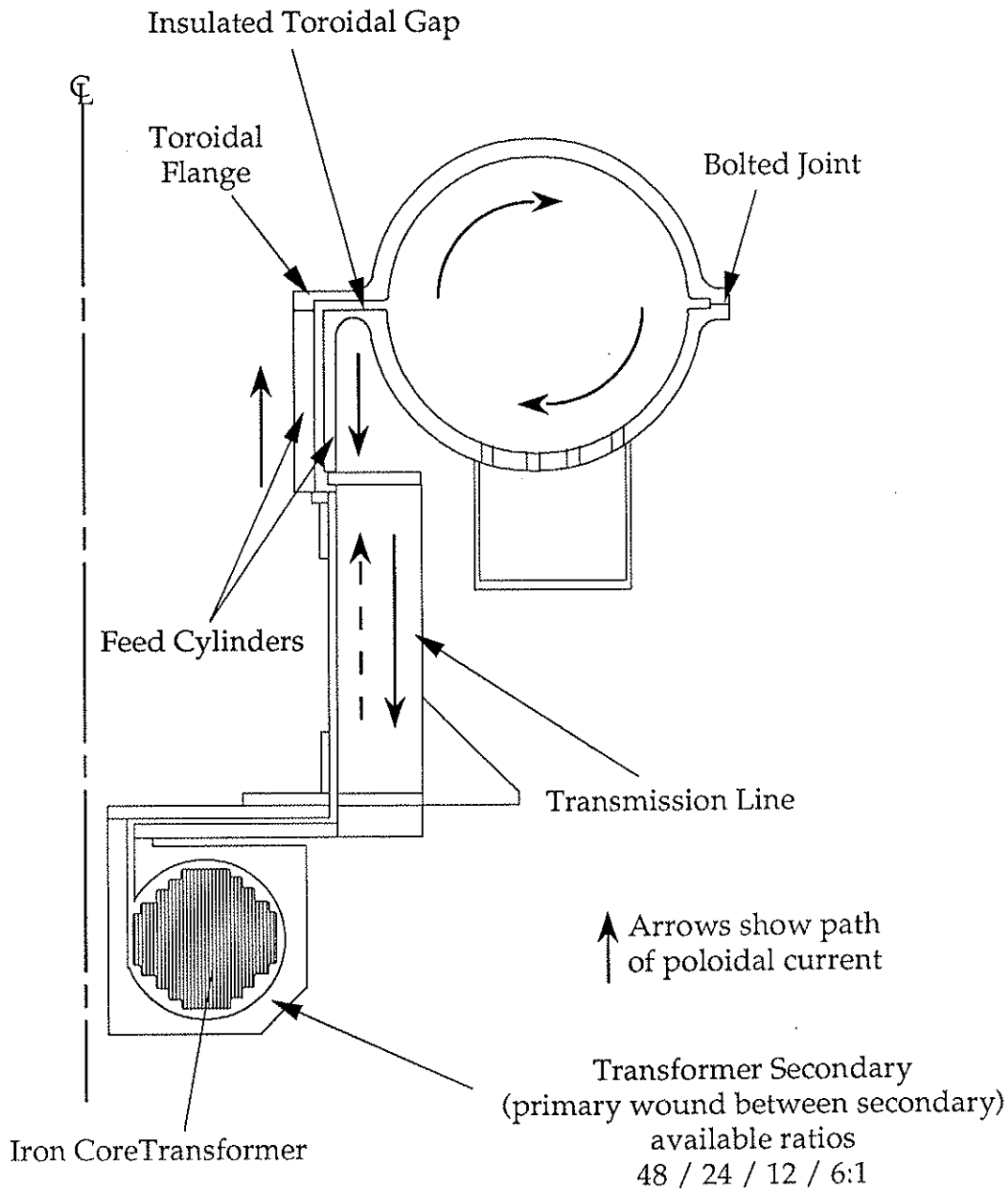

Figure 2.4 The MST toroidal field system.

2.2 DIAGNOSTICS

Several diagnostics are available on MST to measure global discharge parameters. A set of operational diagnostics such as Rogowskii coils are used to measure the toroidal plasma current and poloidal currents in the conducting wall. The average toroidal flux and gap voltages are measured by flux loops. Most of these diagnostics are placed inside the conducting wall, near the plasma edge. These measured quantities are used to calculate RFP parameters , such as F and θ, using the polynomial function model (PFM). [6,7]

To carry out the proposed field error experiments, as well as other experiments on MST, a large number of magnetic pickup coils were installed at various locations.

For magnetic field measurements at the poloidal gap, a 16 coil set was installed at the gap. Each coil set is made of two perpendicular coils to measure the poloidal and radial field. These coils were magnetically calibrated to determine their effective areas and phase delay in the frequency range from 10 to 100 kHz. These coils are distributed around the poloidal gap with roughly equal poloidal separation. The radial position of these coils is about 58 cm, 6 cm away from the plasma edge. The alignment of these coils was made by using an angle finder that is accurate only to $\pm$ 1 degrees at best. This gives a minimum error in the radial field measurements due to poloidal field pickup of about $\pm$ 2% of the poloidal field at the wall. These coils were used during the first year of operation of MST with the bias winding which

resulted in large radial fields about 23% of the poloidal field at the wall. For such a large value of the radial field these coils were more than adequate.

After the MST upgrade of the poloidal field system, the radial field at the gap was expected to be less than 10% of the poloidal field at wall. The physics plans of MST require the radial fields to be less than 2% of the poloidal field at the wall. For these reasons, a new set of magnetic pickup coils was added at the gap. The new set consists of 32 radial and poloidal coils distributed around the poloidal gap at equal poloidal separations. These coils are located inside the shell at a 52 cm radius, at the plasma edge. These coils were aligned to the inside surface of the shell to a fraction of degree. With these coils it is possible to measure radial fields to within a few percent of the poloidal field at the wall with good accuracy.

For fluctuation measurements a large number of magnetic pickup coils were placed on the inside surface of the shell. A set of 64, 3-axis coils was distributed toroidally with equal toroidal separation, all at the same poloidal angle. With this set of coils, measurements of the toroidal and poloidal fields at the wall at a given poloidal angle as a function of the toroidal angle were made. This permitted a Fourier decomposition to determine the toroidal mode spectrum of the plasma. Another set of 16, 3-axis coils that are distributed poloidally with equal poloidal separations at the same toroidal angle was also installed. With this set of coils, the poloidal and the toroidal field at the wall at a given toroidal angle were measured as a function of the poloidal angle. This information provided the poloidal mode spectrum of the plasma.

In conjunction with this extensive set of magnetic diagnostics, MST has a large set of other non-magnetic diagnostics. This includes a single-point Thomson scattering system, a single-chord microwave interferometer, a single-chord charge exchange analyzer and a 2-D soft x-ray array. There is also a large set of visible and ultraviolet spectroscopic diagnostics.

2.3 SOURCES OF FIELD ERRORS

There are many sources of magnetic field errors, such as portholes, magnetic field windings and shell voltage gaps. Portholes are required for diagnostic access but will disturb the wall currents and produce a radial magnetic field that can cause a local disturbance of the magnetic flux surface. This results in enhanced plasma-wall interaction. Portholes must be carefully designed since closely spaced holes may couple and magnetically appear as one large hole. Also, portholes should not have any toroidal symmetry that can cause porthole coupling with plasma modes. These effects may be detrimental to magnetic confinement [8]. Shell voltage gaps are also needed to allow pulsed magnetic fields to enter the conducting shell. This source is the most dangerous and the hardest to fix. Surface currents at the gap faces must be controlled very accurately to eliminate radial fields.

2.3.1 Portholes in the shell

MST has a total of 368 holes in the conducting shell, see figure 2.5. Of these, 175 are for diagnostic purposes. There are four holes 4.5 inches in diameter, and the remainder are mostly 1.5 inches in diameter. There are 193 1.5-inch-diameter holes used for pumping out the conducting shell. There are two types of symmetries associated with these portholes that are likely to produce problems.

The 175 diagnostic holes can be divided into two different sets, each with six groups that are equally spaced around the toroidal direction. This n=6 symmetry may cause or enhance island formation.

The 193 pumping holes are located in the bottom of the device. This may produce radial fields that have an up-down asymmetry which will cause an axisymmetric shift of the plasma. This will result in a mismatch of currents at the poloidal gap, a source of m=1 field errors.

Extensive numerical work was done to study the field errors associated with holes in the conducting shell of MST. [9] The results of these studies, which treat each hole individually as described in great detail in reference 9, showed that there is no evidence of islands around the n=6 resonant surface; thus MST is safe from magnetic islands produced by holes in the conducting shell. It was also found that the pumping holes cause no appreciable shift of the plasma. In summary, the field lines in MST remain well confined in the presence of radial fields from holes in the conducting shell, except for the four

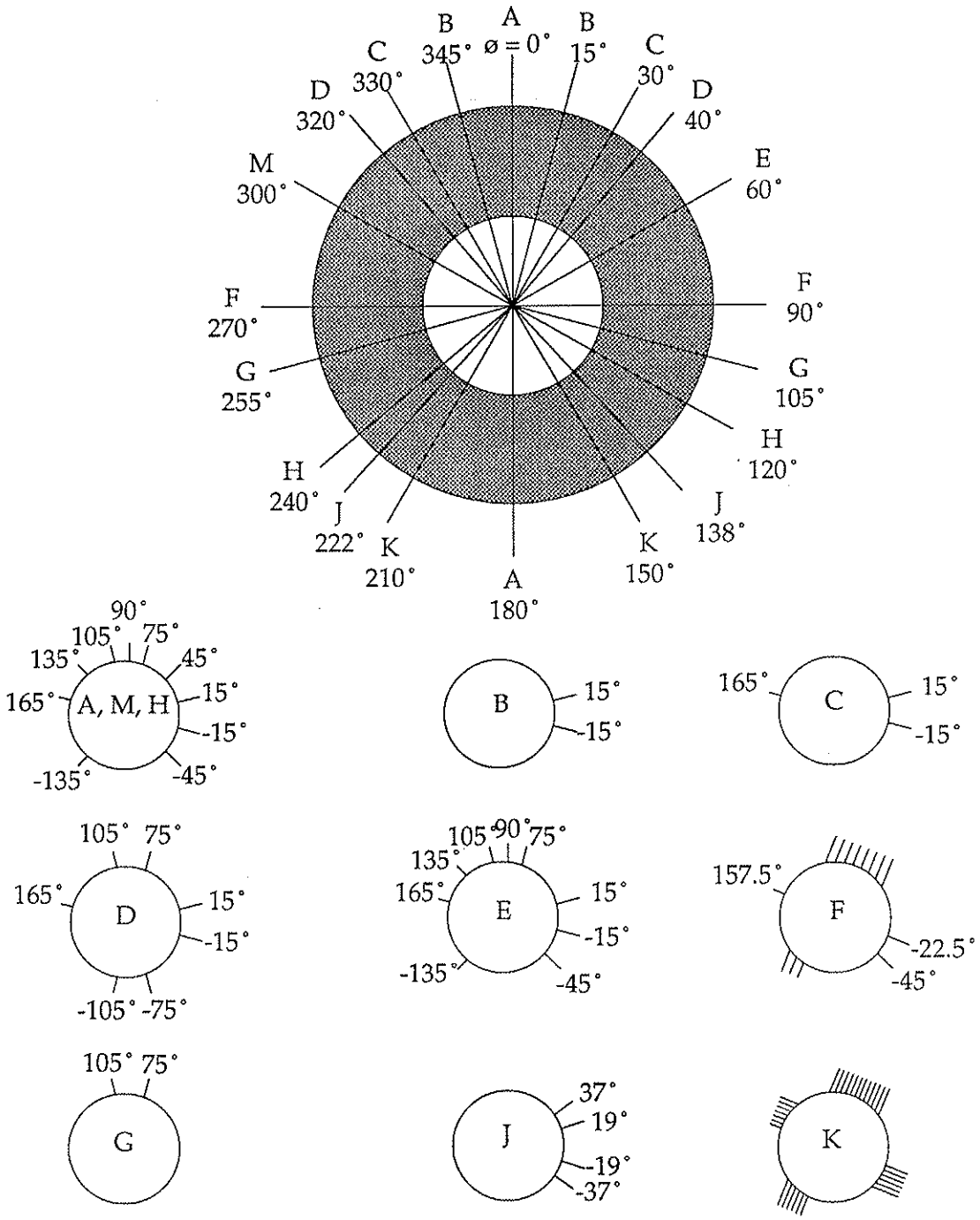

Figure 2.5 The MST porthole layout.

large holes which may be a source of concern for MST. This was verified by the enhanced plasma-wall interaction around these large portholes.

2.3.2 Toroidal field system

The toroidal field system is a unique design[1,2,3] where the conducting shell is used as a one-turn toroidal field winding.

The vacuum toroidal field was measured to have a 1/R dependence as shown in figure 2.6 and to be axisymmetric 60 degrees away from the toroidal gap, as shown in figure 2.7.

The resulting vacuum radial magnetic field at the toroidal gap was measured to contain mostly n = 4 as shown in Figure 2.8-a. The m = 0 component of this n = 4 radial field is less than 0.2% of the vacuum toroidal field on axis. This would produce an island of about 4% of the plasma minor radius around the reversal surface where an m=0 radial field would be resonant. However, with plasma, the spectrum changes, and n = 0 and 1 become the dominant modes shown in figure 2.8-b.

2.3.3 Poloidal field system

The poloidal field system has two windings that may be a source of field errors. The first winding is the bias winding which would produce a dc field error; the second winding is the poloidal field (PF) winding which would produce a pulsed field error.

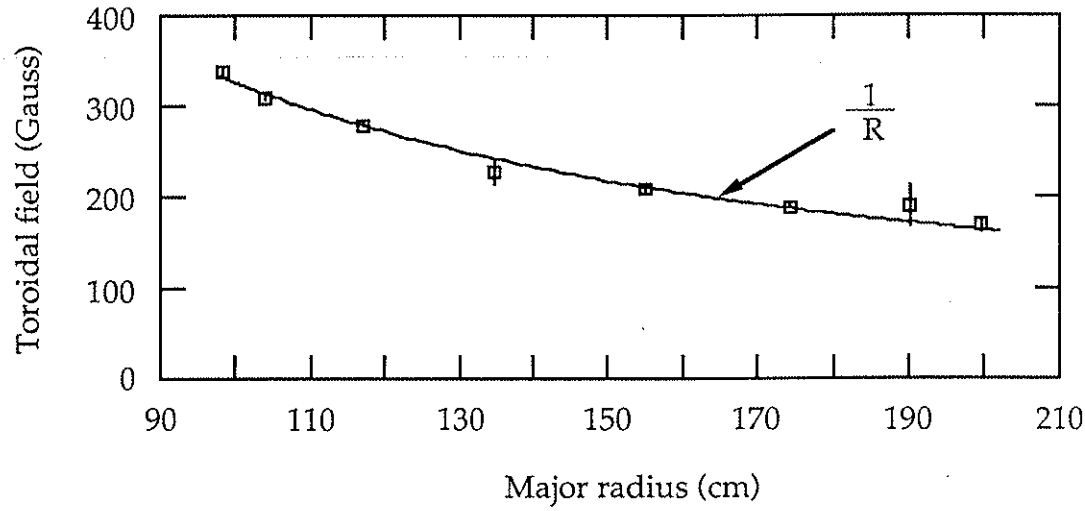

FIGURE 2.6 The vacuum toroidal field at 180 degrees toroidally.

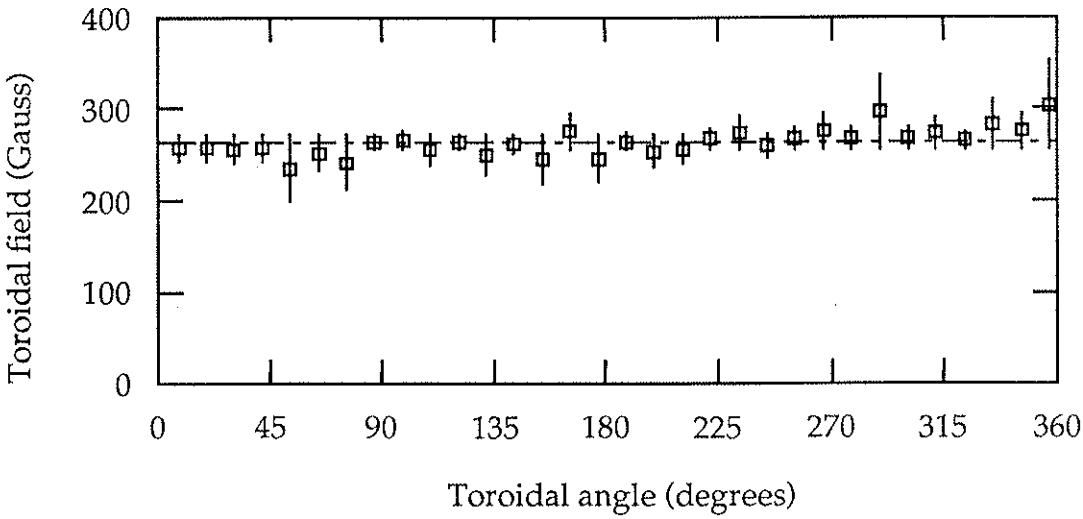

Figure 2.7 The vacuum toroidal field at 241 degrees poloidally.

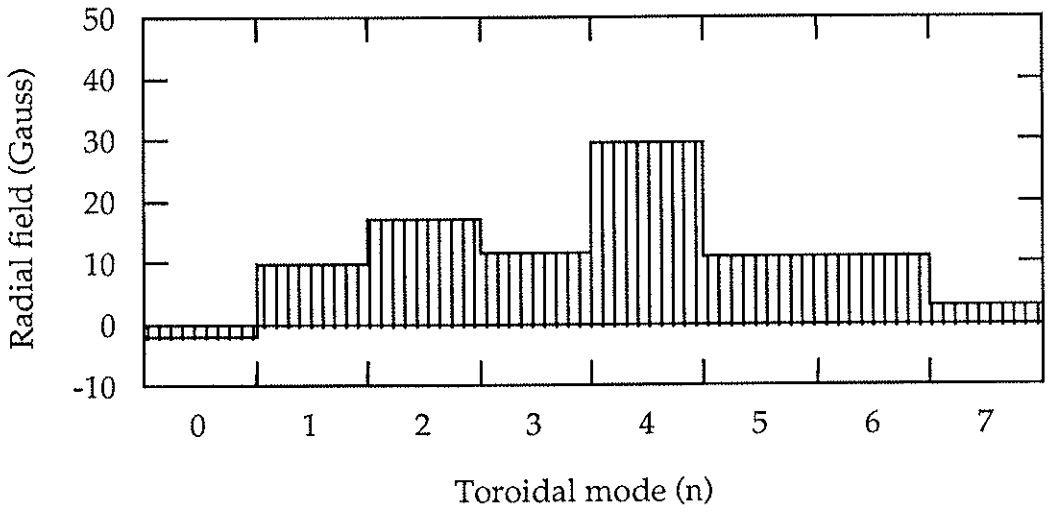

Figure 2.8-a The toroidal mode spectrum of the radial field at the toroidal gap in vacuum.

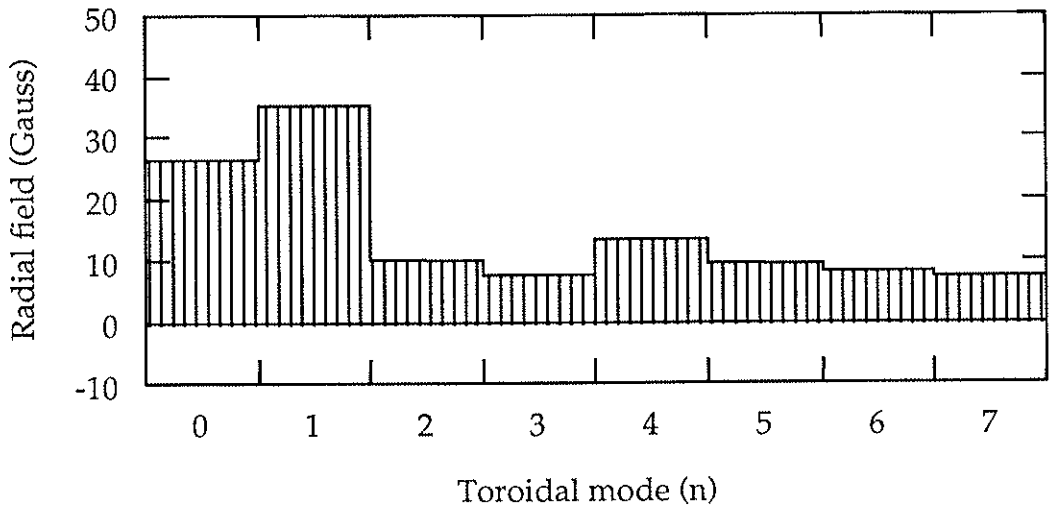

Figure 2.8-b The toroidal mode spectrum of the radial field at the toroidal gap with plasma.

The bias winding is energized by a dc current to reverse bias the iron core. This winding is made of 4 /ø wire placed on the iron core. These turns must be placed in the proper locations along the iron transformer to force all the field lines to be trapped inside the iron core; otherwise some flux will leak out of the iron core and become a source of field error. Any field errors caused by this winding will be a dc field which the conducting shell cannot shield from the plasma. This field error could prevent plasma breakdown if not minimized. A great deal of time and effort was spent to reduce this dc field to levels below the earth's field. The final winding distribution on the iron core produced a dc field error less than 0.5 Gauss inside the volume that would be occupied by the plasma shown in figure 2.9.

During the first year of operation, the bias winding was also used as the Ohmic heating winding as well. However this winding was not optimized for this task, and as a result it produced large pulsed radial magnetic fields at the poloidal gap with an rms value of about 23% of the poloidal field at the wall. Since this winding was placed on a square iron core almost uniformly, a large m = 4 component was expected. The poloidal distribution did not match the poloidal distribution of the plasma surface current, which is mostly m = 1 thereby producing a large m = 1 component of the error field at the poloidal gap.

The permanent Ohmic winding (PF) is designed to minimize the magnetic field errors at the poloidal gap. This is done in two steps. First, by forcing the surface currents to flow radially out on the flange surface once they reach the gap. This is done by piercing the flange, as close as possible to

the gap, with the PF winding, with a distribution show in figure 2.10, that matches the wall currents at the gap. In the second step the surface currents are forced to exit from the inside surface of the flange to the outside surface of the flange and the continuity winding. It is clear at this point that this PF winding design is optimum for minimizing field errors, but it has obvious limitations.

First, there is a current flowing in the inside surface of the flange between the gap edge and the point where the PF winding pierces the flange. This current can be a source of field errors when the PF distribution does not match that of the plasma. This error is found to contain mostly m = 1 and m = 2 components. This error can exist from the beginning of the discharge.

Second, the current that is forced to flow on the outside surface of the flange soaks into the flange due to the finite resistivity of the conductor and produces field errors in the gap. This error has dominantly m = 4 and m = 2 components. This error will dominate late in the discharge.

The first limitation can be corrected by using passive correction coils to eliminate errors with time dependence similar to that of the plasma current. The second limitation requires a complicated waveform shaping or active feedback circuit.

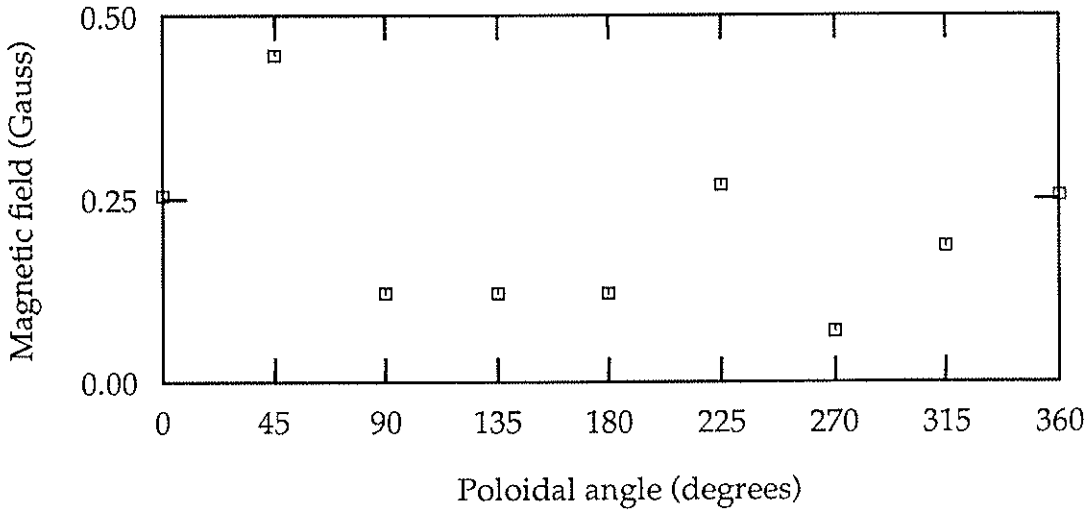

Figure 2.9 The dc magnetic field produced by the bias winding at the plasma edge.

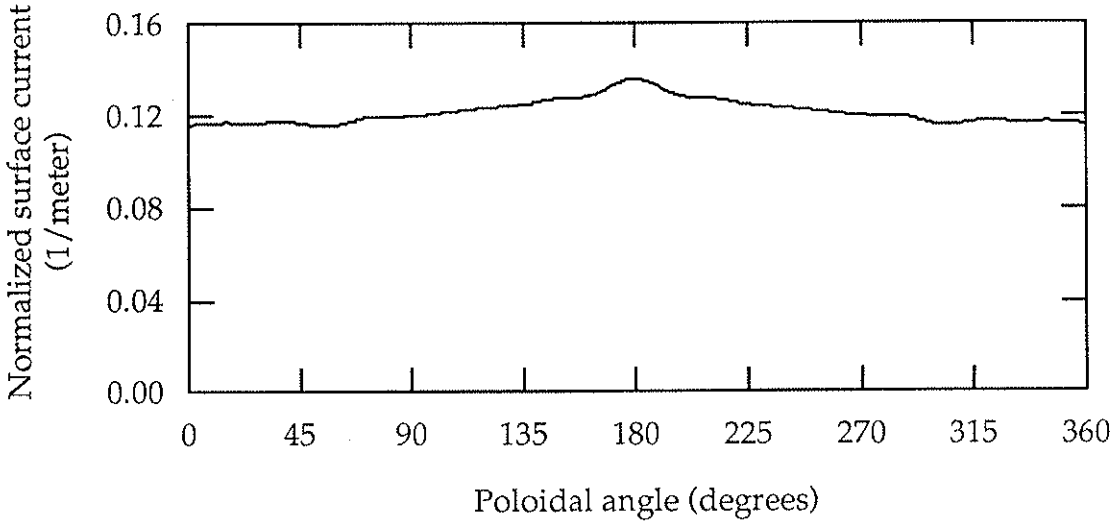

Figure 2.10 The poloidal distribution of PF winding.

REFERENCES

1 R. N. Dexter, D. W. Kerst, T. W. Lovell, S. C. Prager, J. C. Sprott, Fusion Technology in press.

2 Y. Ho, R. N. Dexter, D. W. Kerst, T. W. Lovell, S. C. Prager, J. C. Sprott, The design of MST Reversed Field Pinch, University of Wisconsin Report PLP 956, Nov. 1985.

3 A. F. Almagri, S. Assadi, J. Beckstead, G. Chartas, D. J. Den Hartog, Y. L. Ho, D. W. Kerst, T. W. Lovell, S. C. Prager, J. S. Sarff, W. Shen, C. Spragins, J. C. Sprott, The design of MST Reversed Field Pinch, University of Wisconsin Report PLP 1022, Nov. 1987.

4 D. W. Kerst, Primary System, University of Wisconsin Report PLP 972, March 1986.

5 D. W. Kerst, Poloidal gap and Primary connection, University of Wisconsin Report PLP 955, Oct. 1985.

6 J. C. Sprott, RFP Profile Representations, University of Wisconsin Report PLP 1008 Aug. 1987.

7 J. C. Sprott, Phys. Fluids **31**, 2266 (1988).

8 K. Hattori, K. Itami, Fujita, J. Morikawa, H. Nihei, Z. Yoshida, N. Inone, H. Ji, A. Fujisawa, N. Asakura, K. Yamagishi, T. Shinohara, Y. Nagayama, H. Toyama, K. Miyamoto, Nuclear Fusion **28**, 311 (1988).

9 K. L. Sidikman Ph. D. Thesis, University of Wisconsin-Madison (1990).

3. EXPERIMENTAL RESULTS

Results of the field error experiments performed on MST are presented in this chapter. Field errors at the poloidal gap were reduced by 18% in rms values. This modest reduction of field errors resulted in improved plasma discharges. The plasma loop voltage was reduced by about 31% and the plasma resistivity was reduced by 36%. Reversal duration increased by 16%. The soft x-ray emission profiles are larger and broader. The character of the sawtooth activity as seen on the toroidal field at the wall changed considerably when field errors were reduced. Plasma improvements were observed to have a stronger dependence on the $m = 0$ component of the field error. This dependence agrees well with the presumed vulnerability of RFPs to $m = 0$ magnetic island formation. Field errors were reduced further by a factor of six in rms values when the permanent ohmic winding was installed. With this reduction of field errors plasma loop voltage was reduced by about a factor of two. The discharge duration doubled. At this low level of field errors, the plasma exhibited coherent toroidal modes. These modes are phase-locked to one another to form a localized perturbation. This perturbation rotates toroidally in the ion-diamagnetic drift direction with a speed of about 10^6 cm/sec. Occasionally these modes lock to the conducting wall. This is believed to be caused by the poloidal gap field errors. These locked discharges tend to be much shorter in duration and to have larger loop

voltage. The behavior of locked discharges can be explained by field error instability.

For convenience of presentation only, this chapter will be divided into two parts. The first part will deal with the results of passive correction of field errors and the corresponding improvements in the plasma discharges. The second part will deal with the results of installing the permanent ohmic winding. This winding eliminated the sources of field errors as was described in chapter two.

3.1 OPERATION WITH THE BIAS WINDING.

MST was run for about one year with the bias winding which produced large field errors as expected. One of the surprising results was a large m = 0 component of the radial field at the poloidal gap. Nothing about the machine design led us to expect the presence of an m = 0 component of the radial field. In our attempt to reduce the radial field at the poloidal gap we observed a correlation between plasma improvements and the amplitude of the m = 0 component of the field error. This is consistent with the presumed vulnerability of RFP plasmas to an m = 0 magnetic island formation.

The radial magnetic field at the poloidal gap was measured as a function of poloidal angle and time. Most of the radial field components have a time dependence similar to that of the plasma current and have a peak value when the plasma current is maximum. This occurs at about 15

msec into the discharge. In addition to this slow component of the radial field, there is a fast component associated with the sawtooth activity. These oscillations show up mostly in the m = 0 and m = 1 components of the radial field poloidal mode spectrum. These oscillations cause an inward shift of the plasma, which manifests itself as an increase of the m = 1 amplitude of the radial field. The following analysis is done on the slow component at 15 msec into the discharge where these radial fields are maximum. The field error structure at the poloidal and toroidal gap will be described in section 3.1.1, and the modest correction of these errors as well as the corresponding improvements in the plasma parameters will be described in section 3.1.2. The observed dependence of the plasma quality on the m = 0 component of the field error will be described in section 3.1.3. The variation of field errors with the plasma profiles is the topic of section 3.1.4.

3.1.1 Radial magnetic field at the poloidal and the toroidal gap.

The measured radial magnetic field at the poloidal gap is shown in figure 3.1 where the measured points are represented by the squares. These 16 values of the radial field were used to calculate the amplitudes of the poloidal mode spectrum up to m = 7 using Fourier decomposition of the measured spatial structure. From these calculated modes the full spatial structure is plotted as a solid curve in figure 3.1. The measured radial field has a poloidal magnetic field pickup due to a ± 1 degree alignment error of

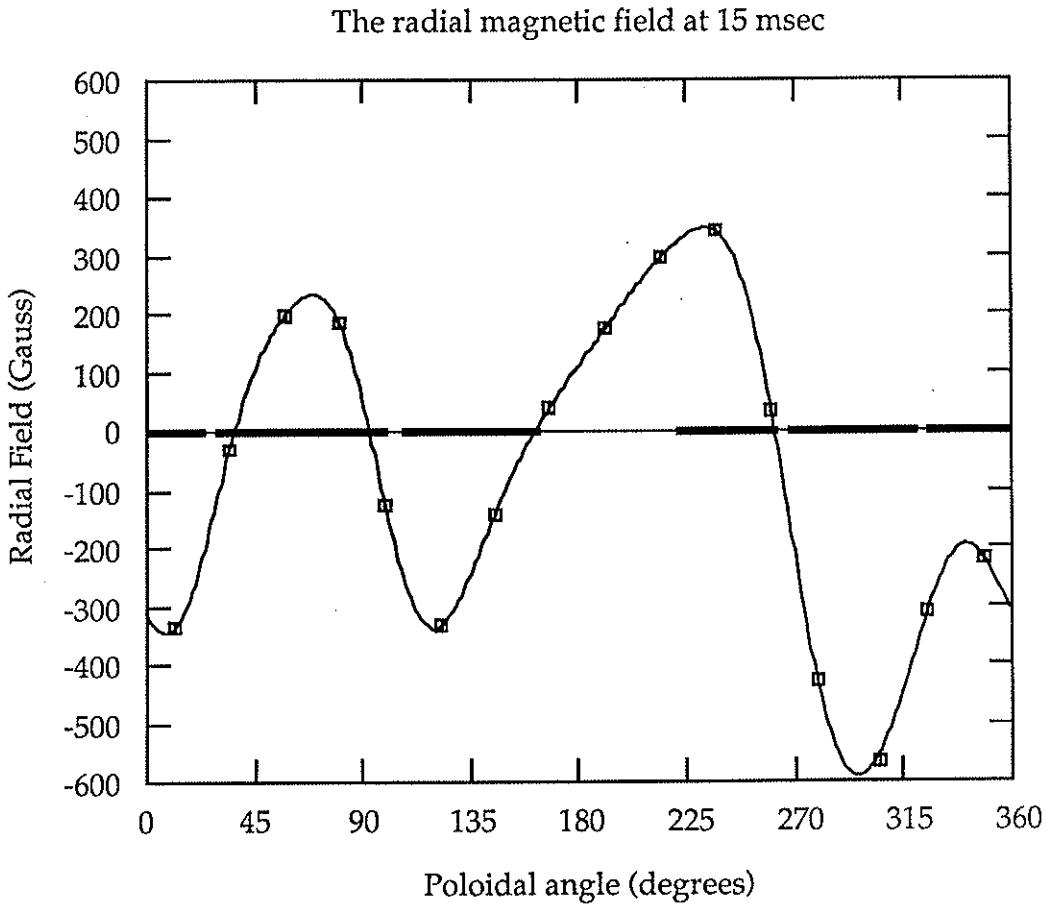

Figure 3.1 The poloidal structure of the radial field at the poloidal gap without field error correction.

the magnetic pickup coils. A misalignment of 1 degree would give an error of 2% of the poloidal field at the wall, about 20 Gauss of systematic error in each measured signal for the cases being analyzed. Errors in the calibration of these coils and errors in the gains of the integrators would add up to about 3% of the value of each signal. This misalignment error in the measurement dominates the other sources of errors. Figure 3.2 shows the calculated amplitudes of these modes, where the errors in the mode amplitudes due to the errors in the raw measurements are about 5 Gauss for the m = 0 and about 7 Gauss for the other components. The dominant modes are m = 1, 2, 4. These results are shot to shot reproducible.

Figure 3.3 shows the measured radial field at the toroidal gap. These measurements were made in the same discharges as the radial fields of the poloidal gap. The coils that are used for the radial field at the toroidal gap have alignment errors of about ± 3 degrees. This would result in an error of about 5 % of the toroidal field at the wall or about 5 Gauss. The toroidal field at the wall where these coils are located is only about 100 Gauss. This ± 5 Gauss systematic error is much smaller than the measured radial field at the toroidal gap which is about 56 Gauss rms. This systematic error in the raw data propagates into less than 3 Gauss of error in the mode amplitudes.

Similar Fourier decomposition is carried out for this radial field. Figure 3.3 shows the calculated spatial structure from these modes as a solid curve. The calculated modes are shown in figure 3.4, where the

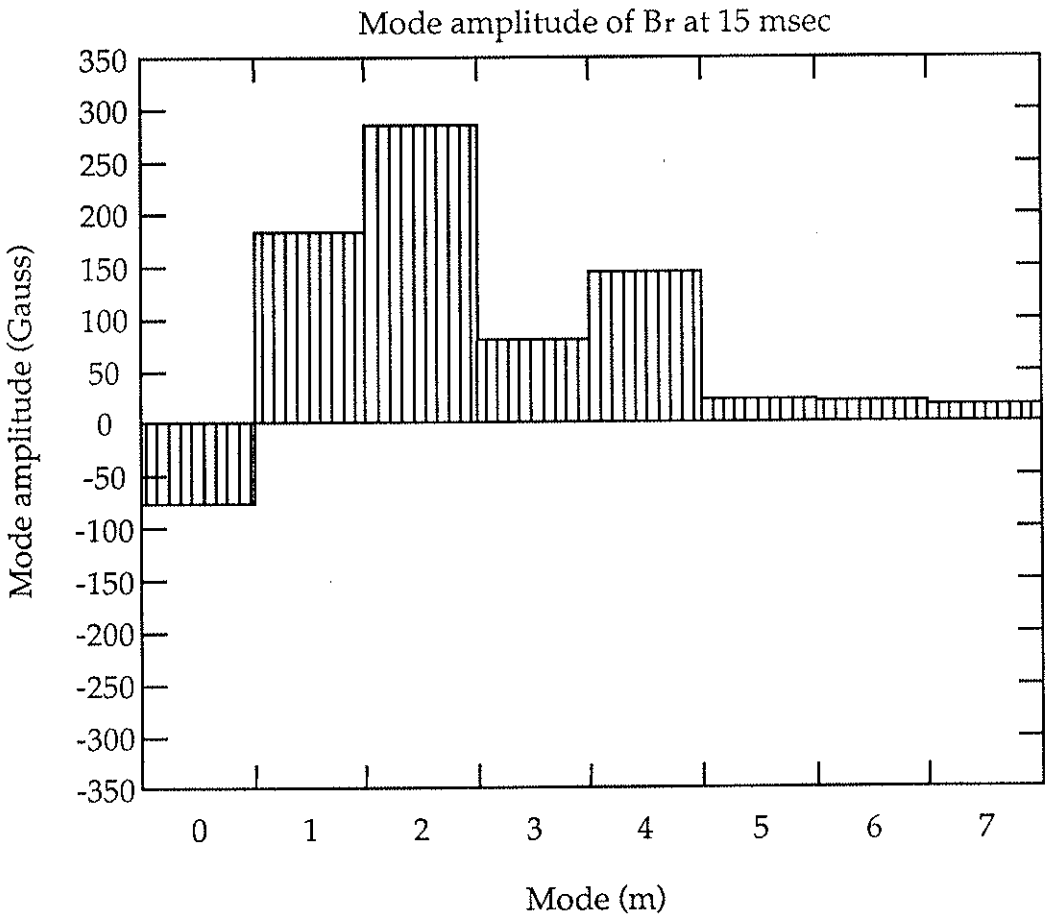

Figure 3.2 The mode amplitude of the radial field at the poloidal gap without any field error reduction.

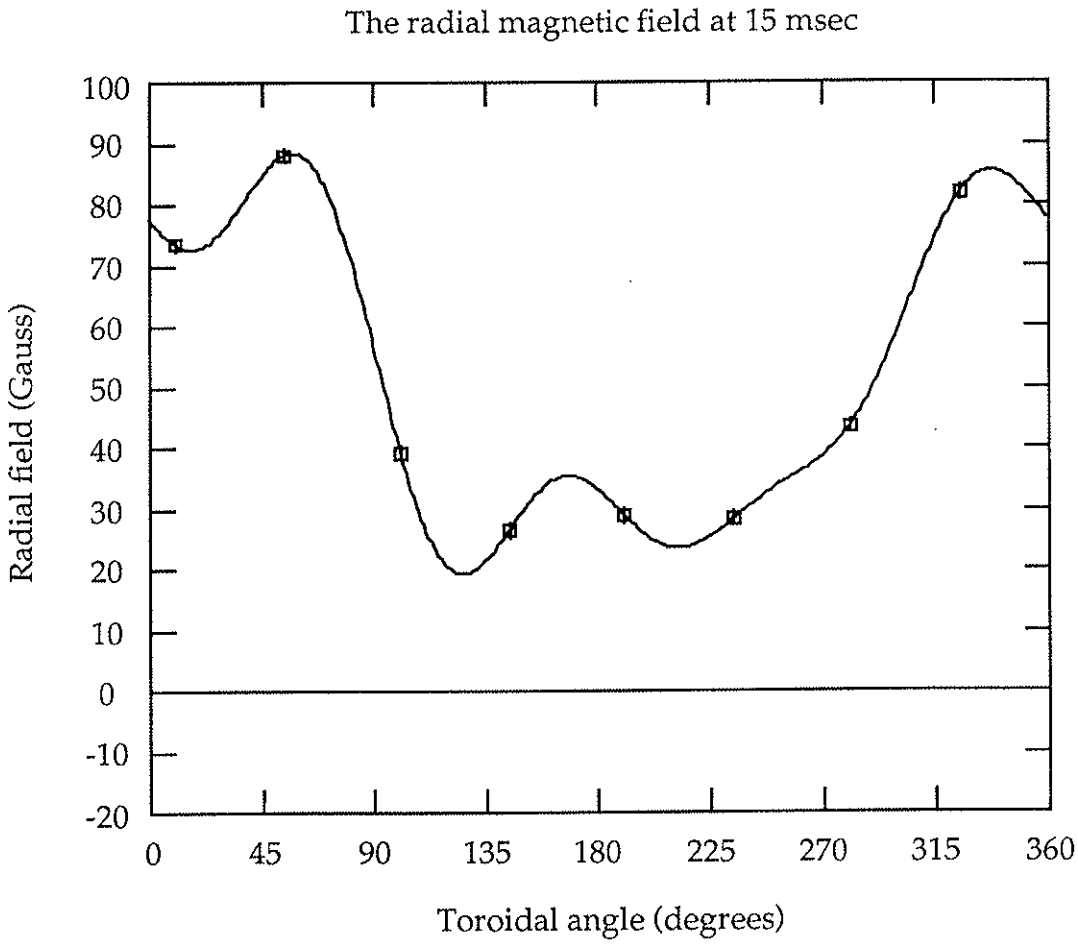

Figure 3.3 The toroidal structure of the radial field at the toroidal gap without any field error reduction.

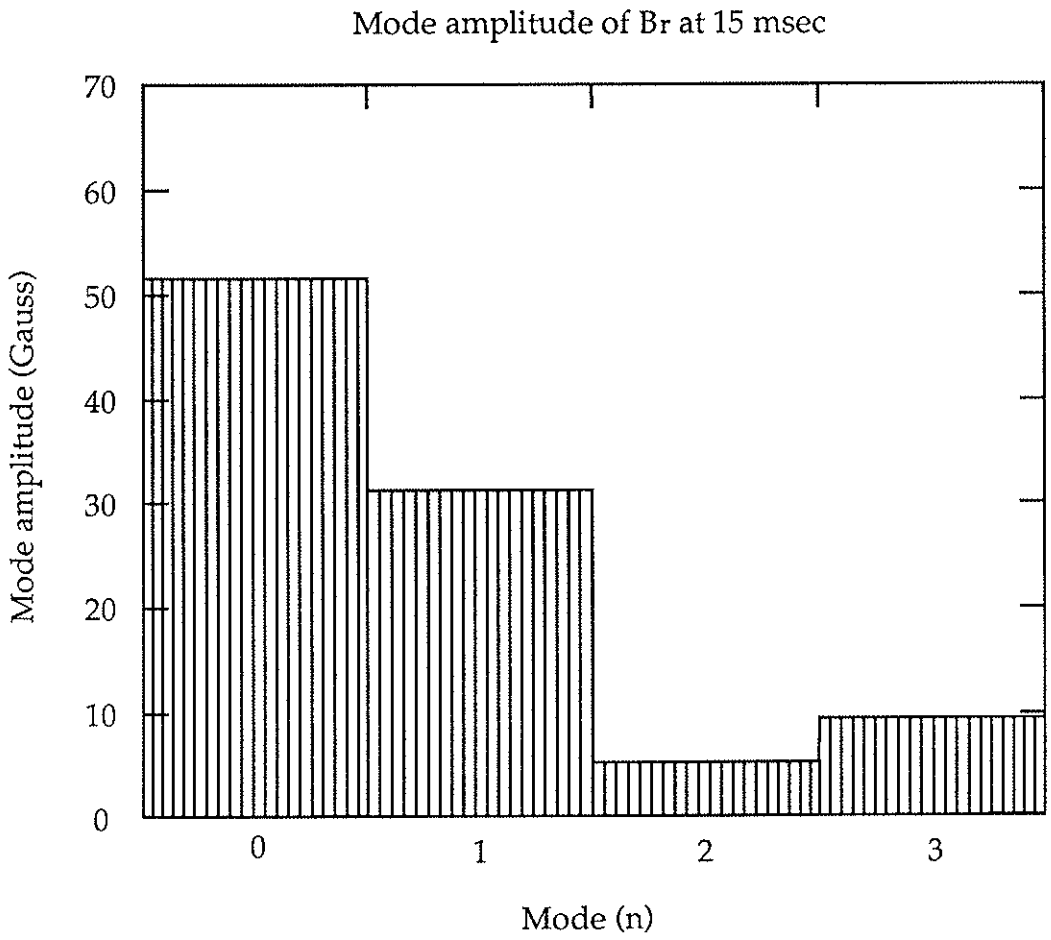

Figure 3.4 The mode amplitude of the radial field at the toroidal gap without any field error reduction.

dominant modes are n = 0 and 1. These n modes have a broad m spectrum associated with them, but all these are non-resonant modes.

3.1.2 Correction of field errors at the poloidal gap.

Since most of the errors have a similar time dependence as the plasma current, it was possible to use a passive correction scheme to reduce these errors at the poloidal gap. Saddle-like coils were placed at the poloidal gap and were driven by the primary current. These coils covered the poloidal locations where the radial field has a peak. Five coils were used to get sufficient poloidal coverage. Figure 3.1 shows the poloidal extent of these coils as a solid line. Due to space limitation, only one turn is used for each coil. As a result we only succeeded in reducing the rms value of the field error to about 17% from 23% of the poloidal field at the wall. Even with this modest reduction we have observed some improvements of the discharge quality. This correction resulted in a factor of two reduction in the radial field at most poloidal locations and some increases at other poloidal locations. Figure 3.5 shows the radial field before and after the correction. The mode amplitudes for the corrected case are shown in figure 3.6. All modes are smaller except the m = 1 component which can be seen in figure 3.5 where the radial field is larger in the poloidal region between 90 and 170 degrees.

One of the results of reducing the radial field at the poloidal gap is a reduction of the radial field at the toroidal gap. Figure 3.7 shows the spatial

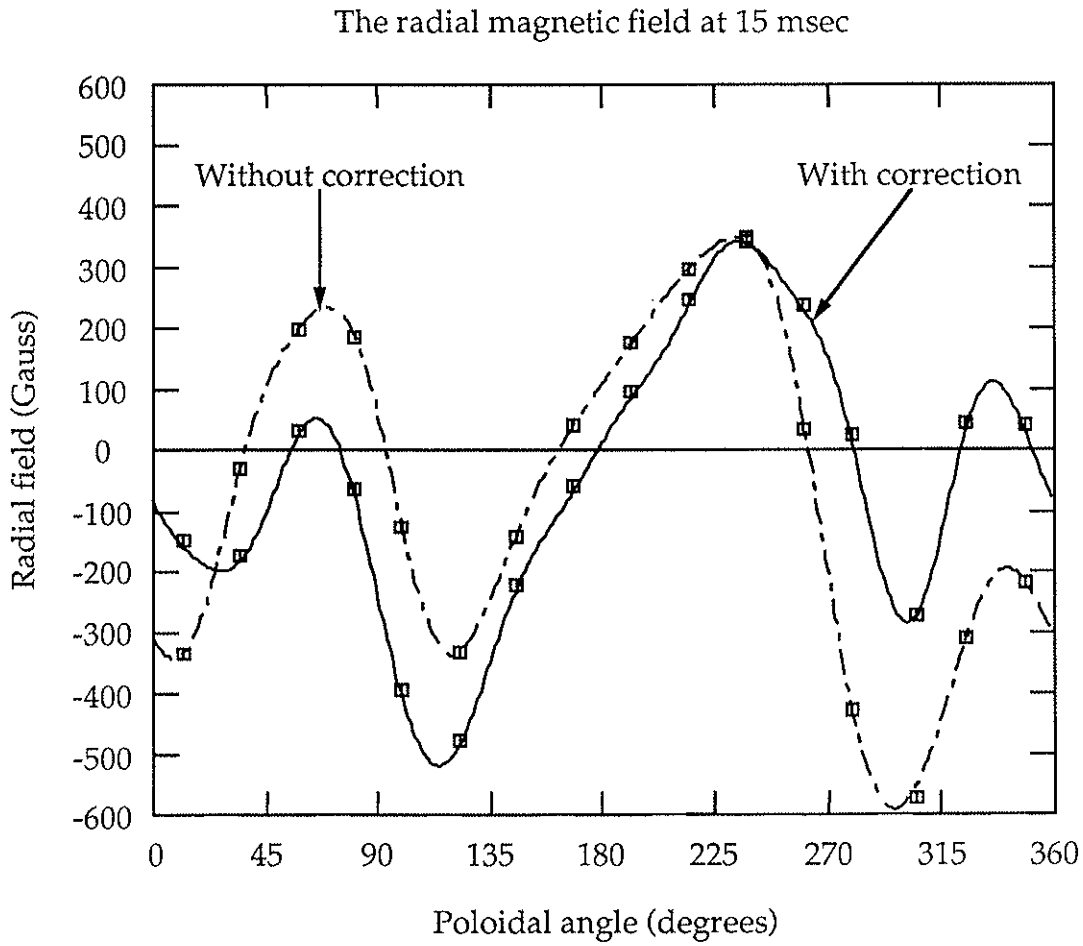

Figure 3.5 The poloidal structure of the radial field at the poloidal gap with (solid curve), and without (dashed curve), field error reduction.

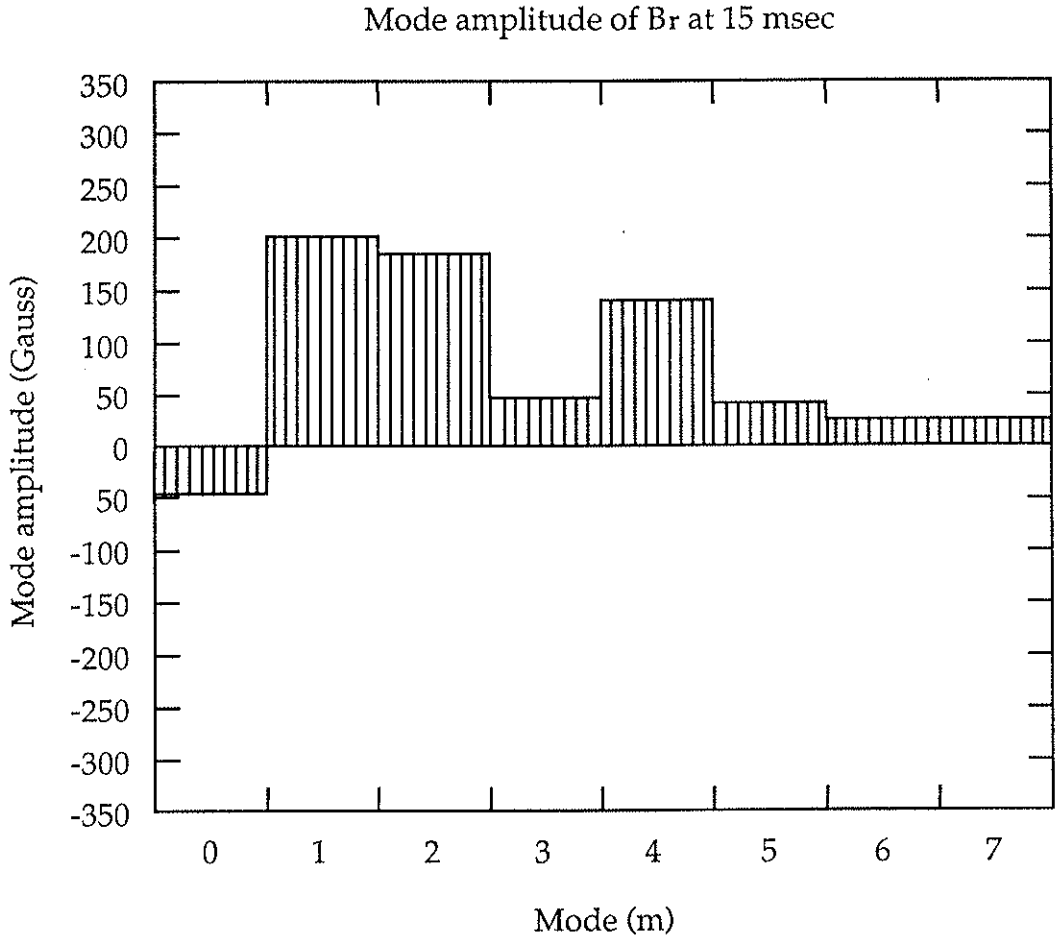

Figure 3.6 The mode amplitude of the radial field at the poloidal gap with field error reduction.

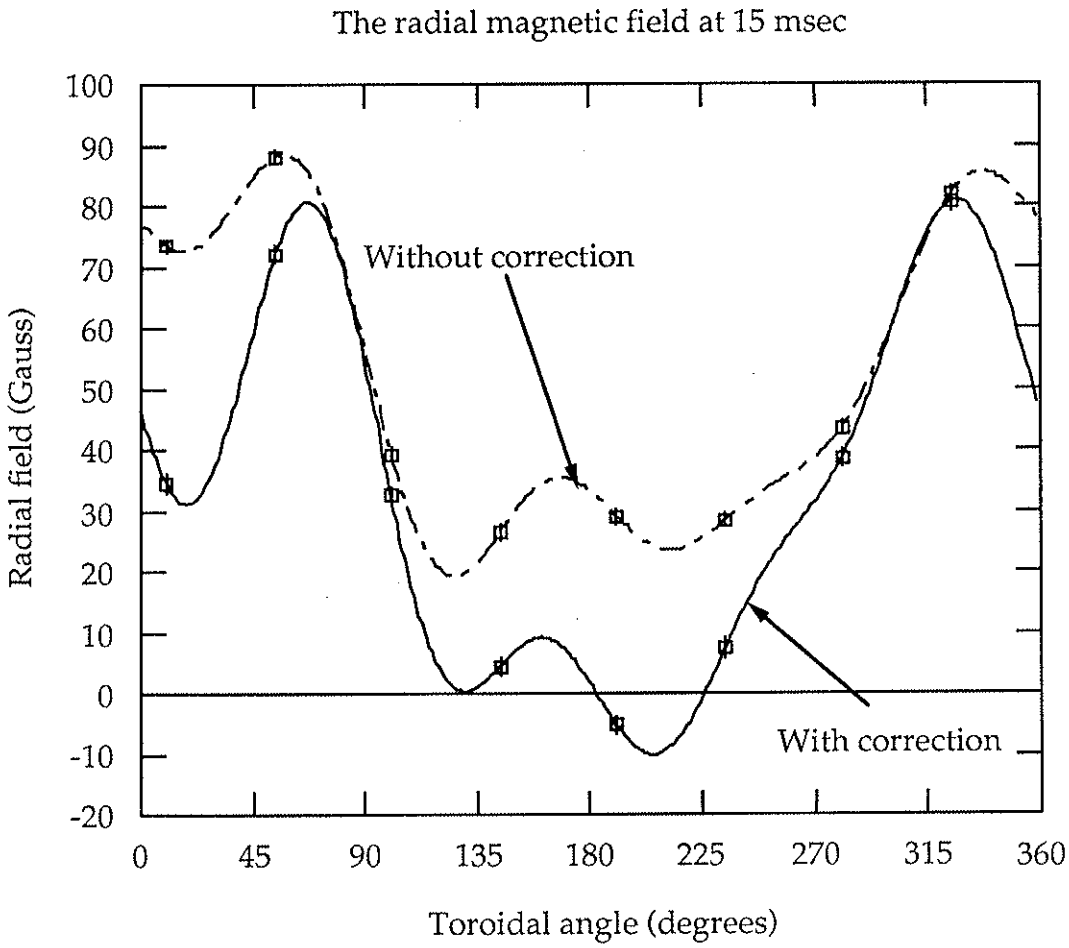

Figure 3.7 The toroidal structure of the radial field at the toroidal gap with (solid curve), and without (dashed curve), field error reduction.

structure of the radial field at the toroidal gap with and without the field error reduction at the poloidal gap. The mode spectrum of these fields shows that most of the changes are in the n = 0 component as is shown figure 3.8. This is the expected result since the two gaps are coupled only though the m = 0 and n = 0 components of the radial field at the poloidal and toroidal gap. That is, the net magnetic flux that exits one gap must all enter at the other gap.

These modest reductions in field errors have resulted in improvements in the plasma equilibrium parameters. These plasma improvements indicate an enhanced plasma confinement and reduced plasma-wall interaction. For this experiment, the bank voltage settings and the initial fill pressure are kept the same for cases of corrected and uncorrected gap field errors. Figure 3.9 shows the plasma current with and without correction. Plasma current and discharge duration increased with the reduction of radial magnetic field at the poloidal gap. Figure 3.10 shows the resistive plasma loop voltage for the same two cases. The loop voltage decreased by about 10 Volts from 32 down to 22 Volts, and the plasma resistivity is reduced by about 36% when the radial field is reduced. The RFP state lasts about 16% longer when the error fields are reduced. This can be seen in figure 3.11 which shows the increase in the reversal duration. The central plasma temperature, as measured by the Thomson scattering diagnostic, increased with reduced field errors. The central plasma density measured by the same diagnostic decreased. Unfortunately the microwave interferometer was not operational for most of these

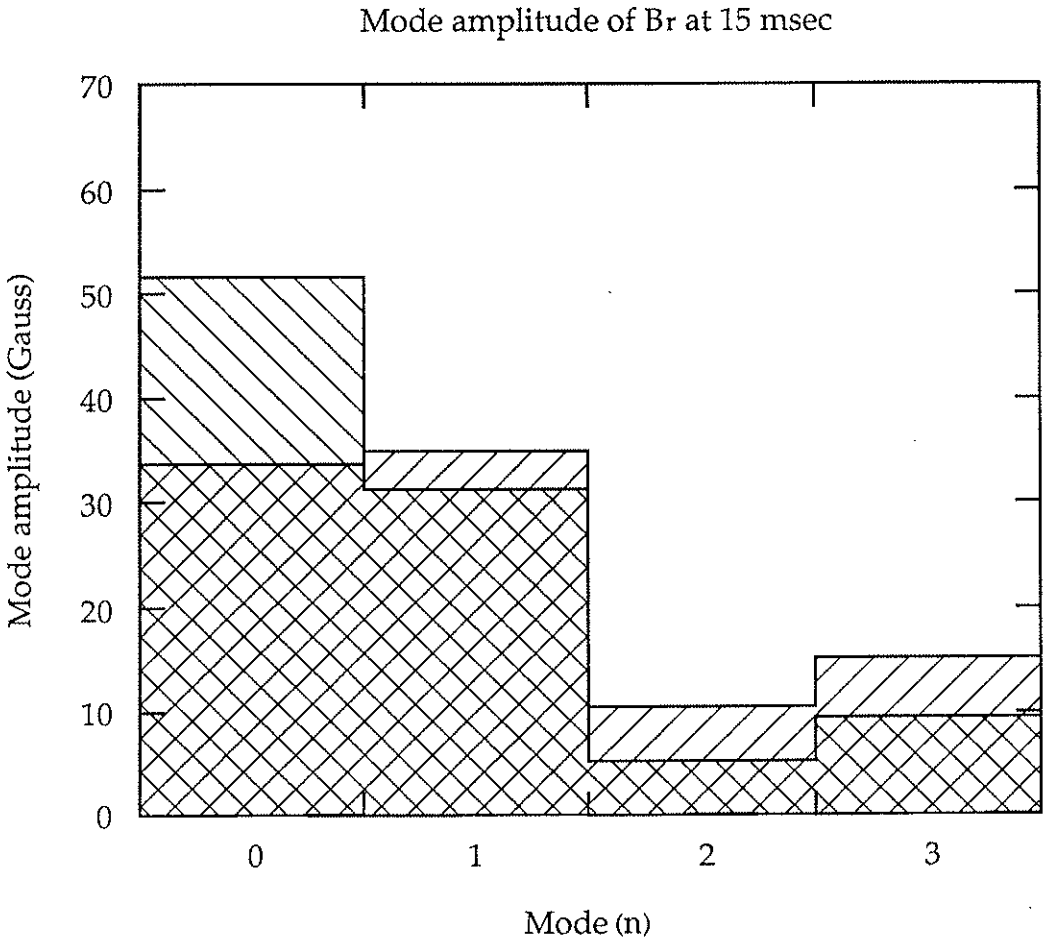

Figure 3.8 The mode amplitude of the radial field at the toroidal gap with (45 degrees lines), and without (135 degrees lines), field error reduction.

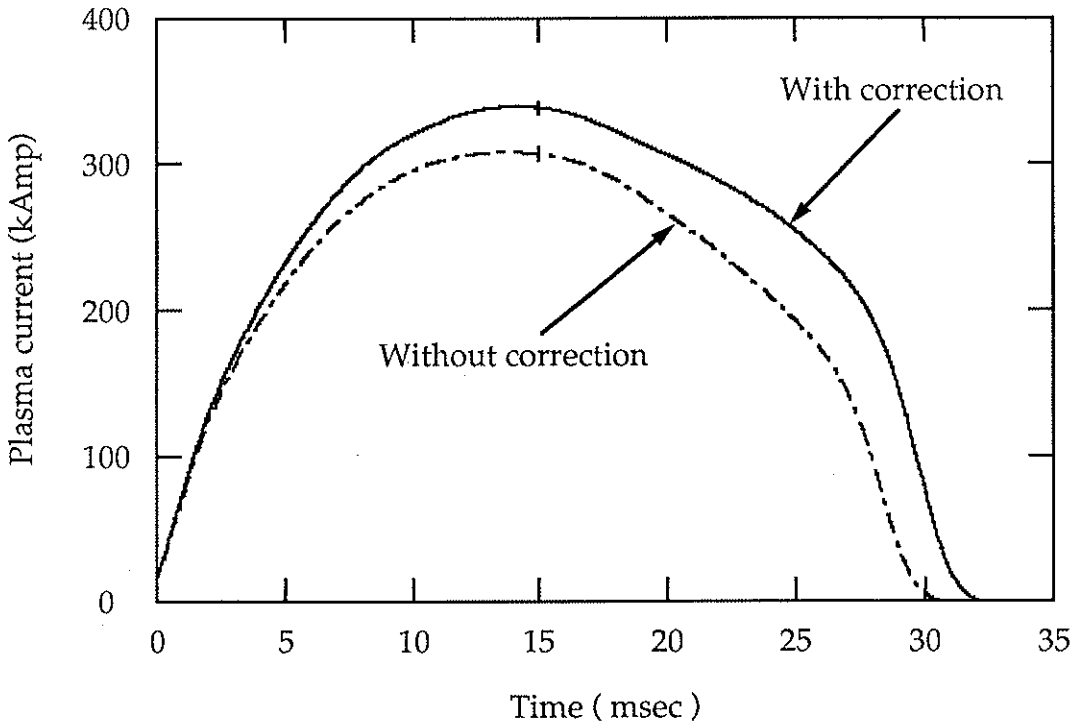

Figure 3.9 The plasma current with (solid curve) and without (dashed) any field error correction.

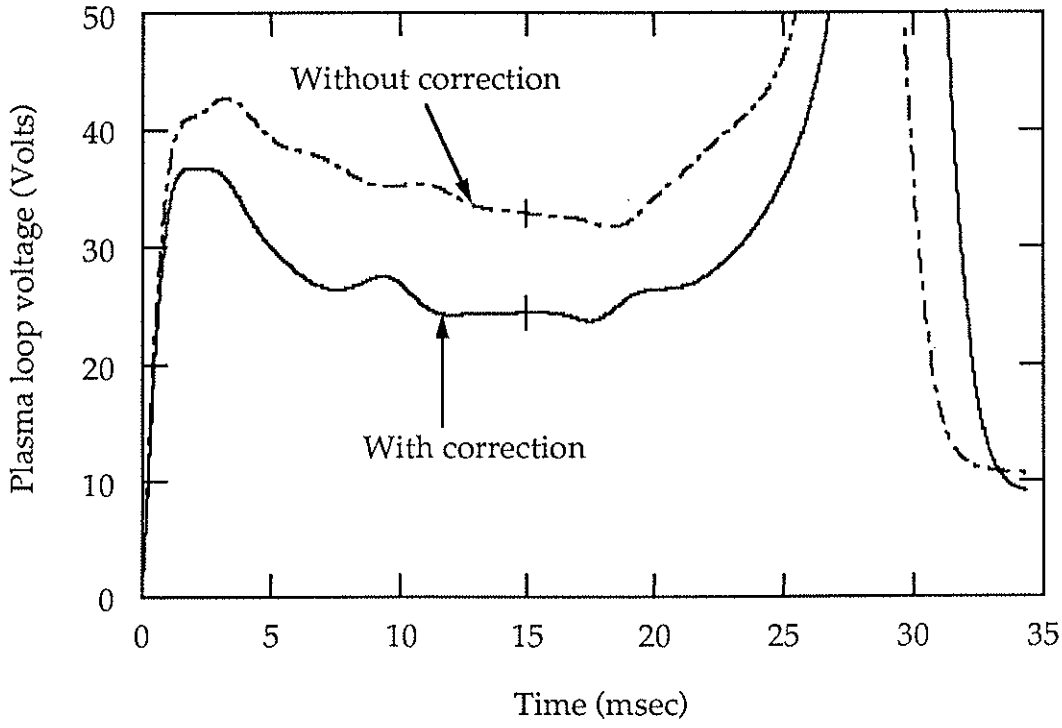

Figure 3.10 The plasma resistive loop voltage with (solid curve) and without (dashed curve) any field error reduction.

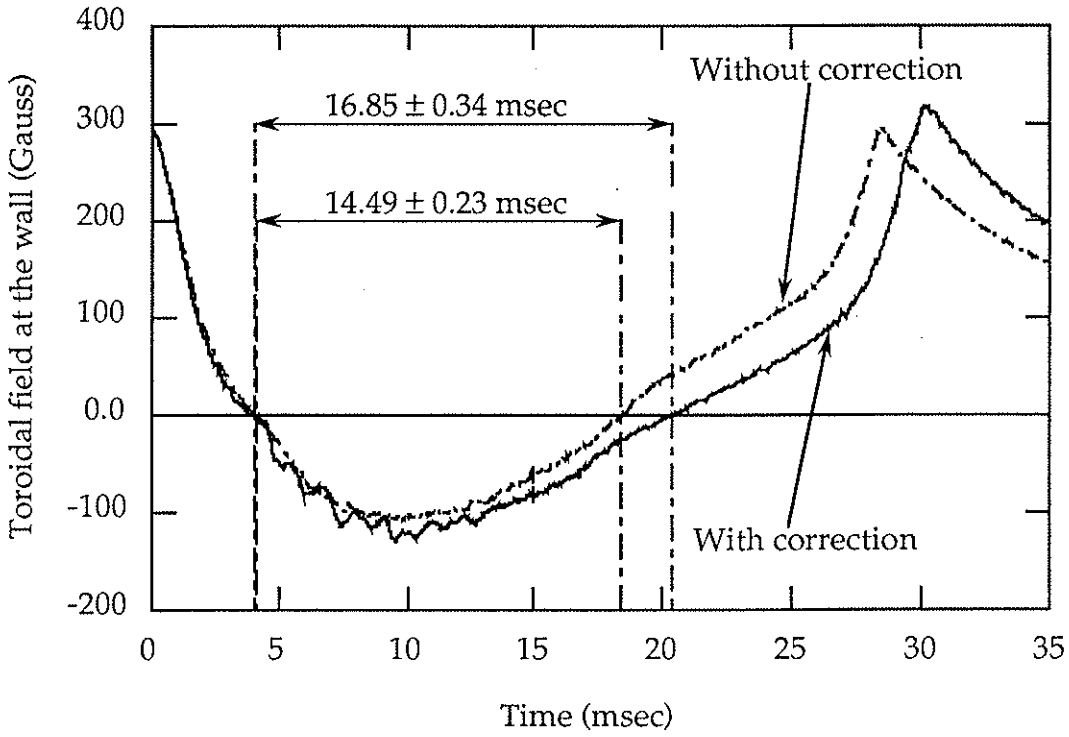

Figure 3.11 The toroidal field at the wall with (solid curve) and without (dashed curve) any field error reduction.

experiments. It is not clear whether the decrease in the central density is due to profile changes or due to an overall reduction of plasma density. The reduction of the plasma loop voltage indicates that there may be some improvements in the energy confinement time with reduced field errors. The soft x-ray signal is about a factor of ten larger when field errors are reduced. The 2-D soft x-ray array is used to do a Fourier-Bessel reconstruction of the emissivity profiles. With error reduction these profiles are very flat, and without error reduction the profiles are narrow as can be seen in figure 3.12. The field error reduction has a strong effect on the behavior of the sawtooth activity or "flux jumps" as seen on the toroidal field at the wall. The change in the toroidal field at the wall due to flux jumps is about a factor of two larger in the corrected case then in the uncorrected case. The time between succeeding flux jumps becomes longer with reduced field errors. Figure 3.13 shows this behavior of the sawtooth with the changes in the field errors. This may suggest how the field errors influence or interact with the plasma dynamics that is responsible for generating these flux jumps. This dynamics is thought to be the nonlinear coupling of plasma modes.

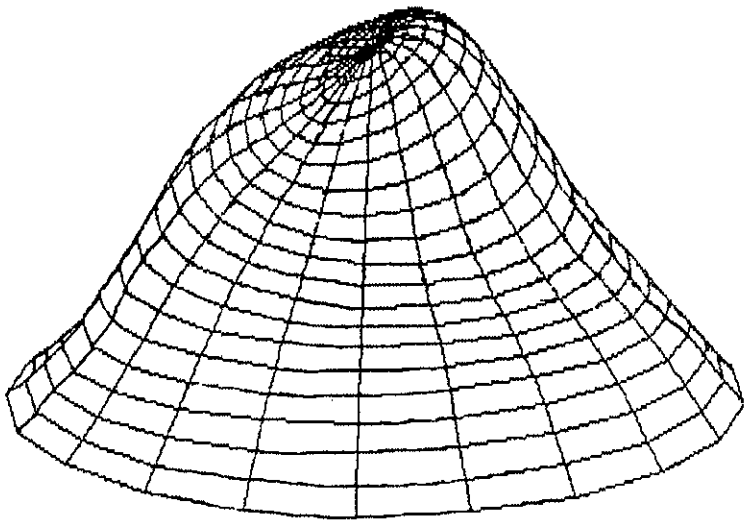

With correction vertical scale = 10.0

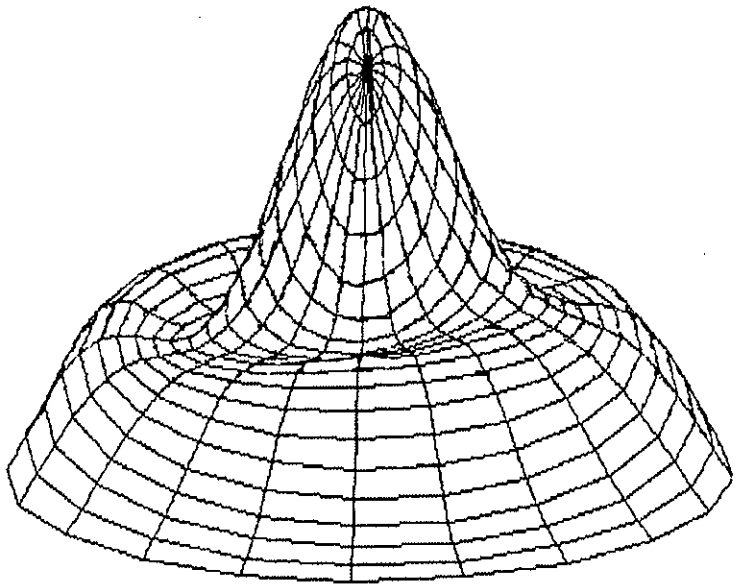

Without correction vertical scale = 1.00

Figure 3.12 The soft x-ray emission profile with (top) and without (bottom) any field error reduction.

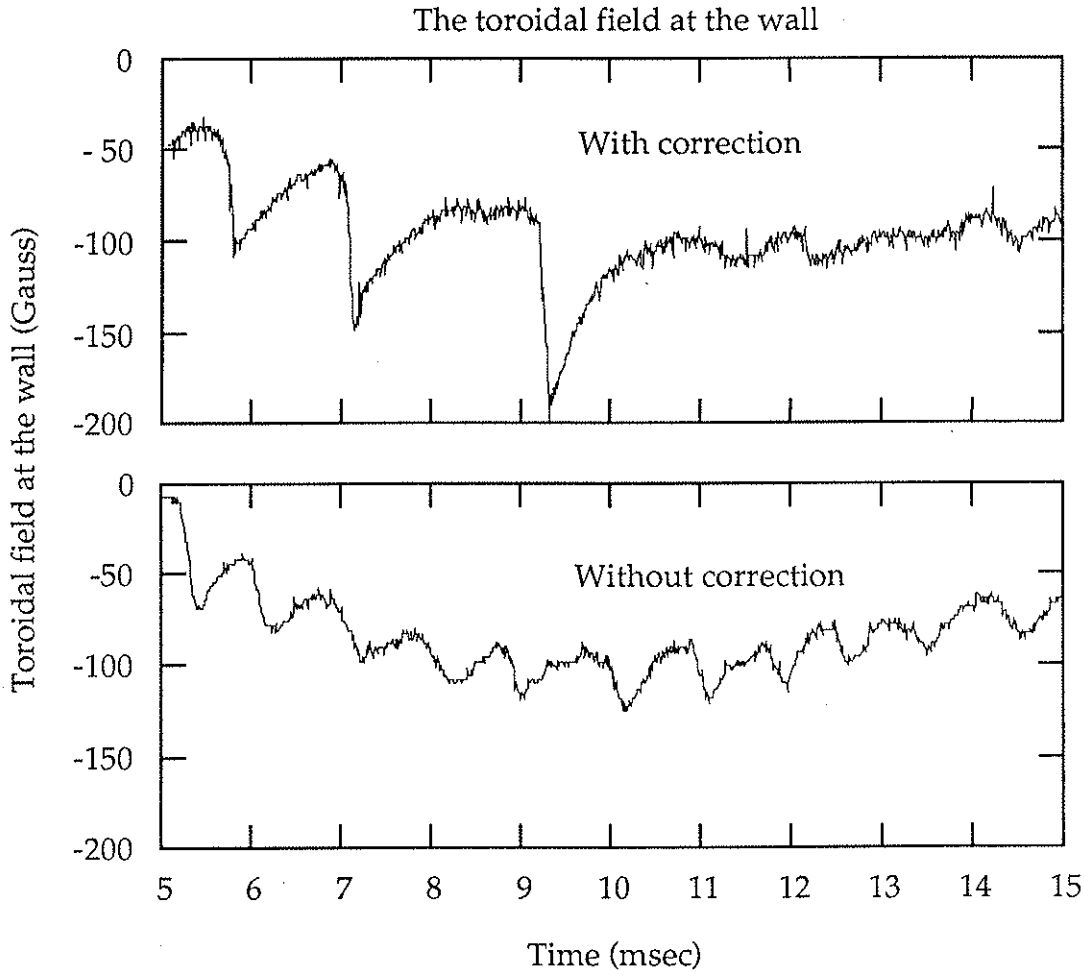

Figure 3.13 The character of the sawtooth-like oscillations (flux jumps) as seen in the toroidal field at the wall with (top) and without (bottom) any field error reduction.

3.1.3 Correlation of plasma improvements with the m=0 component of the field errors.

The observed plasma improvements seem to correlate with the amplitude of the m = 0 component of the radial field at the poloidal gap. Any toroidally localized m = 0 perturbation, such as the m = 0 component of the radial field at the poloidal gap, is very dangerous because such a perturbation has a broad n spectrum and would produce a chain of m = 0 magnetic islands. These islands may overlap and cause the outer region of the magnetic flux surfaces that might be responsible for RFP confinement to be stochastic.

The measured central plasma temperature seems to increase with lower amplitude C_0 of the m = 0 component of the error field as shown in figure 3.14. These changes in the temperature may be a direct result of reduced field errors by reducing transport due to magnetic islands and stochastic field lines or may be an indirect result due to reduced plasma-wall interaction. Reducing field errors will reduce plasma-wall interaction which will affect the plasma density through wall recycling. Without information on the plasma density, figure 3.14 cannot be interpreted as direct cause and effect.

Figure 3.15 shows the correlation between the changes in the plasma resistive loop voltage and the changes in the amplitude of the m = 0 component. This decrease of loop voltage may be an indication of improved plasma confinement with reduced m = 0 perturbation.

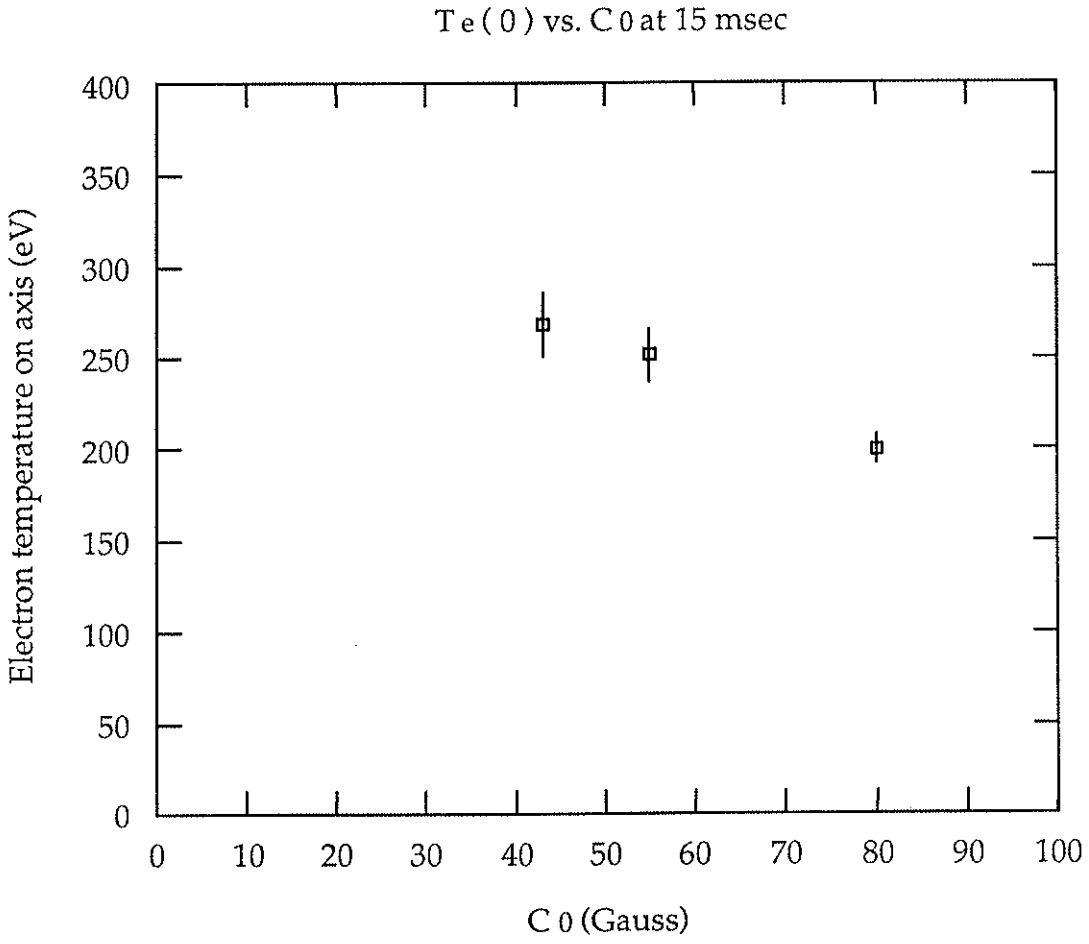

Figure 3.14 The central electron temperature variation with the amplitude of the m = 0 component of the radial field at the poloidal gap.

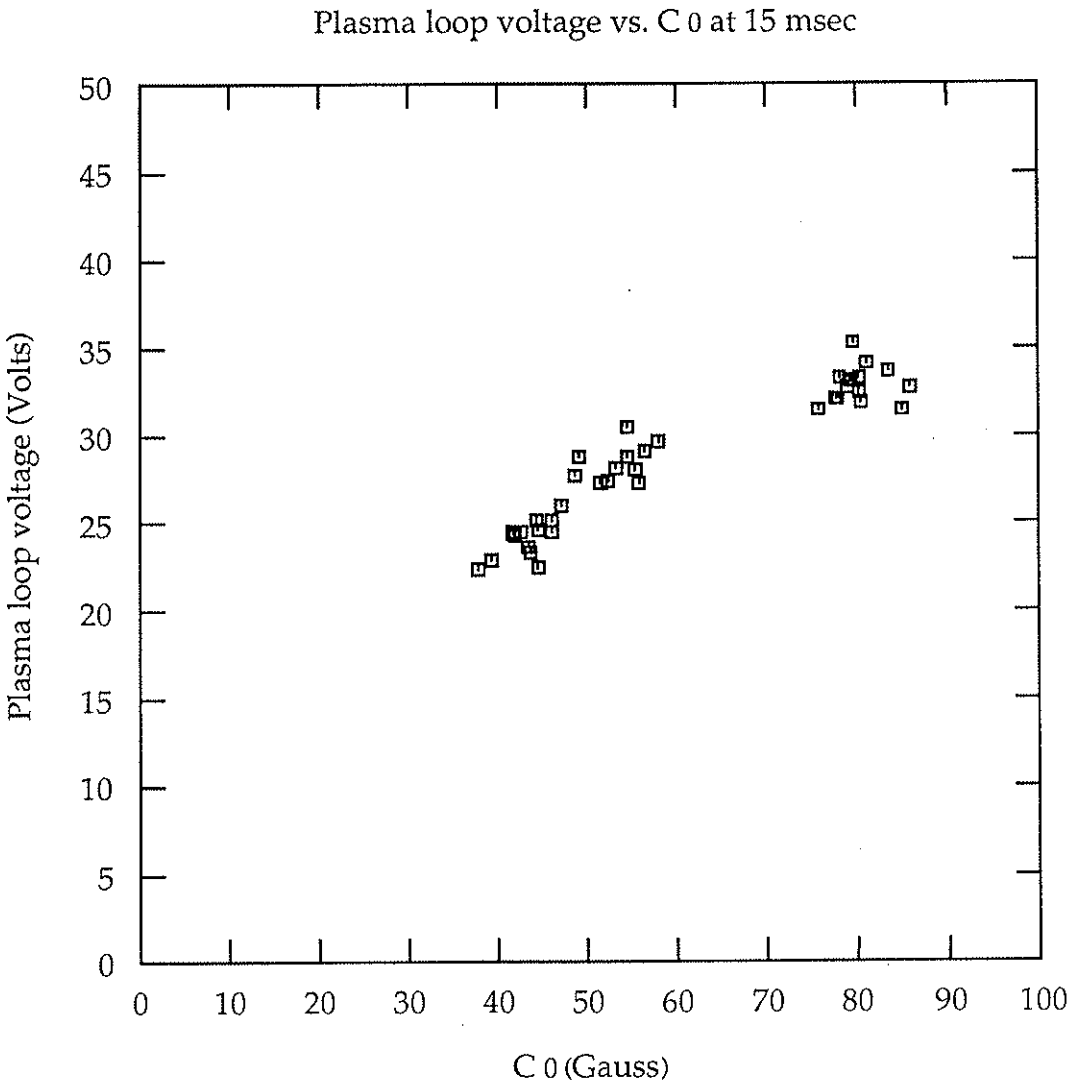

Figure 3.15 The resistive loop voltage variation with the amplitude of the m = 0 component of the radial field at the poloidal gap.

Plasma resistance also decreases with reduced m = 0 perturbation as shown in figure 3.16. The duration of reversal also correlates with the m = 0 error field as shown in figure 3.17.

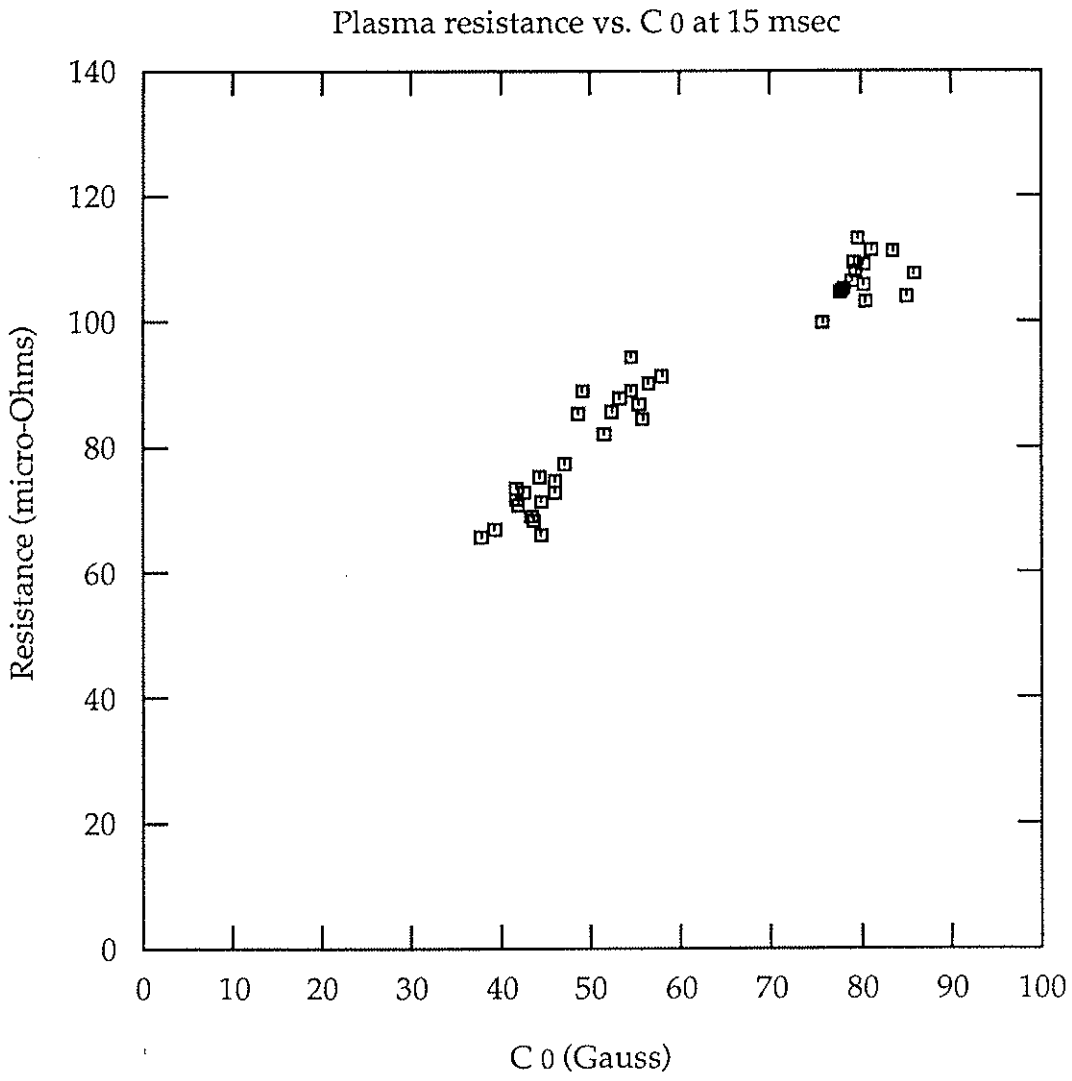

Figure 3.16 The plasma resistance variation with the amplitude of the m = 0 component of the radial field at the poloidal gap.

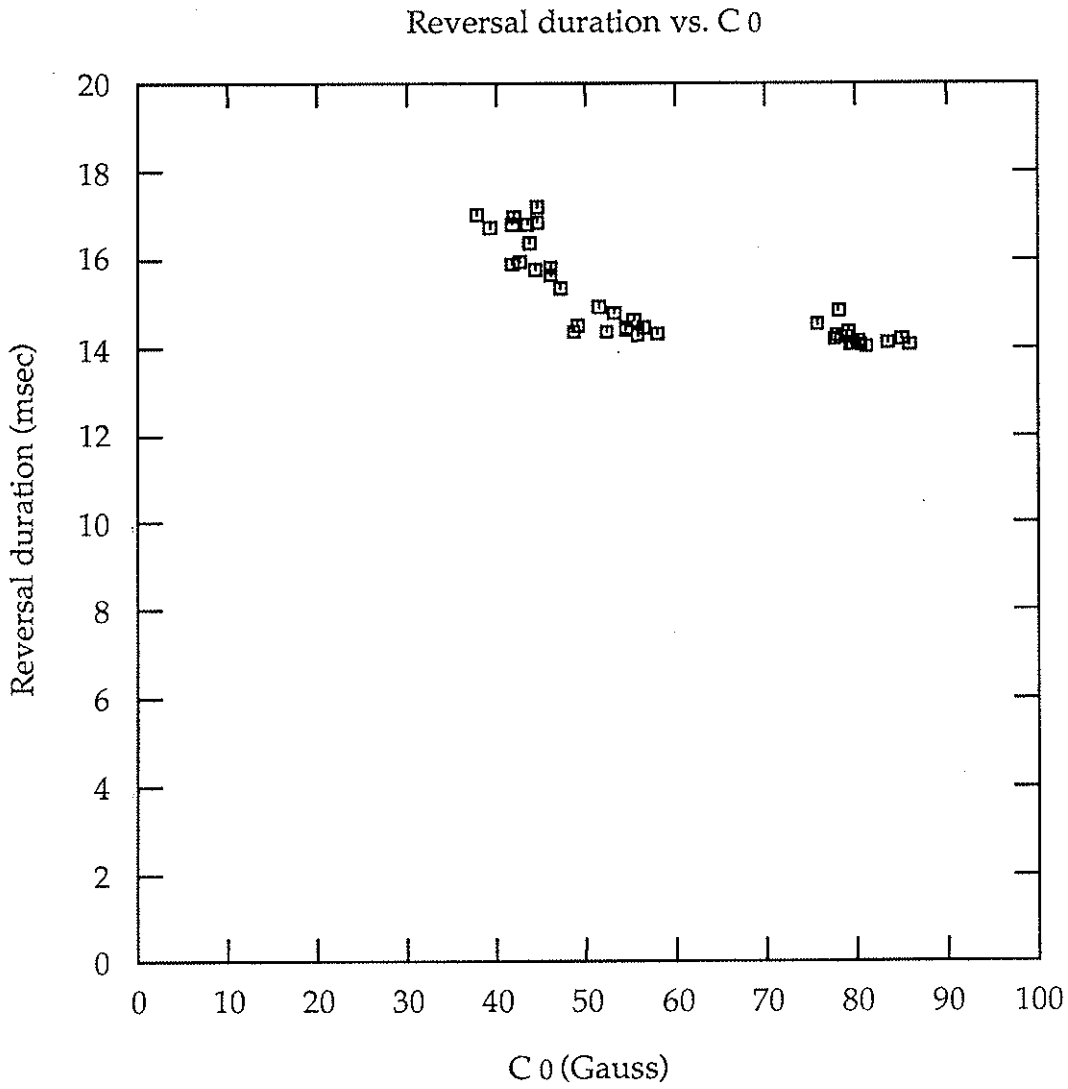

Figure 3.17 The plasma reversal duration variation with the amplitude of m = 0 component of the radial field at the poloidal gap.

3.1.4 Variation of field errors with plasma profiles.

Radial magnetic fields at the gap are produced by the mismatch between the plasma current profiles and the primary winding distribution. There will be a plasma profile which will deviate the least from the primary distribution. For such a current profile, the radial field will be minimum. The shell surface current and the primary winding may have different poloidal structure. When the two distributions have a mismatched m = 1 component, then this difference will result in a radial field with an m = 1 component. Similar results hold for the other m components. Such errors can be minimized by adjusting the current profiles. However, there may be some m component in the Ohmic winding that is not part of the plasma equilibrium or vice versa. Such errors cannot be reduced by changing plasma profiles.

An F-scan experiment was performed to verify these intuitive ideas. Different plasma profiles would correspond to different values of F. It was found that only the low-m component of the radial field has some dependence on F and the high-m component does not vary with F. Figure 3.18 shows the dependence of the m = 0 component of the radial field at the gap. The m = 0 component is small at shallow reversal. Figure 3.19 shows that the m = 1 component has a minimum at shallow reversal (F ~ -0.05). Similarly, the m = 2 component is minimum at F ~ -0.05, as shown in figure 3.20. The high-m components did not exhibit any dependence on F. Figure 3.21 shows the m = 4 component weak

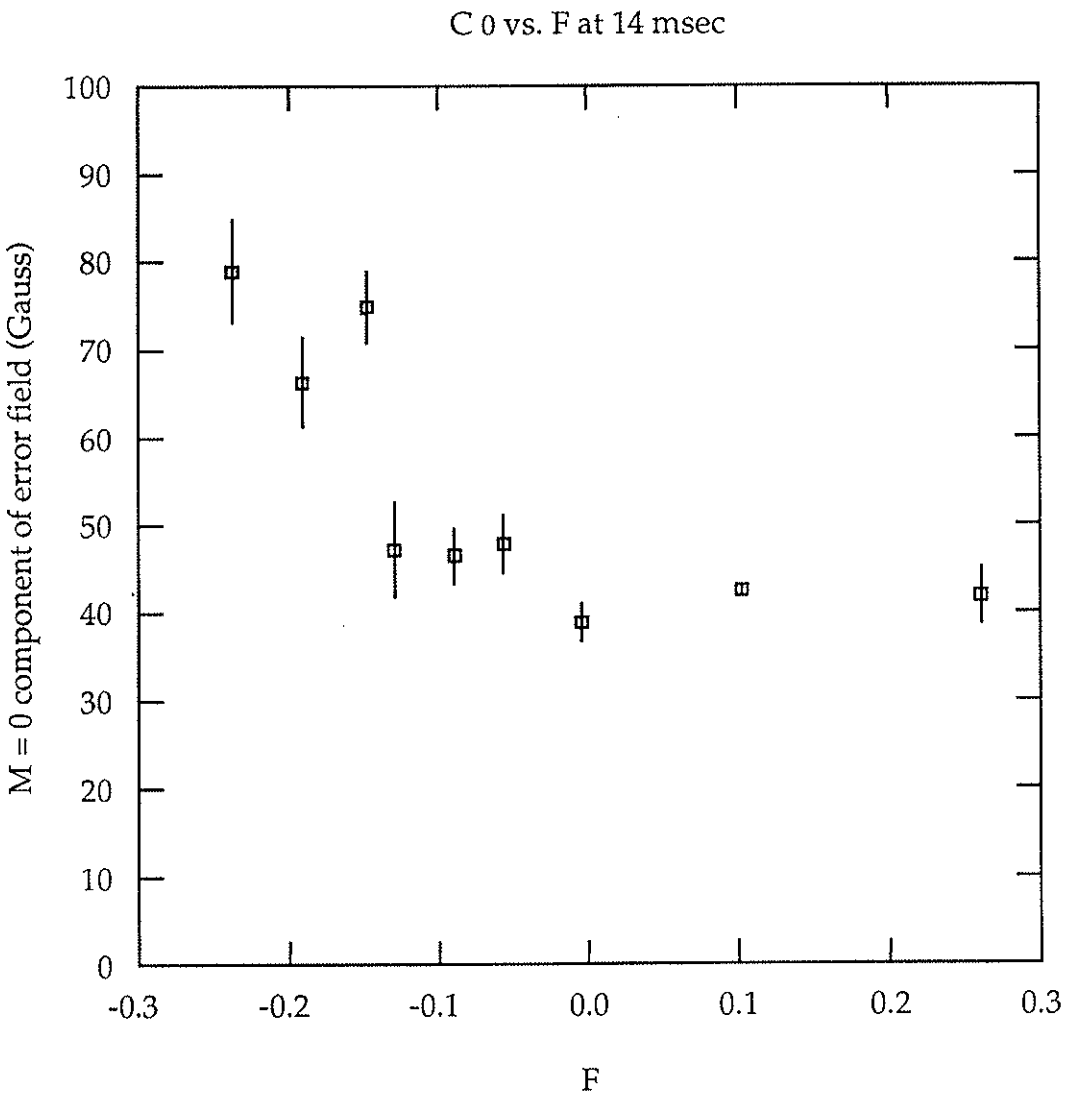

Figure 3.18 The variation of the amplitude of m = 0 component of the radial field with the field reversal parameter F.

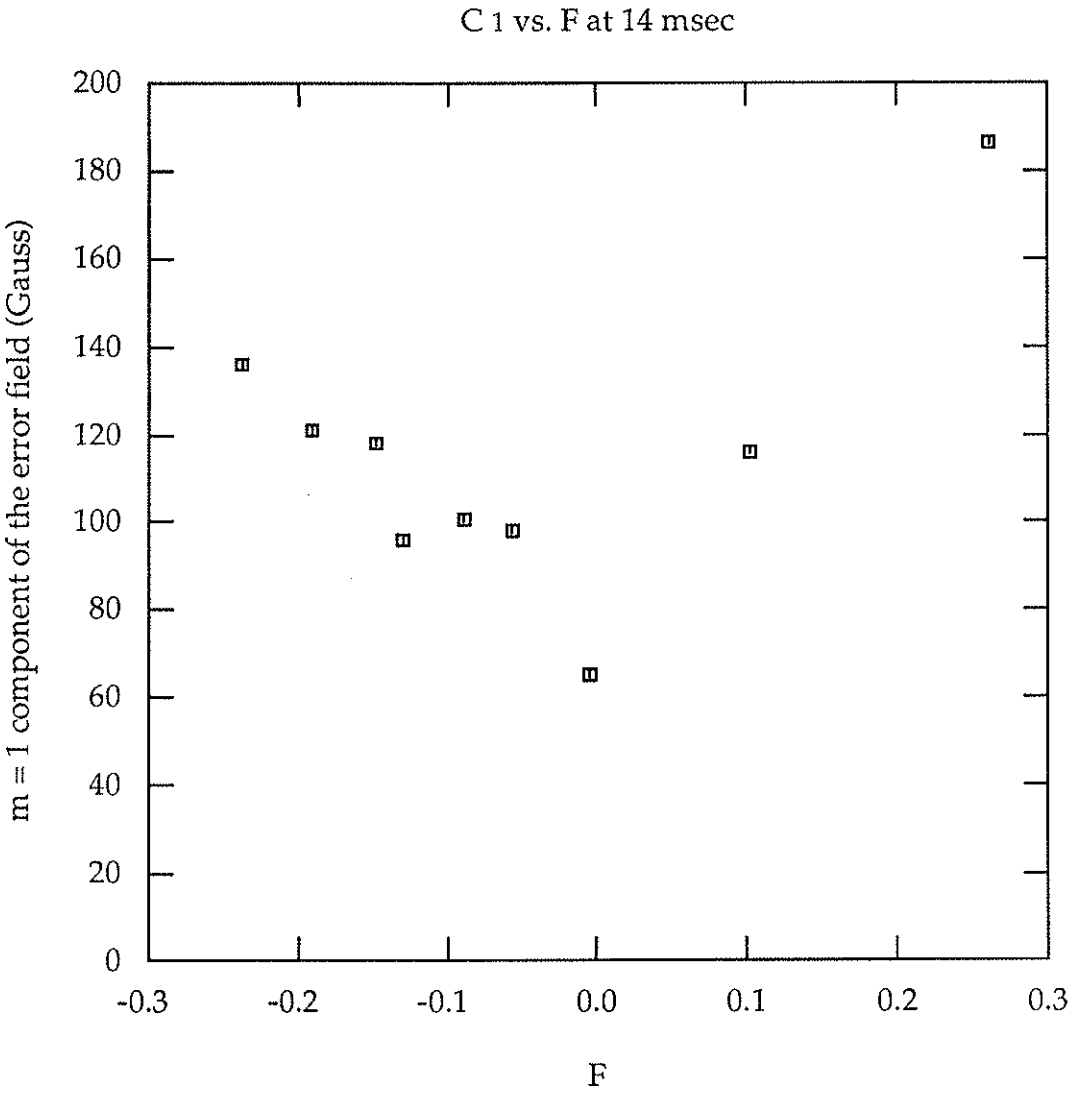

Figure 3.19 The variation of the amplitude of the m = 1 of the radial field with the field reversal parameter F.

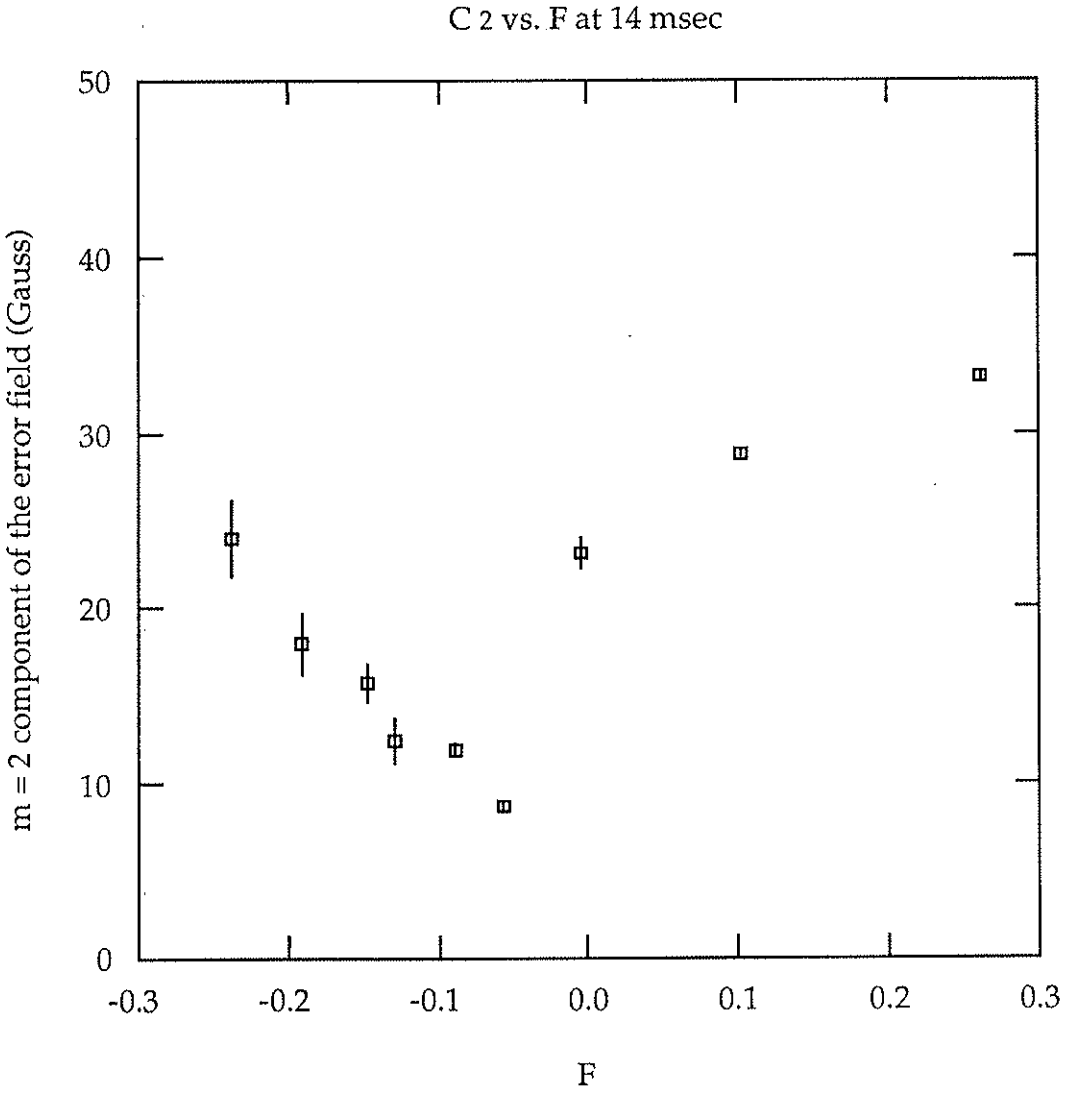

Figure 3.20 The variation of the amplitude of the m = 2 component of the radial field with the field reversal parameter F.

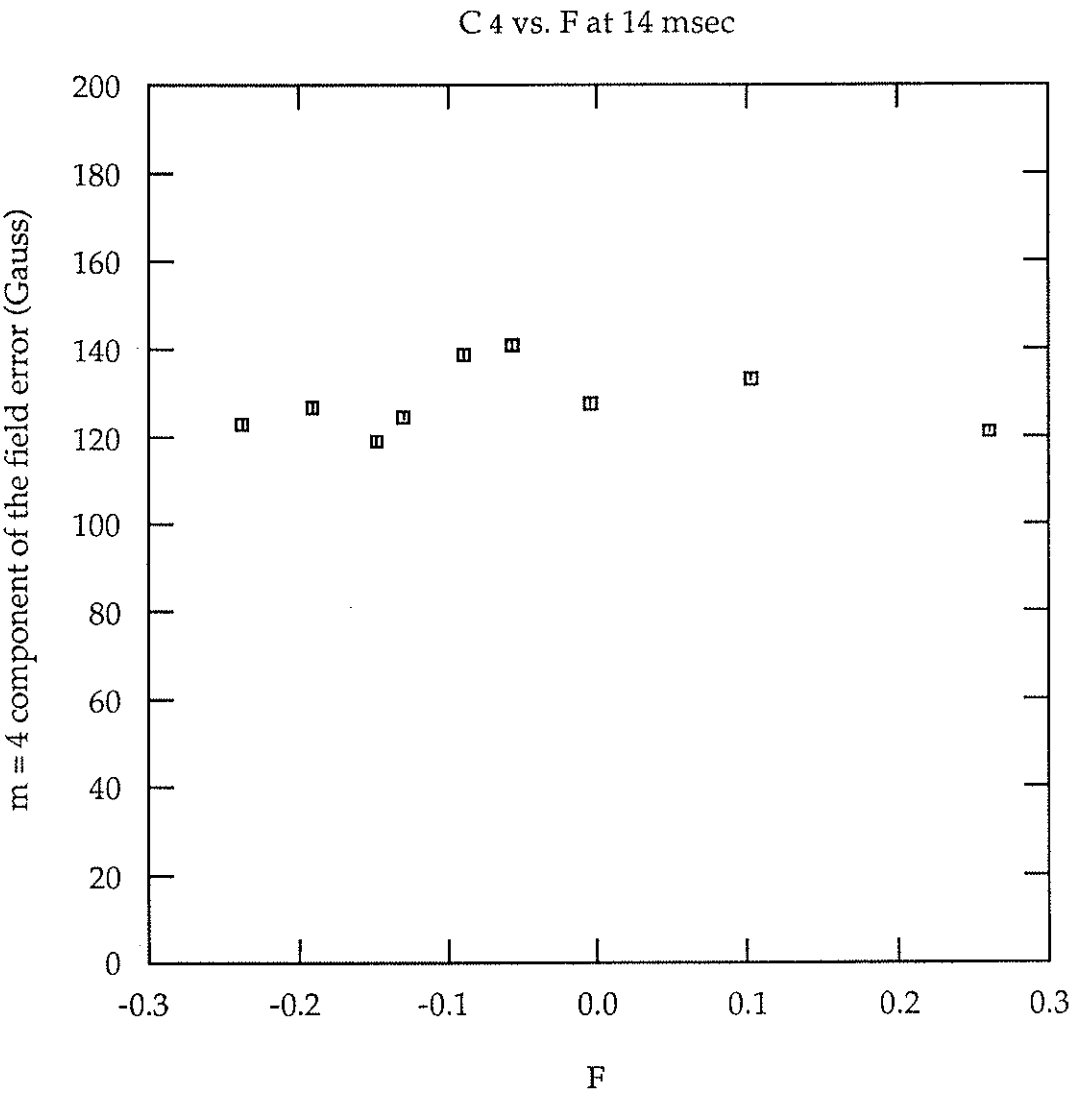

Figure 3.21 The variation of the amplitude of the m = 4 component of the radial field with the field reversal parameter F.

dependence on F. This indicates that the plasma equilibrium does not have these high-m components. The bias winding has a large m = 4 component which is absent in the shell currents as is indicated by the lack of dependence of the m = 4 radial field on F.

3.2 OPERATION WITH THE PF WINDING

After one year of operating MST with the bias winding, the permanent ohmic heating winding, which was designed to match the surface currents in the wall, was installed. With this upgrade of the primary winding system MST has produced much improved plasmas. Field errors are smaller by a factor of about six in rms values down to about 5% of the poloidal field at the wall. With this reduction of field errors, the plasma duration has doubled, loop voltage is smaller by a factor of two down to 12 - 15 Volts from 32 Volts. With these small field errors the plasma exhibited coherent modes in the frequency range from 10 to 40 kHz. These modes were absent in the uncorrected bias plasma. These coherent modes are usually phase locked to one another, forming a localized structure that rotates toroidally. In some discharges we observed an instability that causes the discharge to terminate much earlier than normal discharges. This instability is related to field errors. In these short discharges we observed a sudden increase in the amplitude of the m = 1 component of the radial field at the poloidal gap. At about the same time the rotating structure disappears from the magnetic measurements. It was

observed that the amplitudes of the n = 5 and 7 components of the stationary spectrum increase. The MST plasma equilibrium will be described and some estimates of the value of q on axis will be made in section 3.2.1. The poloidal structure of the field error with the PF winding will be described in section 3.2.2. Comparison of the two cases of large field error (bias) and small field error (PF) plasmas will be made in section 3.2.3. Finally the subject of mode locking in the lab frame and the field error instability will be taken up in section 3.2.4

3.2.1 Equilibrium properties of MST plasma

The poloidal asymmetry of the poloidal magnetic field at the wall is an important equilibrium property for field errors, as will be shown in the next section. We used the magnetic fluctuation measurements to give an estimate of the value of q (safety factor) on axis, where the onset of a particular mode with θ gives an estimate for q(0) versus θ.

For small aspect ratio, the poloidal magnetic field has the following form, to first order in a/R_o,

$$B_\theta(a,\theta) = B_o \left(1 + a\Lambda/R_o \cos(\theta) \right)$$

where a and R_o are the minor and major radius of the plasma respectively. Here, Λ is a constant which measures the poloidal asymmetry of the poloidal magnetic field at the wall. It can be shown[1] that

$$\Lambda = \beta_\theta + l_i/2 - 1$$

where β_θ is the average poloidal beta and l_i is the plasma internal inductance.

From the Fourier decomposition of the poloidal magnetic field Λ is written as

$$\Lambda = a_1 R_o / B_o a \qquad \text{where} \qquad B_o = \mu_o I_p / 2\pi a$$

where a_1 is the $\cos\theta$ coefficient in the Fourier decomposition of the poloidal field and B_o is the $m = 0$ component as given above.

The value of Λ (lambda) was calculated for different values of the pinch parameter. Figure 3.22 shows the measured Λ profile by the squares. The solid curve is the Λ profile for the BFM model with zero poloidal beta. The dashed curve is the Λ profile for the PFM model. The dashed line is the asymmetry factor which was assumed for the design of the PF winding distribution. This indicates that MST should be run at about $\theta = 1.7$ or $F = -0.15$ so that the Λ of the plasma and the Λ of the PF winding are matched. This will minimize the $m = 1$ component of the field error at the poloidal gap.

Figure 3.23 shows the F-Θ diagram for MST. The square points represent the experimental F-Θ diagram. The solid curve shows the F-Θ diagram for the BFM model and the dashed curve shows the F-Θ diagram for the PFM model. The experimental points lie to the right of both models due to beta effects.

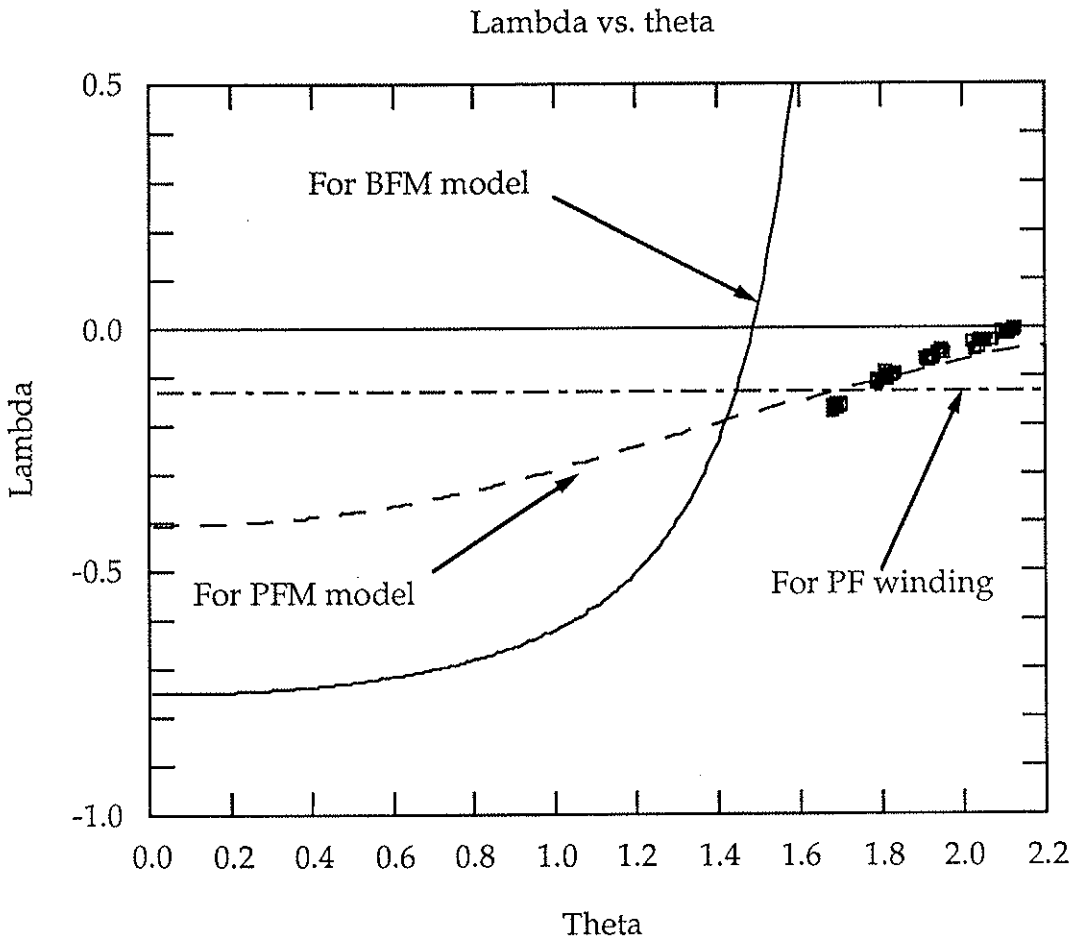

Figure 3.22 The asymmetry factor profile for the BFM model and the PFM model; the squares are the measured lambda from the poloidal field profile, and the dashed line is the assumed lambda of the PF winding current distribution.

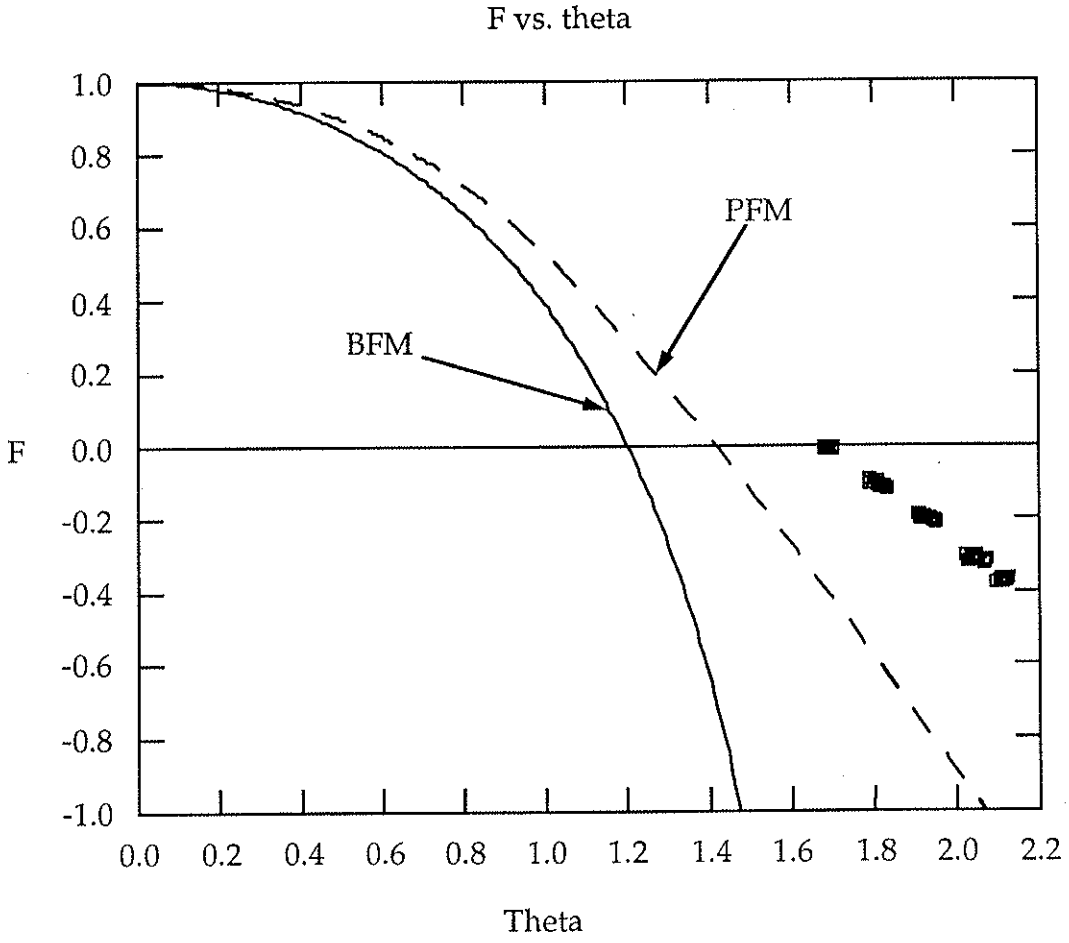

Figure 3.23 The F-θ diagram for the MST plasma shown as squares, the solid curve is for the BFM model, and the dashed curve is for the PFM model.

The toroidal mode amplitudes of the plasma magnetic fluctuations were measured at the same θ values as above. The onset of particular modes with θ may give evidence for q(0). The dominant toroidal modes are always n = 5 - 8, with mostly m = 1. The amplitude of n = 5 was found to be the most sensitive to θ. As θ increases, or F becomes more negative, the amplitude of n = 5 decreases. This may be an indication that q on axis decreased to below 0.2 so that the (1 , 5) mode becomes non-resonant. The higher n modes decrease slightly or do not change as θ is increased. Figure 3.24 shows the amplitudes of n = 5, 6, 7, 8 versus θ.

The value of q on axis is calculated for both models, BFM and PFM, at the same experimental values of θ. These are given by

$$q(0) = a \,/\, R_0\,\theta \qquad \text{for the BFM}$$

$$q(0) = a\,((3 - 2F)\,/(6 - 6F))^{1/2}/R_0 \qquad \text{for the PFM}$$

where F and θ are the measured values, a and R_0 are as defined earlier.

Figure 3.25 shows the calculated values of q(0) as the square points and the dashed lines are for the following values of q = m/n = 1/5, 1/6, 1/7, 1/8. This plot shows that the BFM model is a better fit of the plasma profiles than the PFM, at least in the interior. That is, the decrease in the 1/5 mode with θ better corresponds to the BFM. The plasma profiles are flatter than the PFM profiles and slightly more peaked than the BFM model.

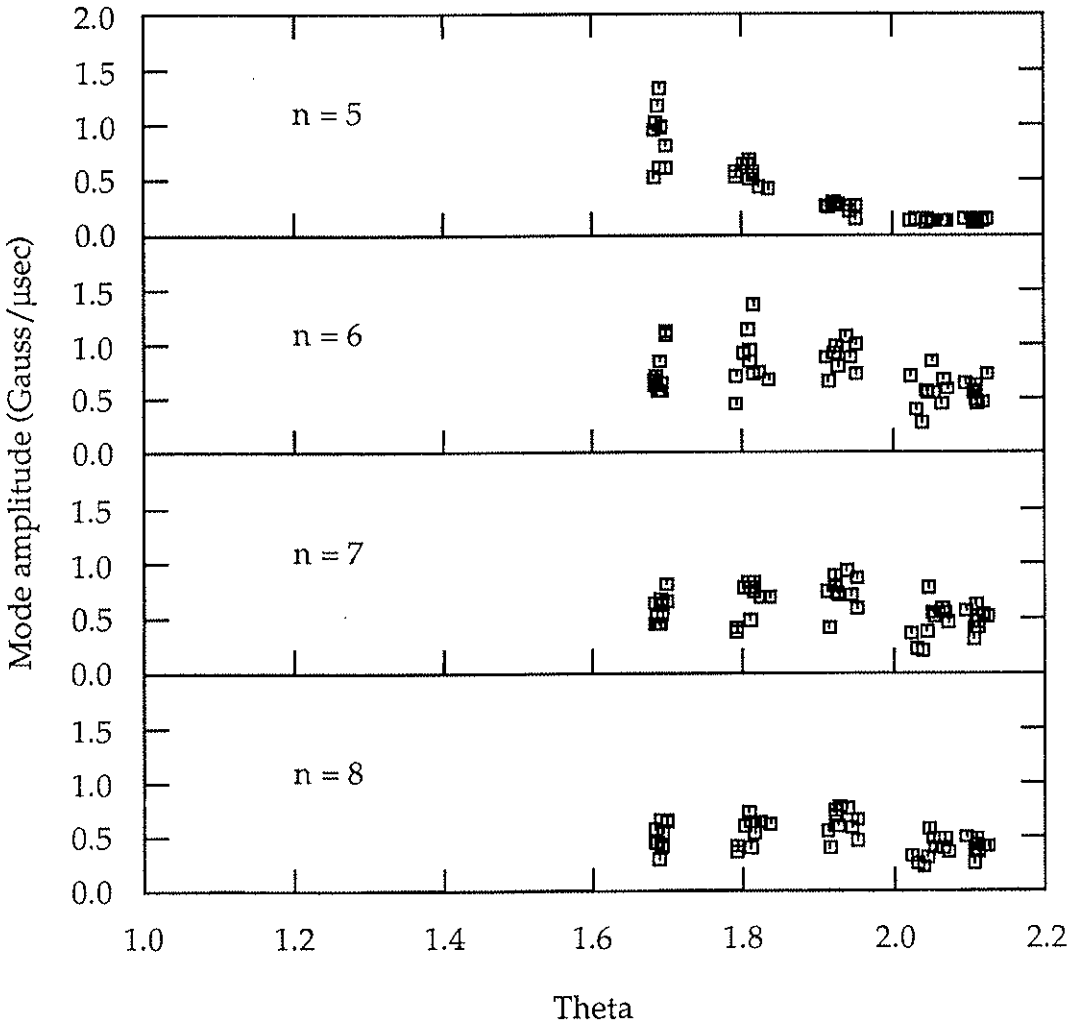

Figure 3.24 The amplitude of the toroidal modes n = 5 to 8 averaged over 1.0 msec at peak current for different values of the pinch parameter theta.

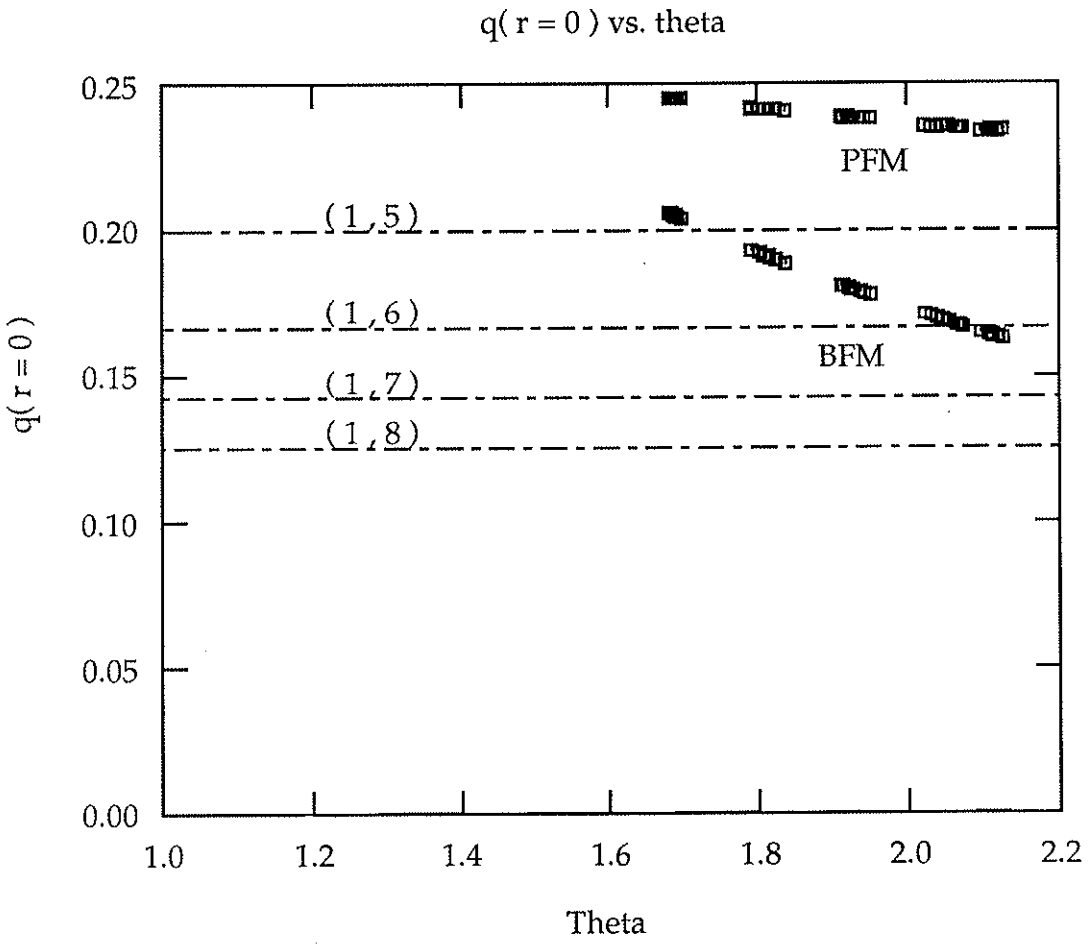

Figure 3.25 The calculated values of q on axis from the measured values of F and theta where the top points are from the PFM and the bottom points are from the BFM. The dashed lines are for the modes m/n = 1/5, 1/6, 1/7, 1/8.

3.2.2 Radial magnetic field at the poloidal gap

The radial magnetic field at the poloidal gap was measured as a function of the poloidal angle and time. The radial field has a new component that was absent in the bias plasmas when field errors were very large. The first component is the slow time scale (plasma current time scale). The second component is the high frequency component associated with the sawtooth activity. The new component is in the frequency range of 10 - 40 kHz. This component is dominantly an m = 1 and is associated with the rotating (1, n) plasma modes.

The measured radial magnetic field at the poloidal gap is shown in figure 3.26 where the measured points are represented by the squares. These 16 values are used to calculate the amplitudes of the poloidal mode spectrum up to m = 7 using Fourier decomposition of the measured discrete spatial structure. The solid curve in figure 3.26 is the full spatial structure reconstructed from the measured values of the radial field. Figure 3.27 shows the calculated poloidal mode amplitudes of the slow component. There are five sources of field error in MST. Some of these produce long-time-scale errors, and some produce short-time-scale errors.

The first source is the mismatch of plasma profiles from the primary winding distribution. This source produces a long-time-scale error. The measured m = 1 component of the field error at the poloidal gap is an example of such error. This error is produced by the difference between the asymmetry factor of the plasma profiles and the asymmetry factor assumed for the primary winding.

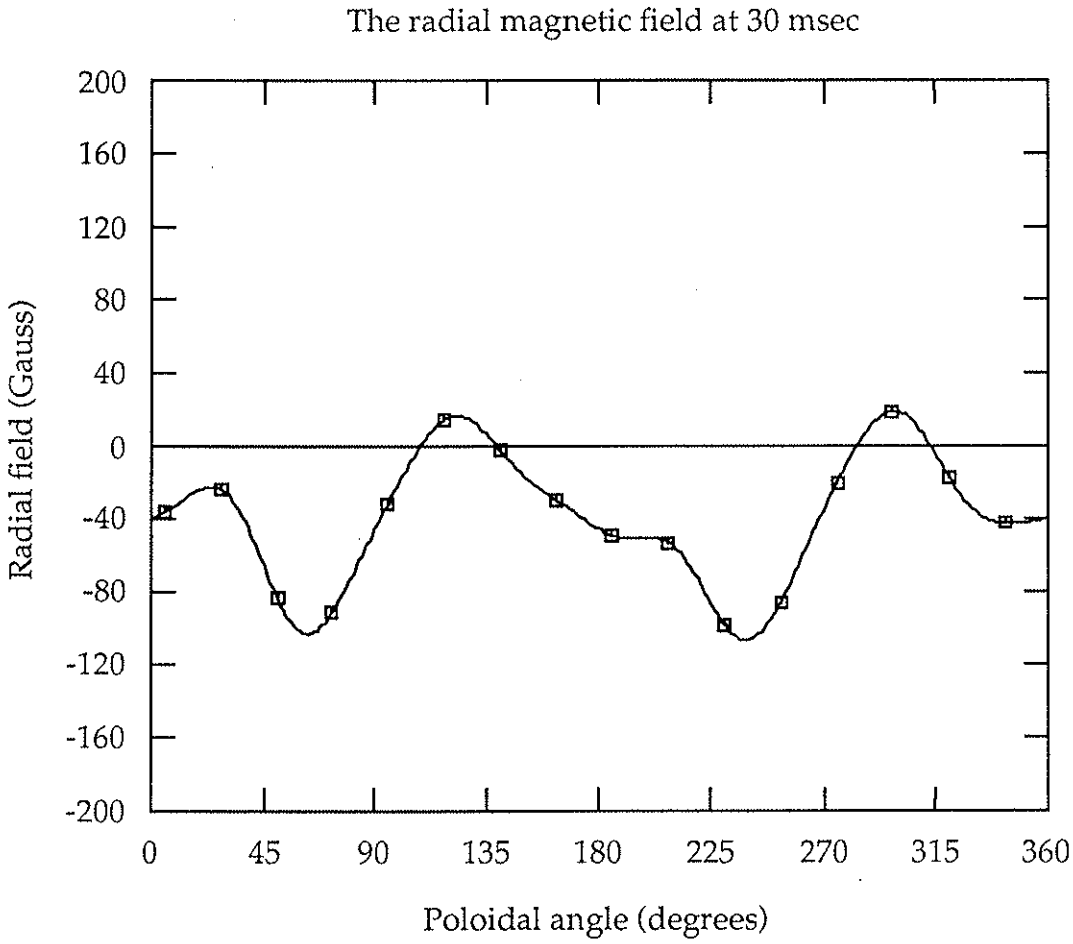

Figure 3.26 The poloidal structure of the radial field at the poloidal gap for the PF winding plasma. The square points are the measured values. The solid curve is the reconstructed full spatial structure.

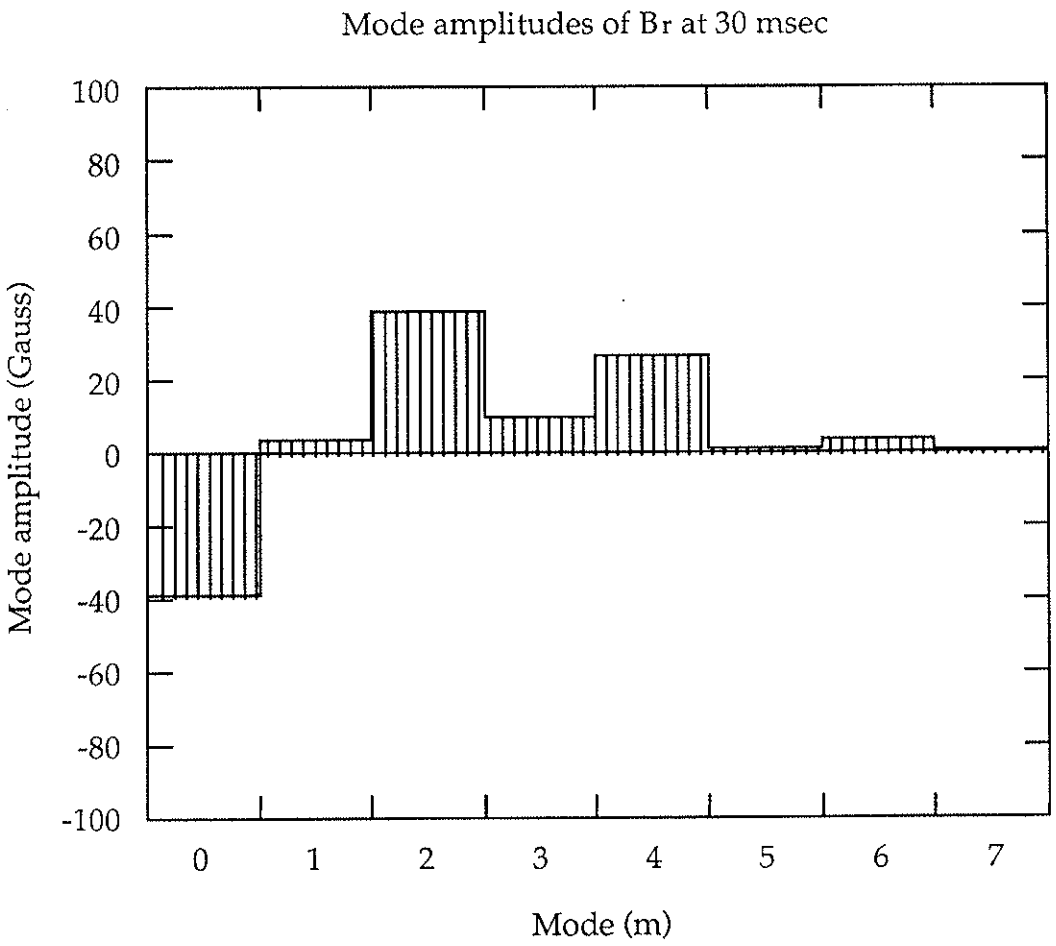

Figure 3.27 The calculated mode amplitudes of the slow component of the field error at the poloidal gap for the PF winding plasma.

Figure 3.28 shows the time trace of the measured m = 1 component of the field error and the measured lambda of the poloidal field at the wall. The m = 1 component is large during the formation stage of the discharge and then decreases as the plasma profiles change and become matched with the PF winding distribution. This is consistent with changes in the measured lambda.

The second source is the finite resistivity of the conducting shell. Currents on the outside face of the poloidal flange will diffuse toward the gap face of the flange. These currents will produce field errors with an m = 4 and 2 component. These errors occur on a longer time scale which is of the order of the soak-in time scale. Figure 3.29 shows the time trace of the m = 4 and 2 components of the field error. These two components of the field error have a linear dependence on the plasma current as can be seen in figure 3.30. This figure shows the amplitude of the m = 4 and 2 component at peak plasma current for different values of plasma current. This is an expected result since the currents that produce these errors are some fraction of the plasma current.

The third source produces the m = 0 component of the field error. This source is not fully understood. This source couples the poloidal and the toroidal gap. This component does not depend on the plasma current. In the same current scan where the amplitudes of m = 2 and 4 modes changed with current, the m = 0 at peak current did not change. In this current scan the field reversal parameter F was held constant. This agrees well with the F scan experiment described in section 3.1.4 where the m = 0

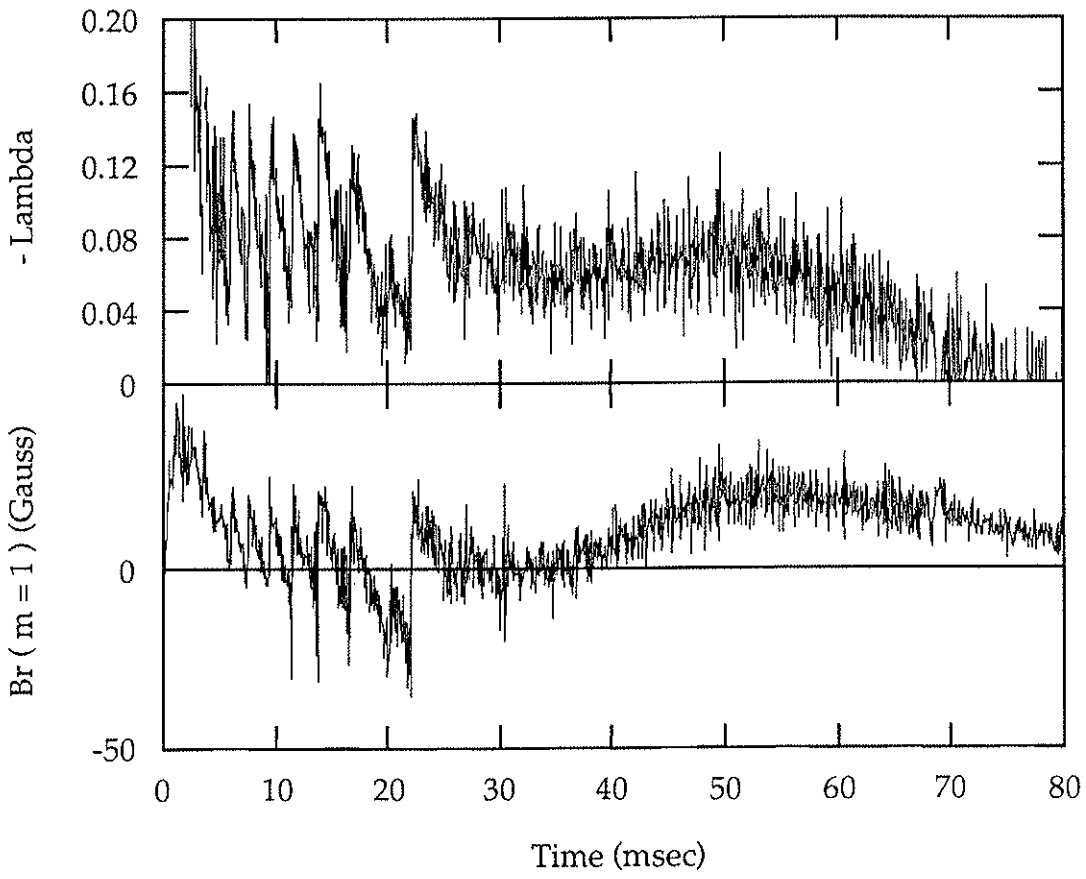

Figure 3.28 The time traces of the asymmetry factor and the m = 1 component of the field error at the poloidal gap. The waveform of the field error is consistent with the changes in the measured lambda.

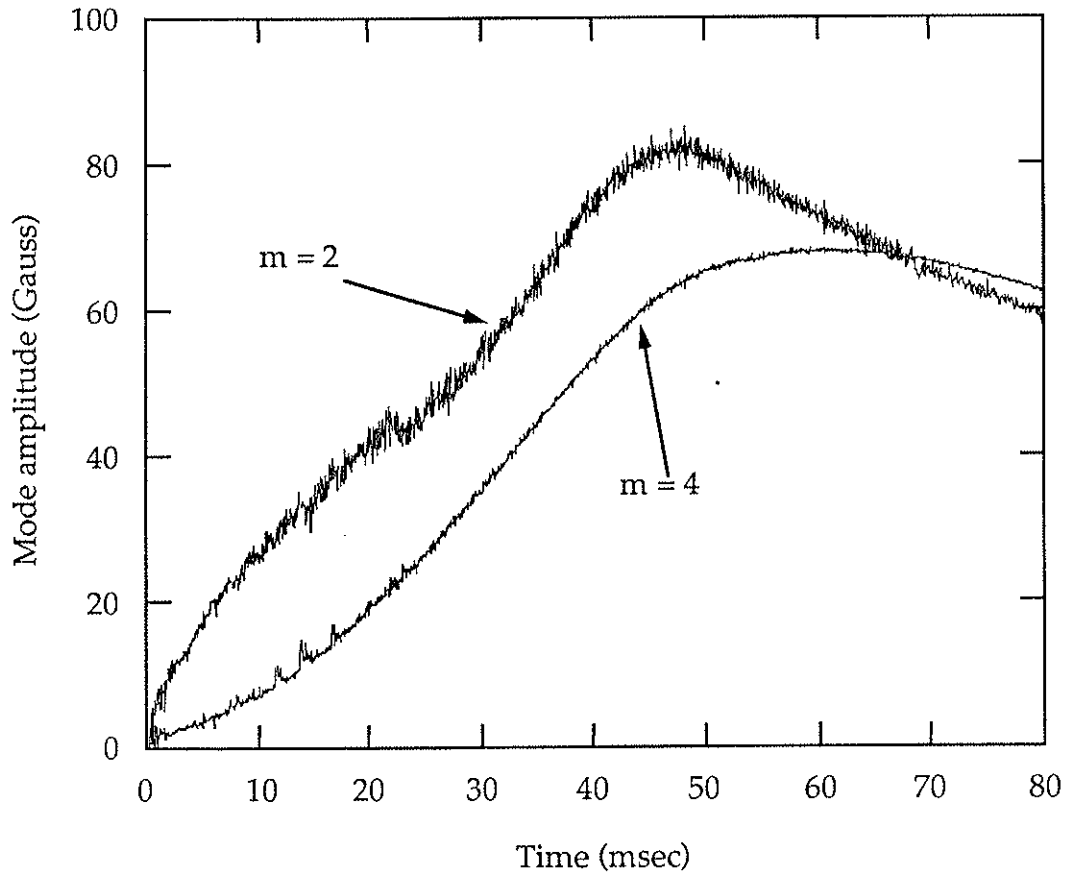

Figure 3.29 The time dependence of the m = 2 and 4 components of the field error at the poloidal gap shows the finite resistivity effect of the poloidal flange. The m = 2 can be divided into two time scales. One part is proportional to the plasma current and the rest is due to soak-in.

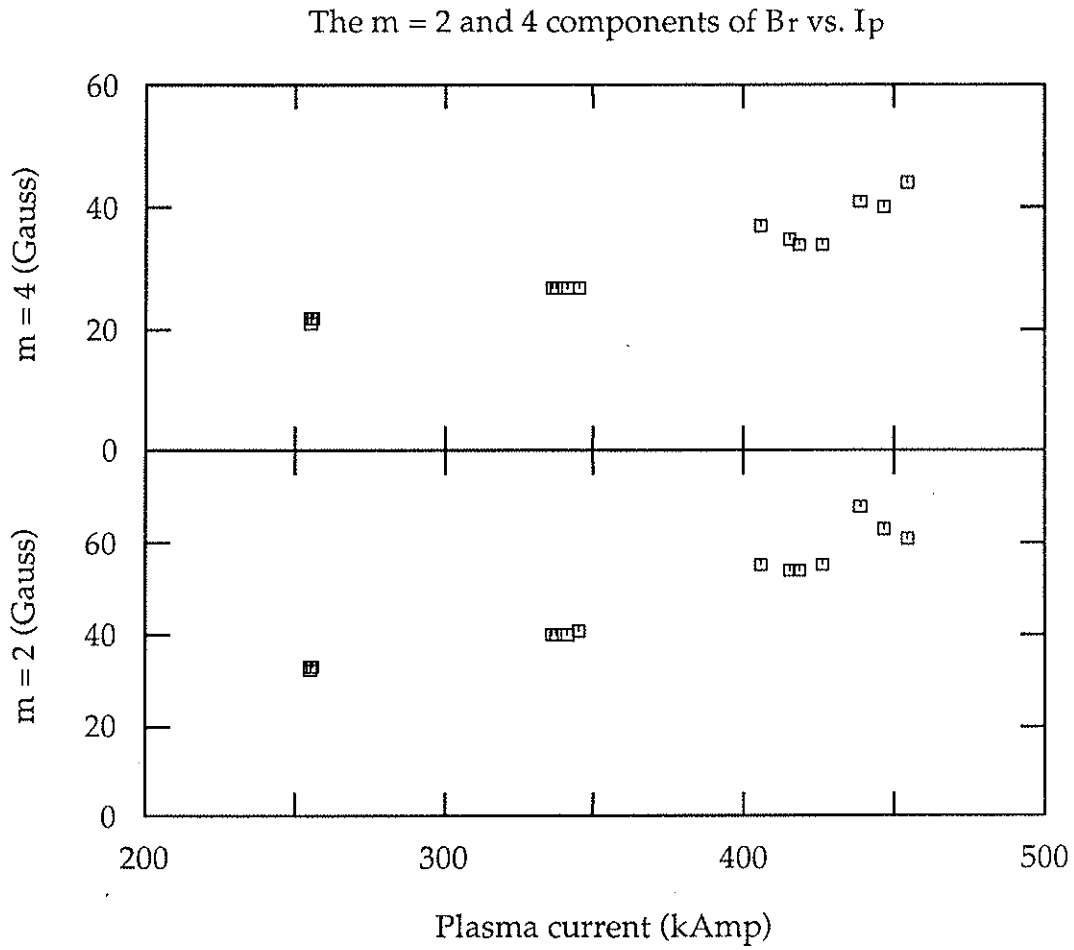

Figure 3.30 The m = 2 and 4 component of the field error at the poloidal gap at peak plasma current at a constant F. This plot shows the linear dependence of these components on the plasma current.

had a strong dependence on F see figure 3.18. Figure 3.31 shows the m = 0 component and F at 30 msec into the discharge (peak current) where they have no dependence on plasma current.

The fourth source is the sawtooth activity. It produces field error components on the same time scale as the flux jump. This error shows most strongly in the m = 0 and 1 components of the field error. This is consistent with the profile changes that results in the generation of the sawtooth activity. This can be seen in figure 3.32 which shows the time trace of the m = 0 and 1 component.

The fifth source is the rotating coherent magnetic fluctuations. These magnetic fluctuations which are dominantly m = 1, rotate toroidally in the lab frame. As these perturbations rotate they disturb the equilibrium wall currents. This results in a oscillating field error at the poloidal gap. When this part is isolated from the raw signals of the error field and Fourier decomposed it is found that it is dominantly m = 1 as expected. This m = 1 has the same frequency range (10 - 40 kHz) as the coherent magnetic fluctuation (1, n) of the plasma. Figure 3.33 shows the amplitude and the phase of this component. This field error is about 1.0% of the poloidal field at the wall. This type of field error is very hard to correct due to its high frequency.

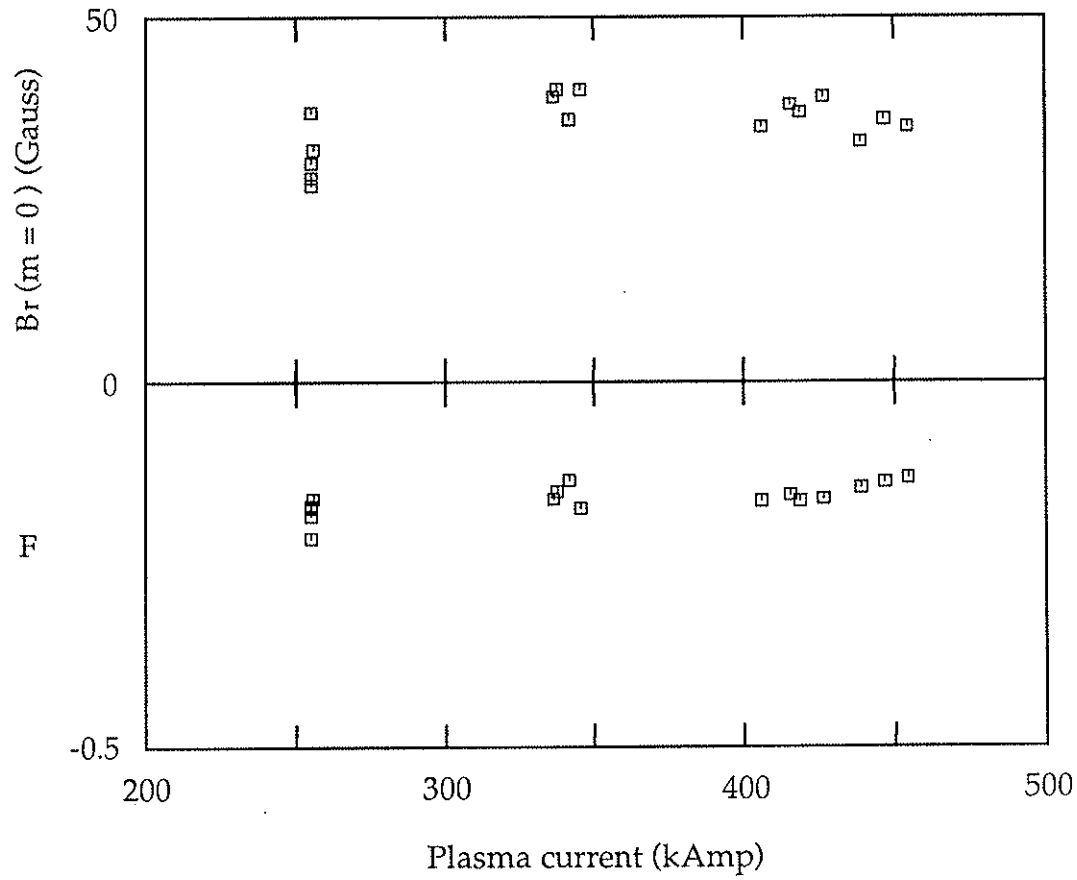

Figure 3.31 The m = 0 component of the field error at the poloidal gap at peak plasma current versus plasma current at a constant F. This plot shows the independence of the m = 0 component from the plasma current. The lower plot shows the value of F for this current scan.

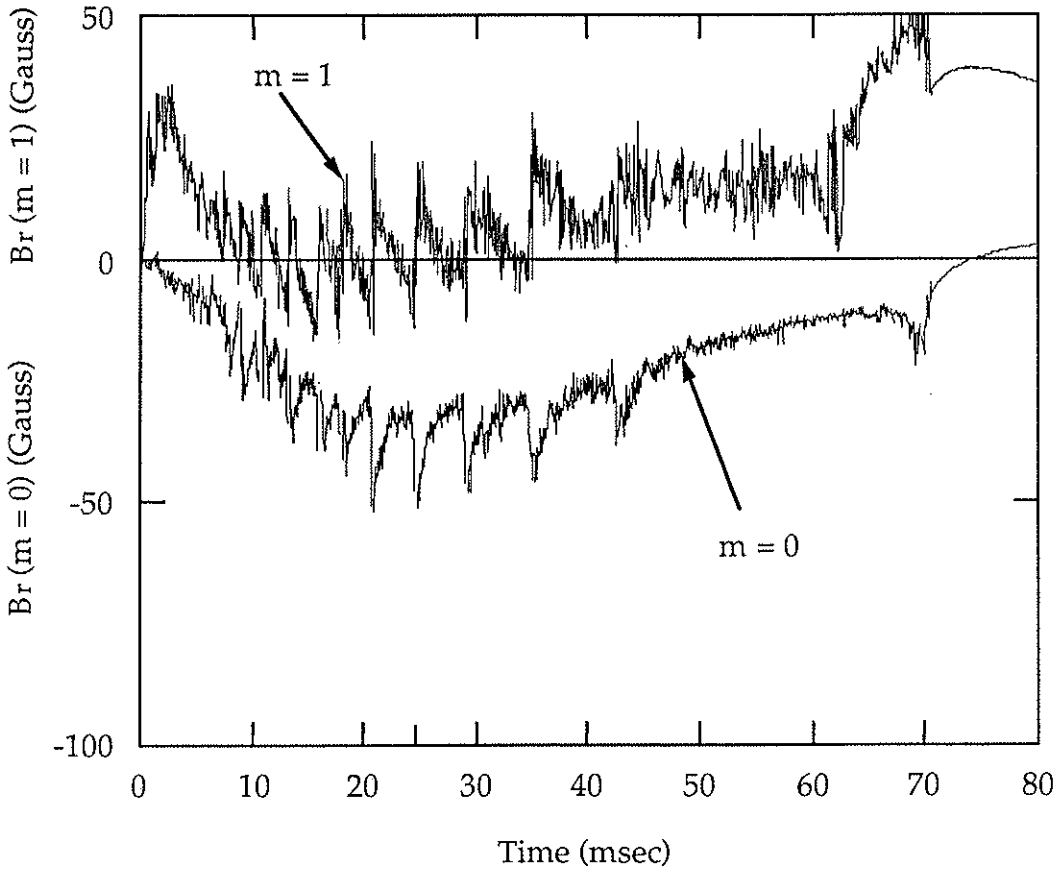

Figure 3.32 The time traces of the m = 0 and 1 components of the field error at the poloidal gap. This plot shows the effect of the flux jump on the field error where it causes an increase in the amplitude of the m = 0 and 1 components only.

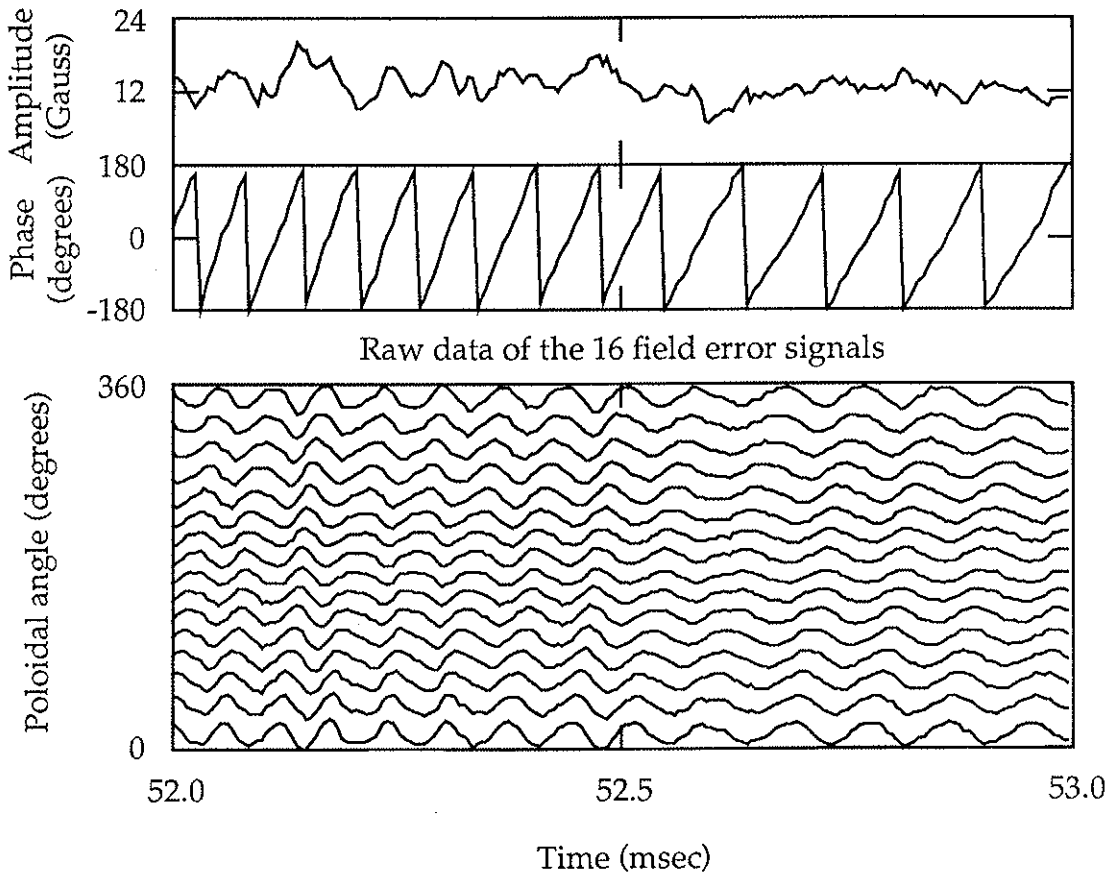

Figure 3.33 The component of the field error that is produced by the coherent plasma modes as they cross the poloidal gap. This error is mostly an m = 1 mode. The top plot shows the amplitude of the error. The middle plot shows the phase. The bottom plot shows the raw data in the same order of their poloidal locations with the long-time-scale component removed.

3.2.3 Comparison of bias and PF plasmas

The PF winding installation is the major design step in reducing field errors in MST. As was stated earlier, the PF winding has a poloidal structure of an assumed plasma equilibrium similar to that obtained in experiment. The rms of the radial field is about a factor of six smaller with the PF winding than with the bias winding. Figure 3.34 shows the poloidal structure of the radial field in the poloidal gap. The solid curve is for the PF plasma and the dashed curve is for the bias winding. The changes in the mode amplitude for these two cases is shown in figure 3.35. The amplitude of m = 1 is reduced by a factor of 9, m = 2 is reduced by a factor of 5, and m = 4 is reduced by a factor of 8. The most dramatic effect of the PF winding, through reduced field errors, is the increase in the discharge duration from 30 msec to about 75 msec. This is also partly due to improved power crowbaring of the poloidal field circuit. The resistive loop voltage is also reduced to about 16 Volts from about 32 Volts with the bias winding. The loop voltage was later reduced more by few Volts to about 13 Volts by reducing some of the remaining field errors. Figure 3.36 shows a trace of plasma current and loop voltage where the solid curves are for the PF winding and the dashed curves are for the bias winding. Figure 3.37 compares the oscillating component of the radial field which is dominantly m = 1. With the bias plasma these oscillations are absent because the plasma (1 , n) modes are locked to the wall due to large field errors. However, for the corrected bias plasma these oscillations were

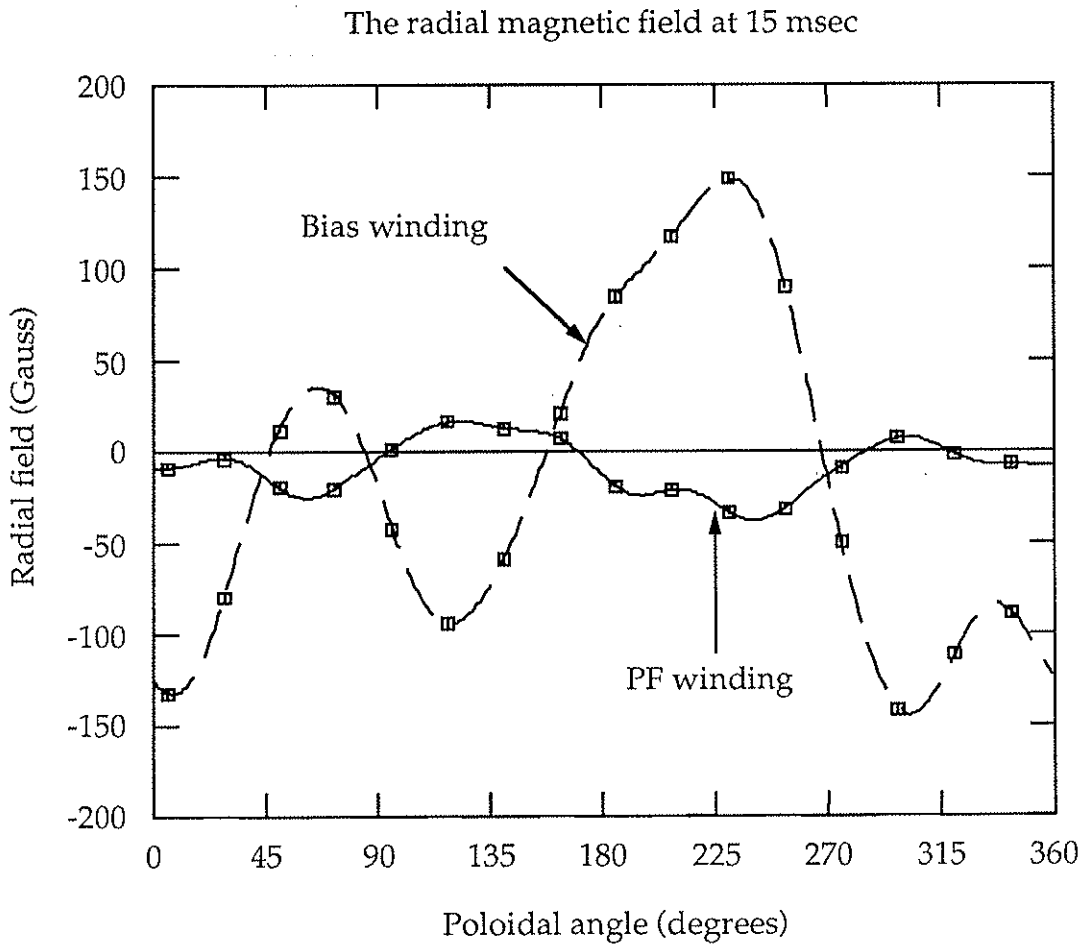

Figure 3.34 The poloidal structure of the radial field at the poloidal gap. The solid curve is for the PF winding plasma and the dashed curve is for the bias winding plasma for the same plasma current.

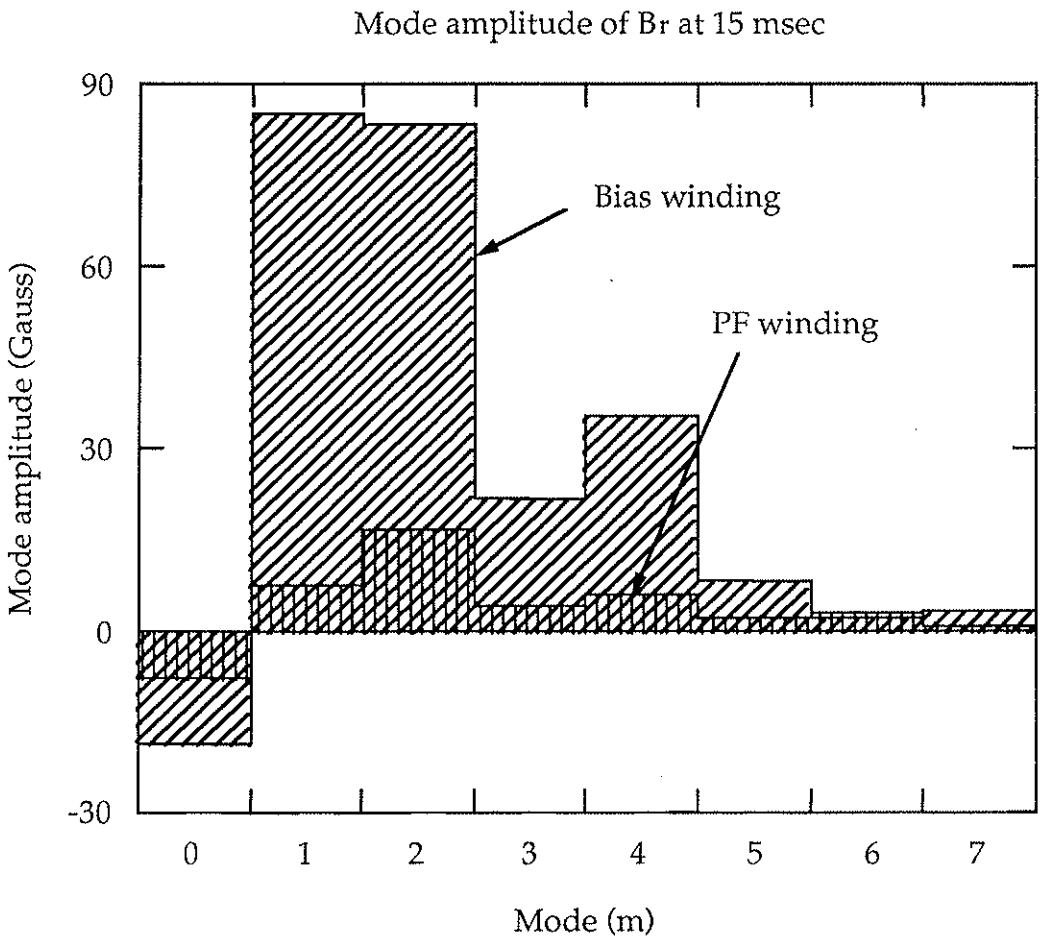

Figure 3.35 The mode amplitudes of the radial field at the poloidal gap for both cases of the PF and bias winding. The vertical lines are for the PF and the 45 degrees lines are for the bias winding.

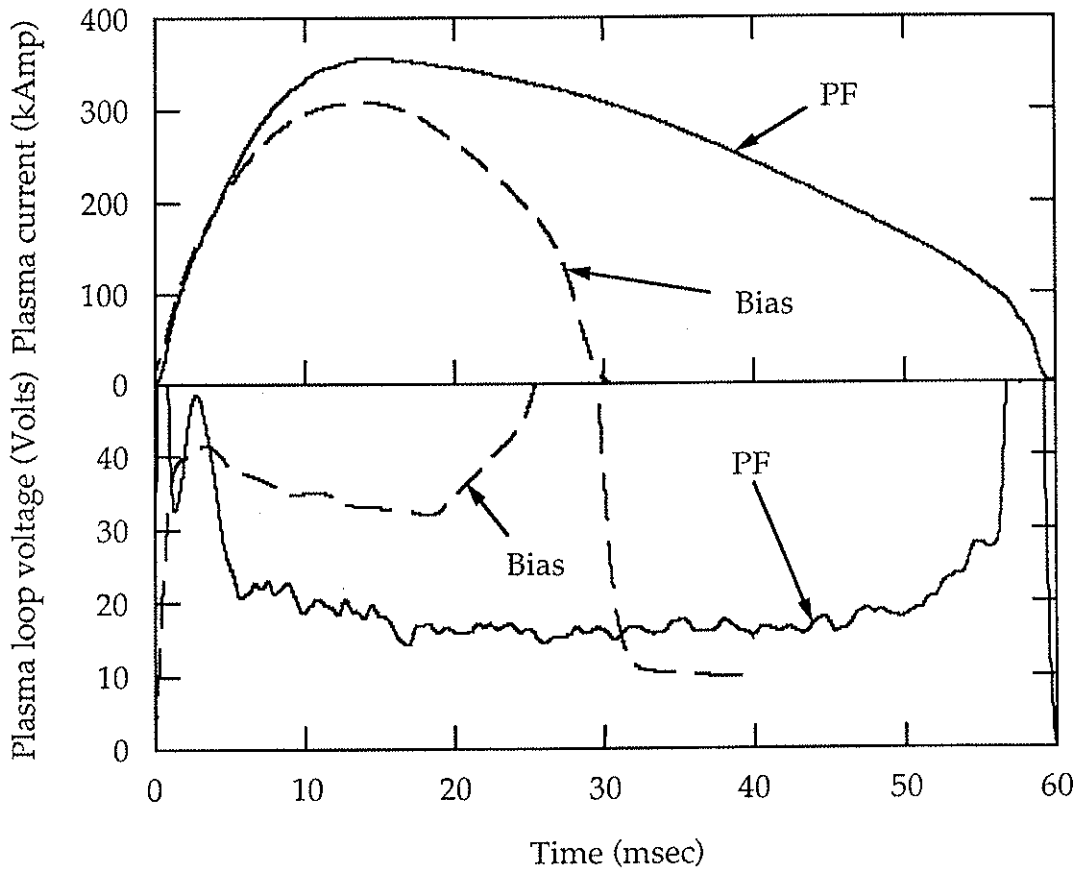

Figure 3.36 The time trace of the plasma current and resistive loop voltage for both cases of PF and bias winding.

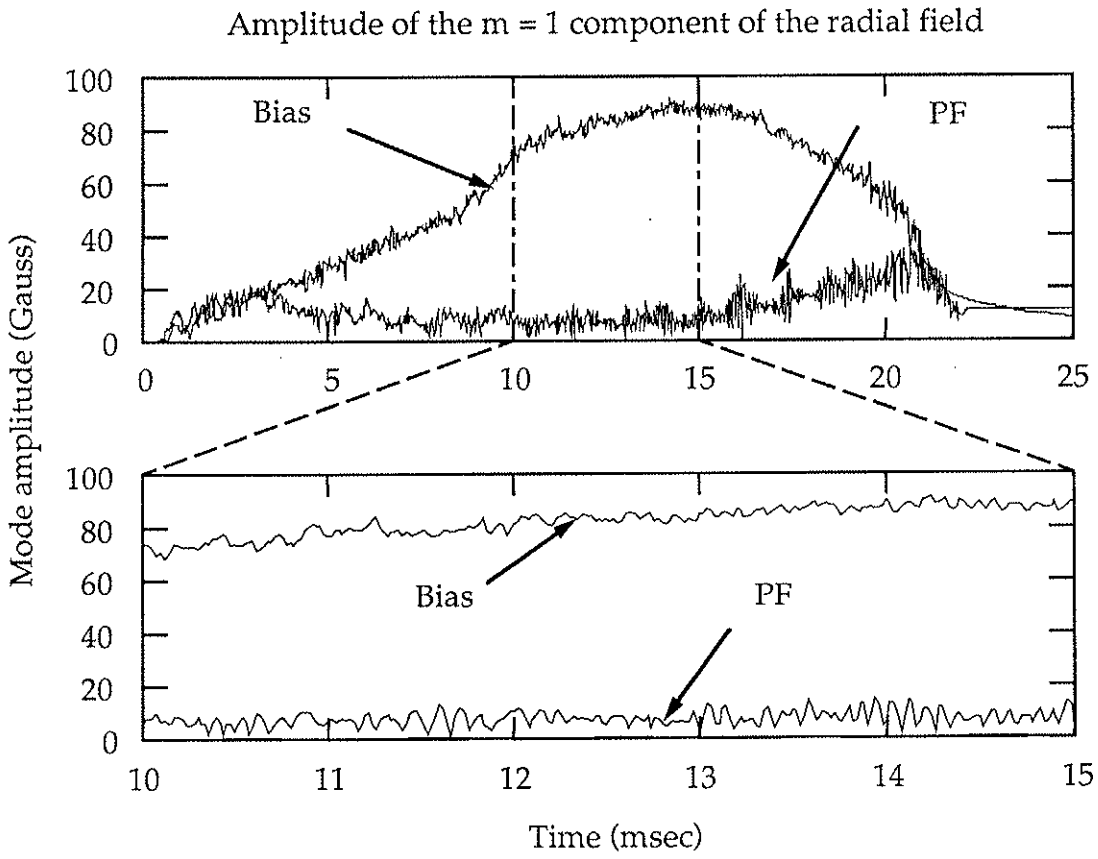

Figure 3.37 The time trace of the m = 1 component of the field error at the poloidal gap for both cases of PF and bias winding. The lower trace is an expanded time window showing the absence of the coherent oscillation with the bias winding.

present early in the discharge occasionally. Also, some comparison of the high frequency toroidal modes was made. Figure 3.38 shows the two point correlation measurement of the toroidal mode spectrum in the low ($2 < f < 50$ kHz) and high ($50 < f < 250$ kHz) frequency range. The magnetic fluctuation in both frequency ranges seems to be suppressed and the spectrum is narrower in the low field error plasma.

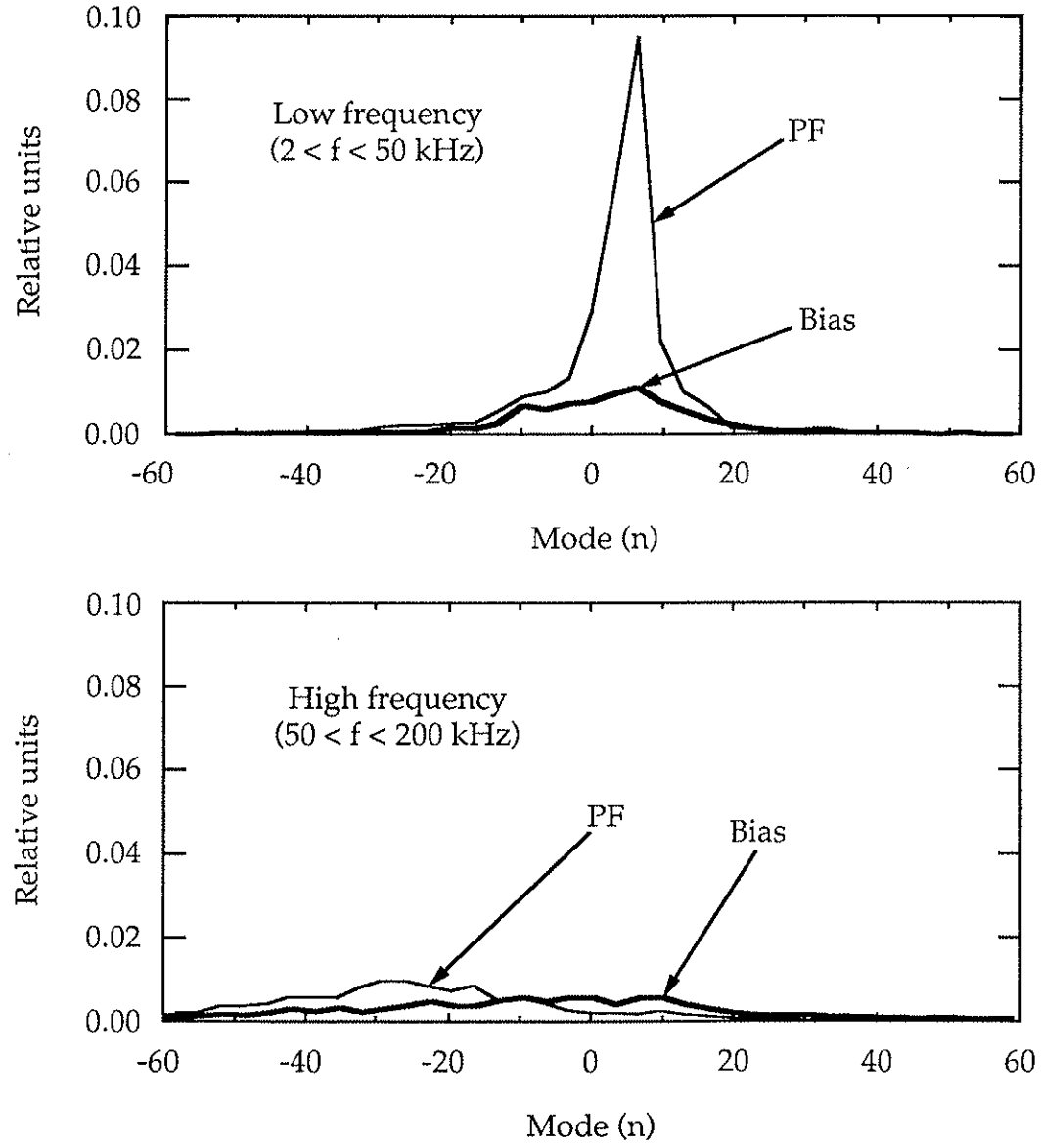

Figure 3.38 The toroidal mode specrtum of the magnetic fluctuation from two-point correlation measurements at two frequency ranges. In the low frequency range the magnetic fluctuations are dominated by the coherent modes when the field errors are small(PF). In the high frequency range the spectrum is shifted due to field errors (Bias).

3.2.4 Mode locking and field error instability

Measurements of the toroidal mode fluctuation spectrum shows that the spectrum changes from a single mode to many modes throughout the discharge. When the spectrum is broad, the dominant modes (1, n = 5 - 8) phase lock to one another to form a localized perturbation. This localized perturbation starts to rotate in the ion diamagnetic drift direction with varying speed (~ 10^6 cm/sec). This perturbation is similar to the previously observed "slinky" on OHTE[2] and other devices.

Figure 3.39 shows the raw data from 32 coils placed toroidally around the device in the same order as their toroidal locations. This plot shows the broadening of the toroidal spectrum in time. Before 19.3 msec the spectrum is narrow; after that the spectrum broadens and the localized perturbation forms. In some discharges these helical modes stop rotating and lock to the wall. If this happens early in the discharge then usually it occurs at a sawtooth event, but there are some cases where the modes stop rotating late in the discharge where there is no sawtooth activity. Once the modes stop rotating the discharge characteristics change. The most drastic change is that the discharge duration becomes much shorter. In general, the sooner the instability takes place, the shorter the discharge. The duration of discharge can be reduced by as much as a factor of two from 80 msec long to about 40 msec long. In many ways these short discharges are similar to the BIAS plasma. The other obvious change is the presence of a large rising m = 1 component of the radial field at the poloidal gap, as is

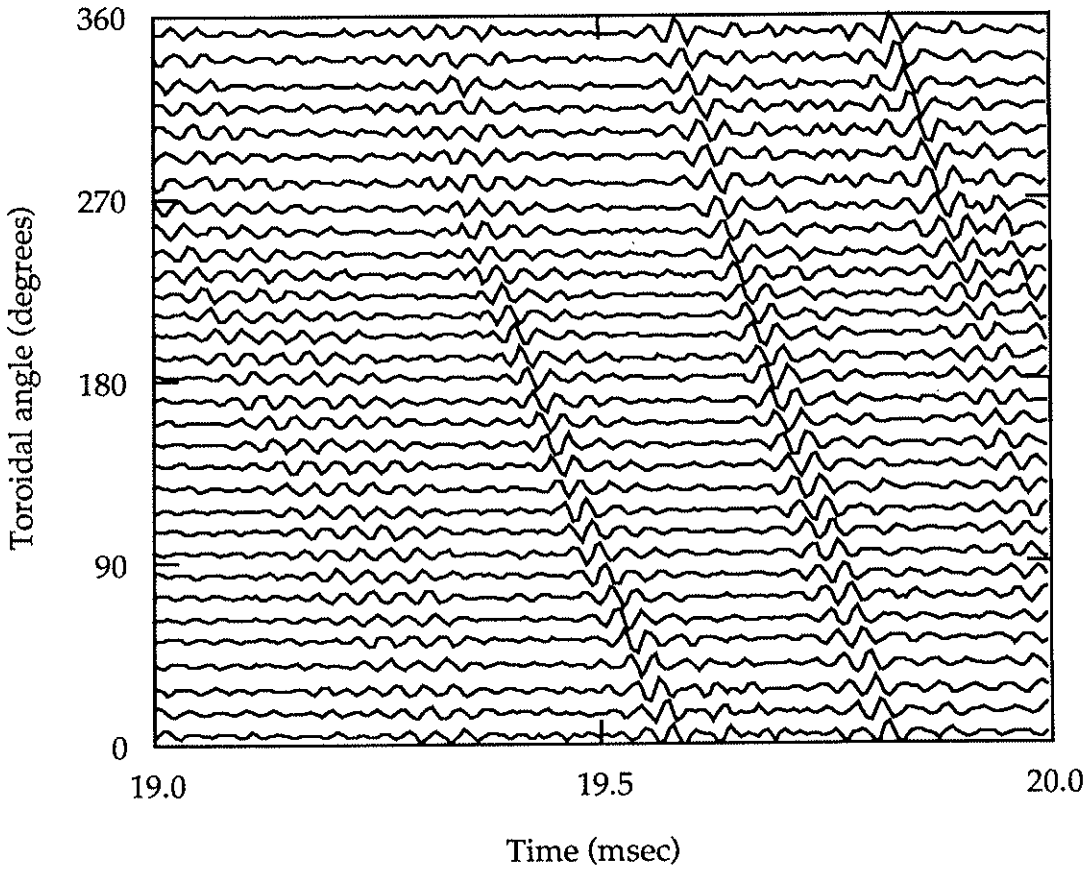

Figure 3.39 The raw data of 32 coils placed toroidally around the device with the slow component of the poloidal field removed. This shows the formation of the localized perturbation when the dominant toroidal modes phase lock to one another. This perturbation rotates toroidally in the ion diamagnetic drift direction at about 10^6 cm/sec.

shown in figure 3.40. Once the toroidal rotation stops the m = 1 oscillation seen in the radial field at the poloidal gap disappears as well; as can be seen in figure 3.41.

Measurements of the m = 1 component of the radial field at the poloidal gap (0 degrees toroidally) shows that when the modes lock to the wall the plasma moves below its equilibrium position. This is then followed by inward motion in major radius. The downward motion is proportional to the horizontal radial magnetic field which is given by the cos(θ) coefficient. This horizontal field increases quickly from the noise level to a constant value. This indicates that the plasma at the poloidal gap makes a downward jump and stays in that position until the discharge terminates. The vertical magnetic field, which is proportional to the inward motion, is given by the sin(θ) coefficient. This vertical field increases in time indicating that the plasma at the poloidal gap is moving inward until it terminates. This is shown in figure 3.42.

Measurements of the m = 1 component of the poloidal field at 180 degrees away from the gap shows that the plasma moves up above its equilibrium position which is followed by inward motion until the discharge terminates. This is shown in figure 3.43.

The opposite vertical motion at the gap and 180 degrees away shows that the plasma locks to the wall with an odd toroidal mode number. This mode is stationary or of the same time scale as the plasma current. Accurate measurements of the stationary spectrum requires a high degree of alignment of the pickup coils and a good resolution of the electronics

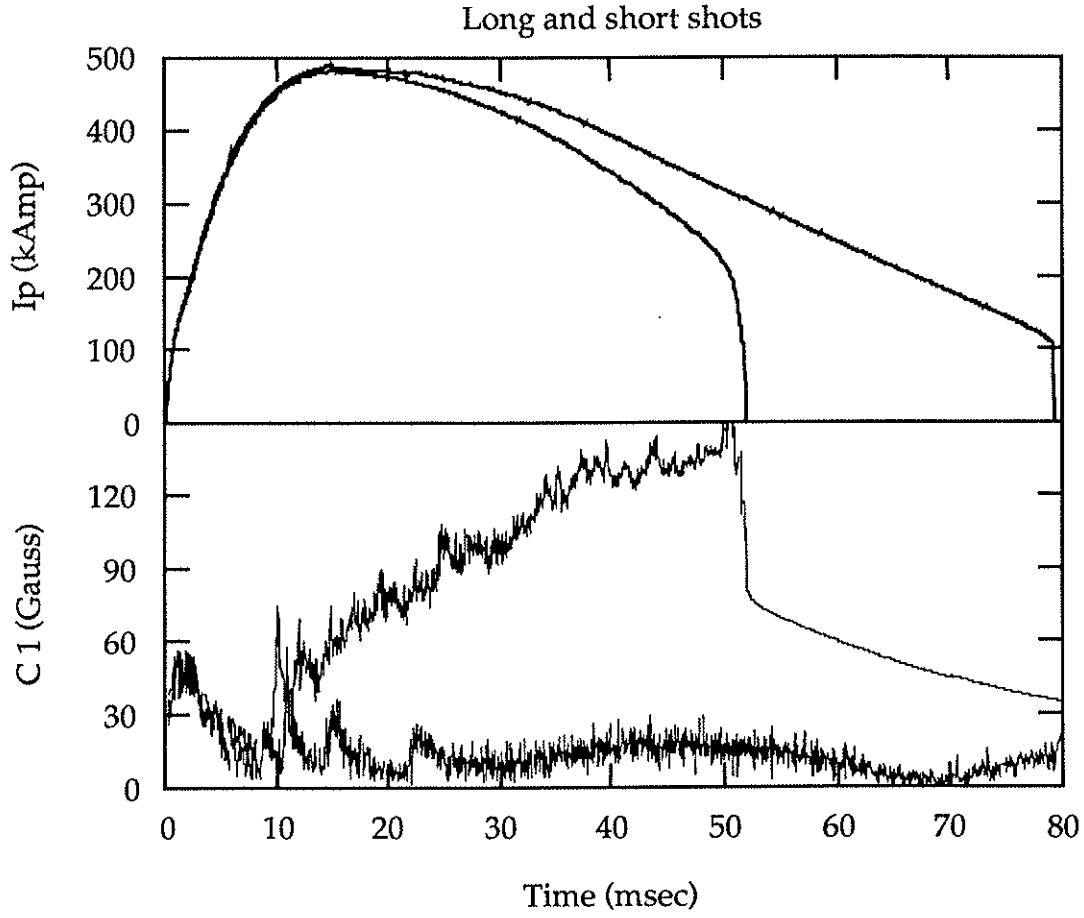

Figure 3.40 The plasma current and the m = 1 component of the field error at the poloidal gap for locked and unlocked discharges. The short shot is always acompanied by a large m = 1 field error.

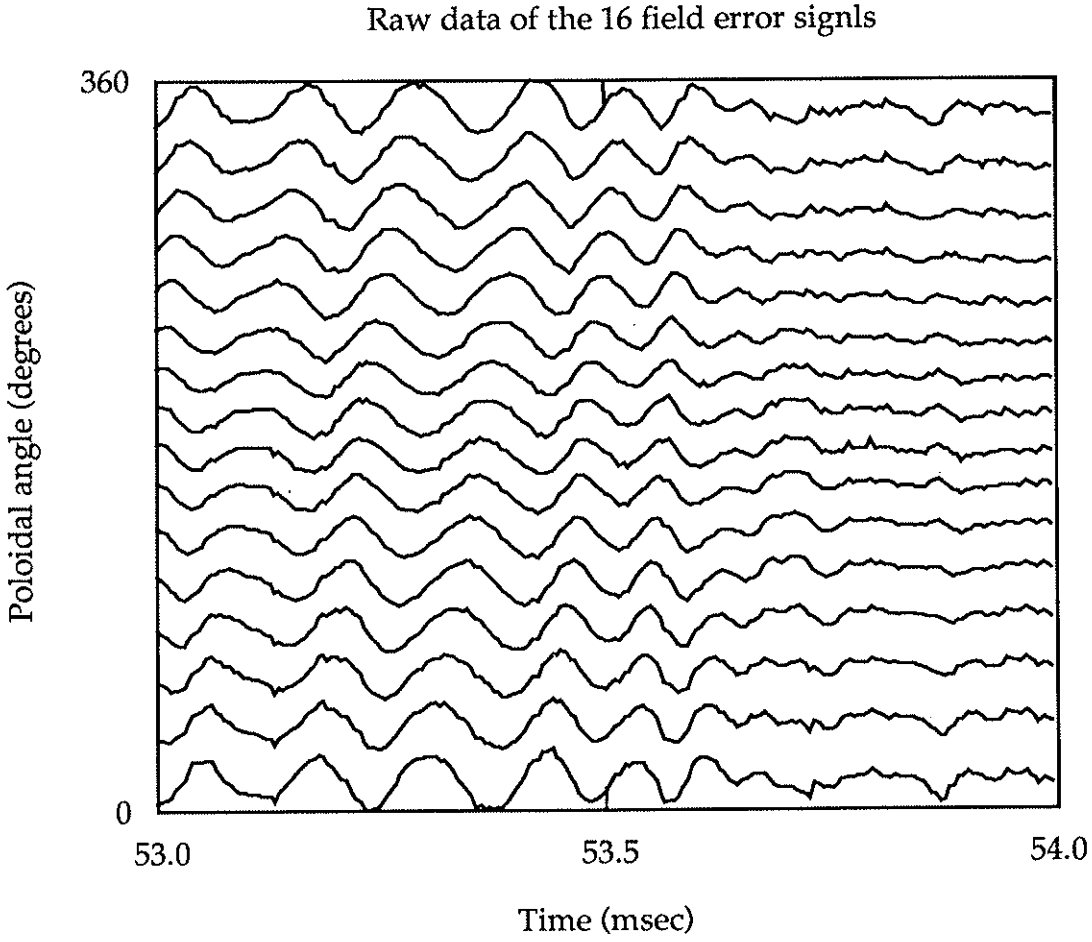

Figure 3.41 The raw data of the field error at the poloidal gap showing the disappearance of the coherent oscillation associated with the rotating toroidal modes.

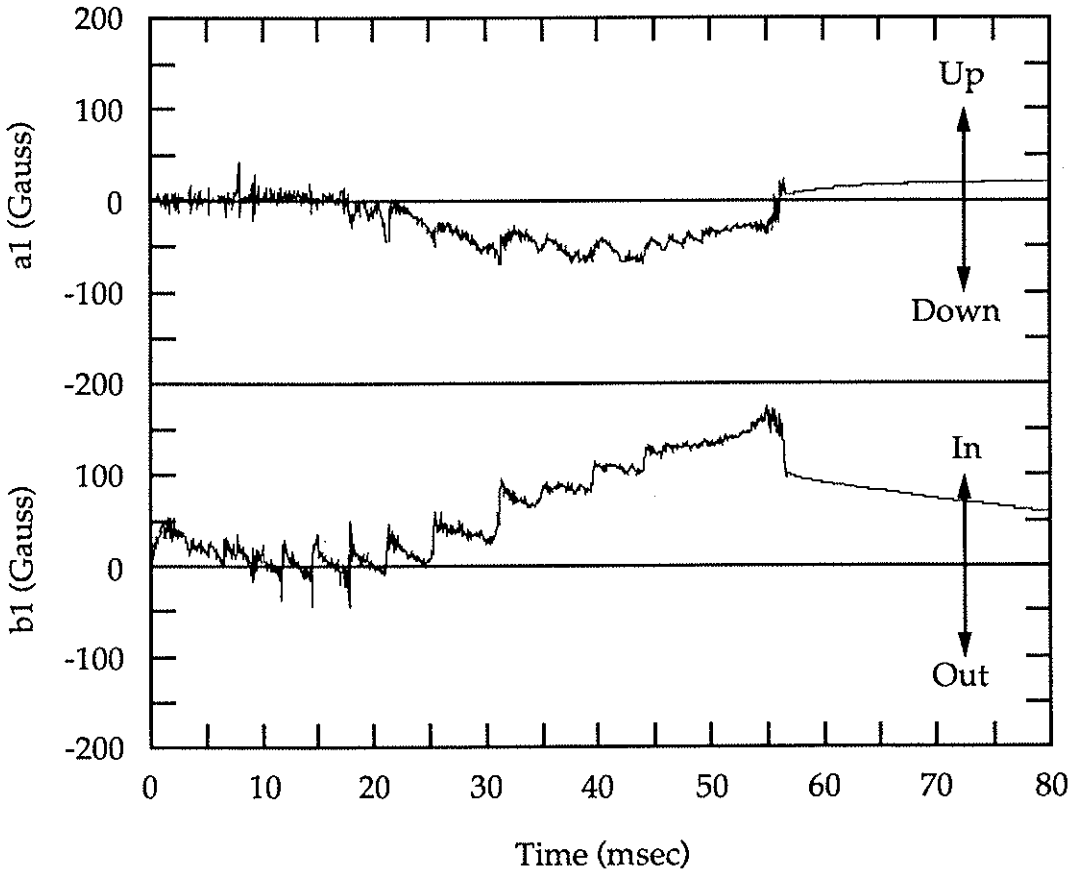

Figure 3.42 The sine and cosine coefficient of the m = 1 component of the radial field at the poloidal gap show the downward motion of the current profiles which is followed by an inward motion of the current profiles at the poloidal gap.

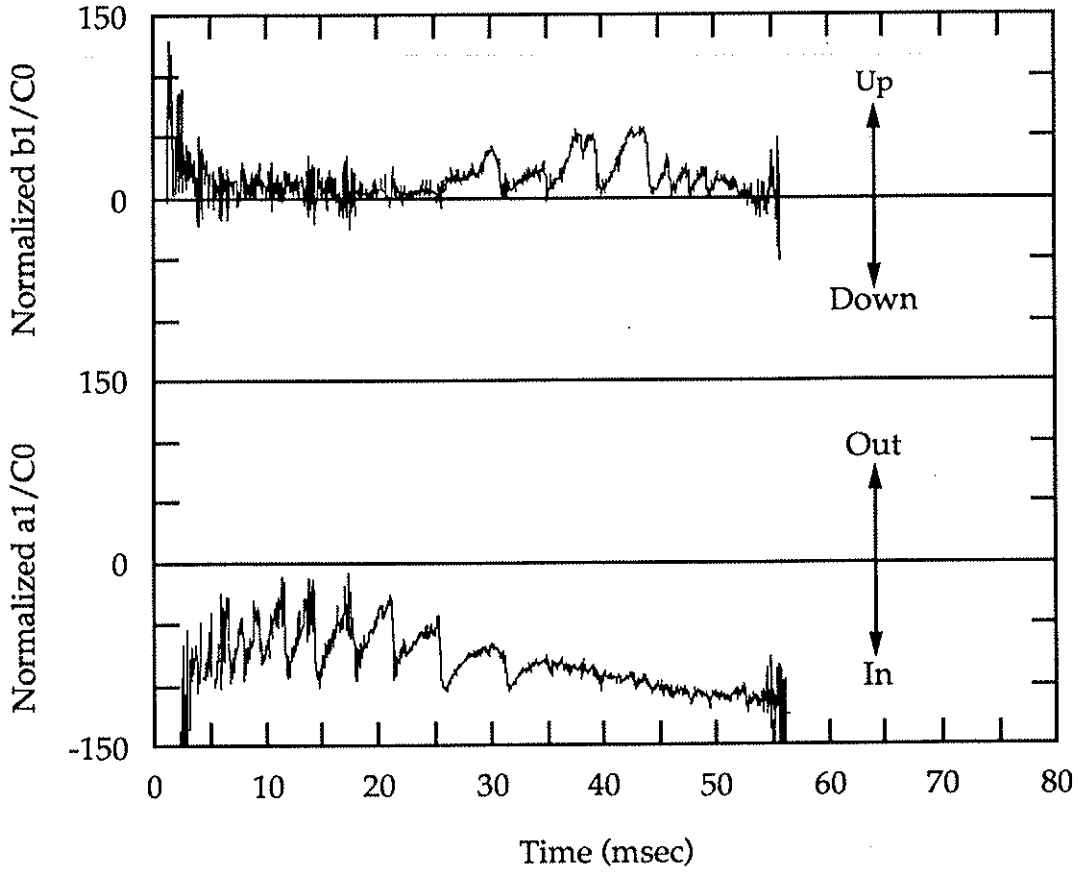

Figure 3.43 The sine and cosine coefficient of the m = 1 component of the poloidal field at 180 degrees away from the poloidal gap show the upward motion of the current profiles which is followed by an inward motion of the current profiles.

used, such as integrators. This problem arises due to the leakage of the large n = 0 component into the higher n stationary modes which are of the same frequency as the n = 0 mode. This problem does not effect the fluctuating modes whose frequency is different from the stationary n = 0 component. However, we have observed that the amplitude of the n = 5 and n = 7 do change and become larger for the locked discharges, while the n = 0 amplitude does not change. Since the n = 0 component does not change, this means that the leakage of n = 0 into the higher n's is the same for both locked and unlocked discharges. Therefore the change in the amplitude of the higher n's indicates that n = 5 and 7 stationary modes do exist in the locked discharges. The amplitudes of the stationary spectrum is expected to be about 2% of the poloidal field at the wall. The observed change in the amplitude of the stationary n = 5 and 7 from unlocked to locked discharge is about 0.6%, as shown in figure 3.44. Helical plasma will produce a radial magnetic field at the toroidal gap of a similar n spectrum as the helical plasma itself. The radial field measurements at the toroidal gap does not get spoiled by leakage from the small n = 0 component of the toroidal field at the wall. Measurements of the radial field at the toroidal gap will also tell us which stationary modes are forming as the plasma locks to the wall as well. This measurement will done in the near future.

The observed characteristics of the locked discharge can be explained by the following mechanism: the plasma forms into a stationary kink due to tearing instability which locks to the wall, perhaps due to the plasma-field error interaction. The inward motion of the plasma that follows the

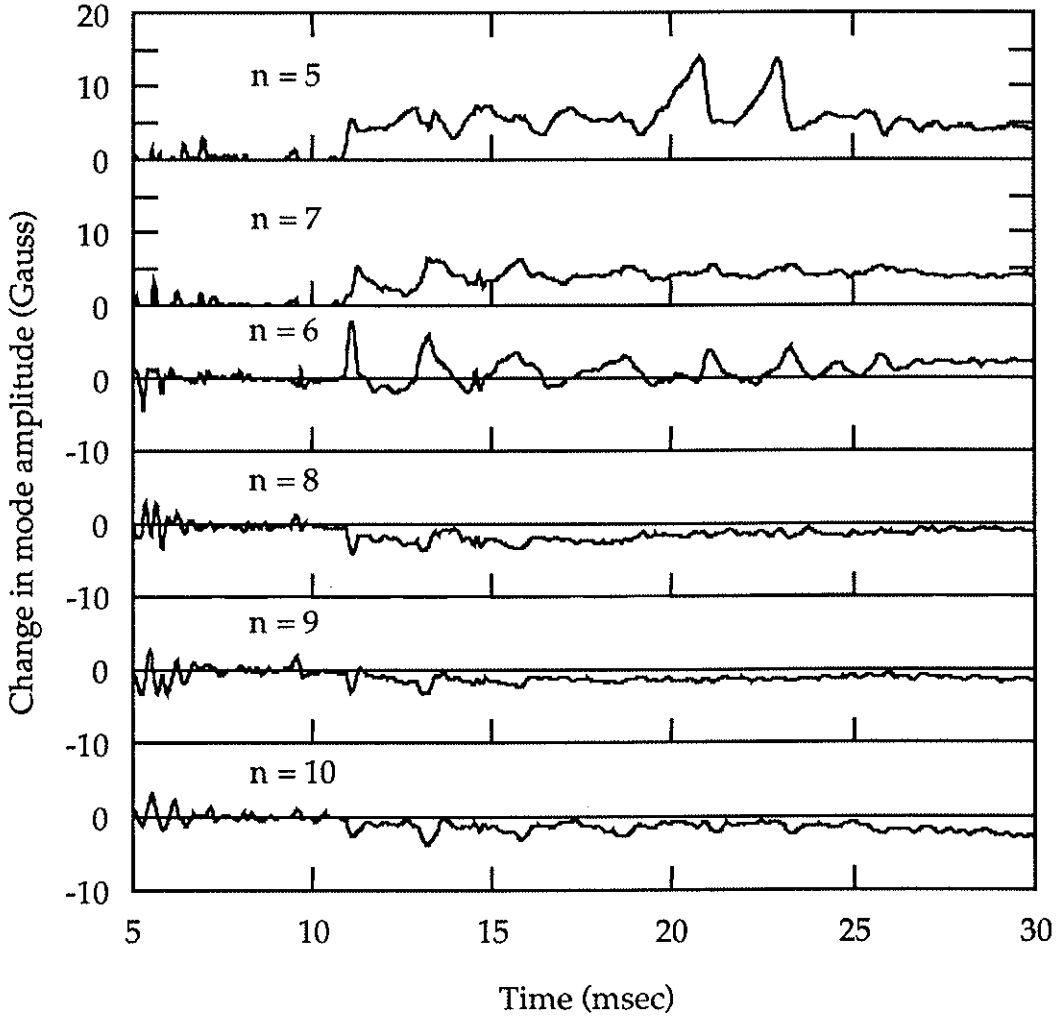

Figure 3.44 The change in the amplitude of the stationary toroidal modes of n = 5 to 10. Only the amplitudes of n = 5 and 7 change when the discharge locks.

mode locking can be explained by Kerst field error instability.[3] This instability assumes that the plasma is in the form of a helix of $n \neq 0$. The helical plasma will interact with with the toroidal gap and produce a radial error field at the toroidal gap of toroidal mode number similar to that of the helix. This radial field will develop a toroidal component away from the toroidal gap. The toroidal component of this error field will interact with the vertical component of the helical plasma current. This produces an axisymmetric inward force that will cause the plasma to move inward. Kerst has calculated the required vertical magnetic field to oppose this inward motion to be proportional to the toroidal gap width. There are two bad effects that happen once the plasma forms into a stationary helical mode. First, the wall will provide less restoring force to this inward motion (low frequency). Second, the effective gap width will become larger with time due to resistive effects. The inward force or the vertical field required to oppose it will increase in time due to gap widening, while the conducting shell restoring force will decrease. Since the toroidal gap widens up on the wall resistive time scale, then one would expect the required vertical field to oppose the inward motion to also increase with a similar time scale. The measured m = 1 component of the radial field at the poloidal gap is a measure of the necessary vertical field to stabilize the plasma against the inward motion. The m = 4 component of the radial magnetic field at the poloidal gap is due to the soak-in effect through the poloidal flange. The m = 1 component of the radial field at the gap and the m = 1 component of the poloidal field at 180 degrees away have the same

time scale as the m = 4 component of the radial field at the gap. Figure 3.45 shows the waveform of the m = 4 and 1 components of the radial field and the m = 1 of the poloidal field. This suggests that the inward motion of the plasma once it forms into a stationary helical mode may be due to the field error instability.

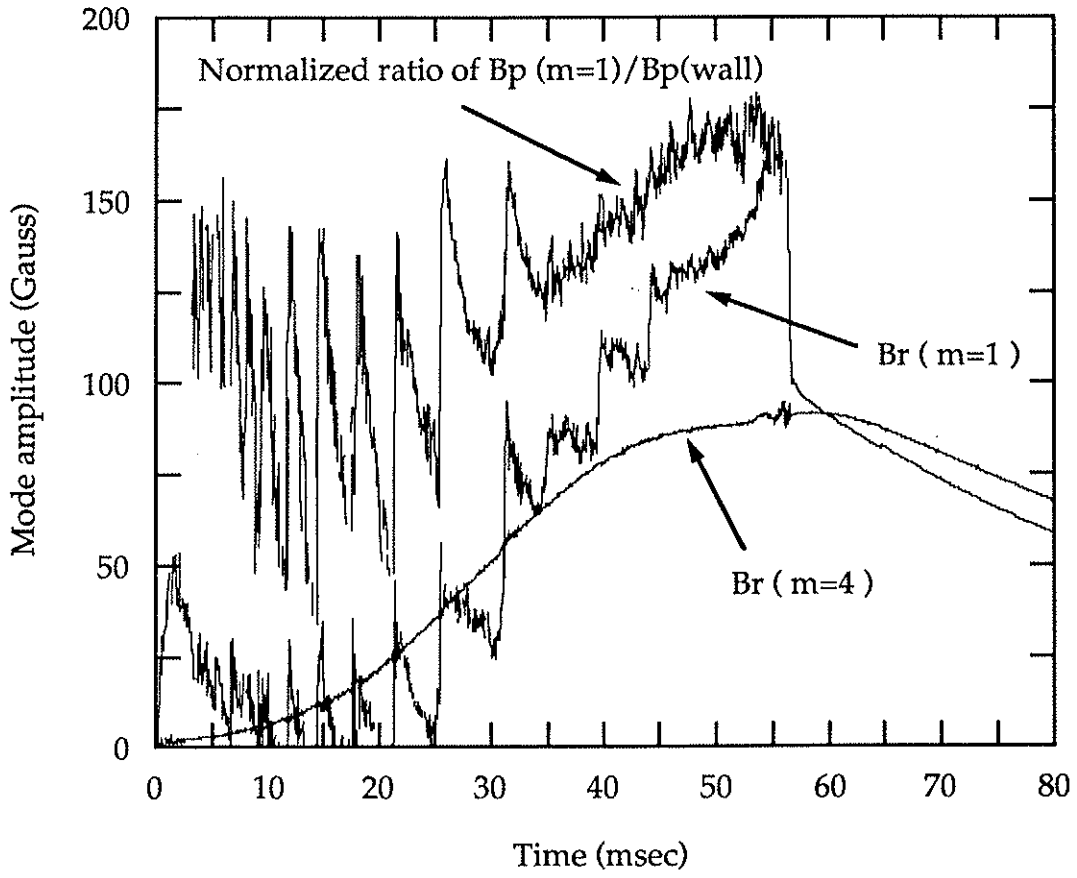

Figure 3.45 The time trace of the m = 1 and 4 component of the radial field at the poloidal gap, and the normalized ratio of m = 1 over m = 0 of the poloidal field at 180 degrees toroidally. This shows that the inward motion of the current profiles at the gap and 180 degrees away is on the time scale similar to the soak-in time scale.

3.3 Internal radial magnetic fields and magnetic islands.

An estimate of the magnetic island width associated with the measured radial magnetic fields at the poloidal gap can be made using the following simple calculations. The measured radial field is used as the boundary condition for the internal field profiles in vacuum in a cylindrical geometry. The basic assumption here is that the plasma does not influence the these internal profiles.

In vacuum one can solve $\nabla^2 \phi = 0$ to obtain the radial field profiles given by $\mathbf{B} = \nabla \phi$ The toroidal Fourier decomposition of the measured radial field at the gap can be used as the boundary condition to determine $B_r(r, \theta, z)$. The amplitudes of the radial fields at the resonant surface (r_s) are given in terms of the modified Bessel function $I_m(x)$ by

$$B_r(m=0,n) = \frac{2b_0}{n\pi} \sin\left(\frac{nd}{2R}\right) \frac{I_1\left(\frac{nr_s}{R}\right)}{I_1\left(\frac{na}{R}\right)}$$

$$B_r(m=1,n) = \frac{2b_1}{n\pi} \sin\left(\frac{nd}{2R}\right) \frac{I_0\left(\frac{nr_s}{R}\right) - I_2\left(\frac{nr_s}{R}\right)}{I_0\left(\frac{na}{R}\right) - I_2\left(\frac{na}{R}\right)}$$

where b_0 and b_1 are the amplitudes of the m = 0 and 1 components of the radial field at the poloidal gap, d is the poloidal gap width, and a and R the minor and major radii.

The magnetic island width is given by

$$w(m,n) = 4\sqrt{\frac{r_s B_r(m,n)}{n B_\theta \left|\frac{dq}{dr}\right|_{r_s}}}$$

where r_s is the radius of the resonant surface, $B_r(m, n)$ is the amplitude of the m and n component of the radial field at the resonant surface, B_θ is the poloidal field, and dq/dr is the gradient of the safety factor at the resonant surface. The BFM profiles are used to determine r_s and the gradient of q at r_s.

For the m = 0 island one can show that the island width is given by

$$w(0,n) = 4\sqrt{\frac{a R B_r(0,n)}{2\theta n B_\theta}}$$

where θ is the pinch parameter.

For the m = 1 island one can show that the island width is given by

$$w(1,n) = 4\sqrt{\frac{a R B_r(1,n) g}{2\theta n B_\theta}}$$

where

$$g = \frac{\frac{r_s\theta}{a}}{\frac{j_0(\frac{2\theta r_s}{a})}{j_1(\frac{2\theta r_s}{a})} - \frac{\theta r_s}{a}\left(1 + \frac{j_0^2(\frac{2\theta r_s}{a})}{j_1^2(\frac{2\theta r_s}{a})}\right)}$$

For the m = 0 field error component all n's are resonant at the reversal surface but the largest island is the n = 1. From the measurement of B_r and B_θ at the peak current of the discharge using an effective gap width of about 10 cm the width of the m = 0 and n = 1 island is about 5 cm. At higher n the island width goes as

$$w(0, n) = \frac{w(0, 1)}{\sqrt{n}}$$

The measured m = 0 component of the radial field at the gap was observed to be independent of the plasma current. This means that the m = 0 island width will be even smaller for higher-current discharges.

For the m = 1 magnetic islands we have two types of discharges, locked and unlocked.

For the unlocked discharges the m = 1 component of the field error at the poloidal gap is about 20 Gauss. For these discharges the island width for the resonant modes of m = 1 and n = 5 - 10 are small and do not overlap. The width of the m = 1 and n = 5 island is about 1.5 cm, and the higher n's are smaller by $1/\sqrt{n}$.

For the locked discharges, the m = 1 component of the field error becomes large as the poloidal field is decreasing. The resulting m = 1 islands are large and overlap. The width of the m = 1 and n = 5 island is about 6 cm. Figure 3.46 shows the m = 1 island widths and their overlap for the locked discharge.

These calculations are only a rough estimate due to two problems. The first is the toroidal effects for the calculated radial field profiles and

the island width equation which is only valid for small island widths. The second problem is the plasma interaction with the field errors. The plasma may amplify or attenuate the error magnetic field in the plasma region.[4,5]

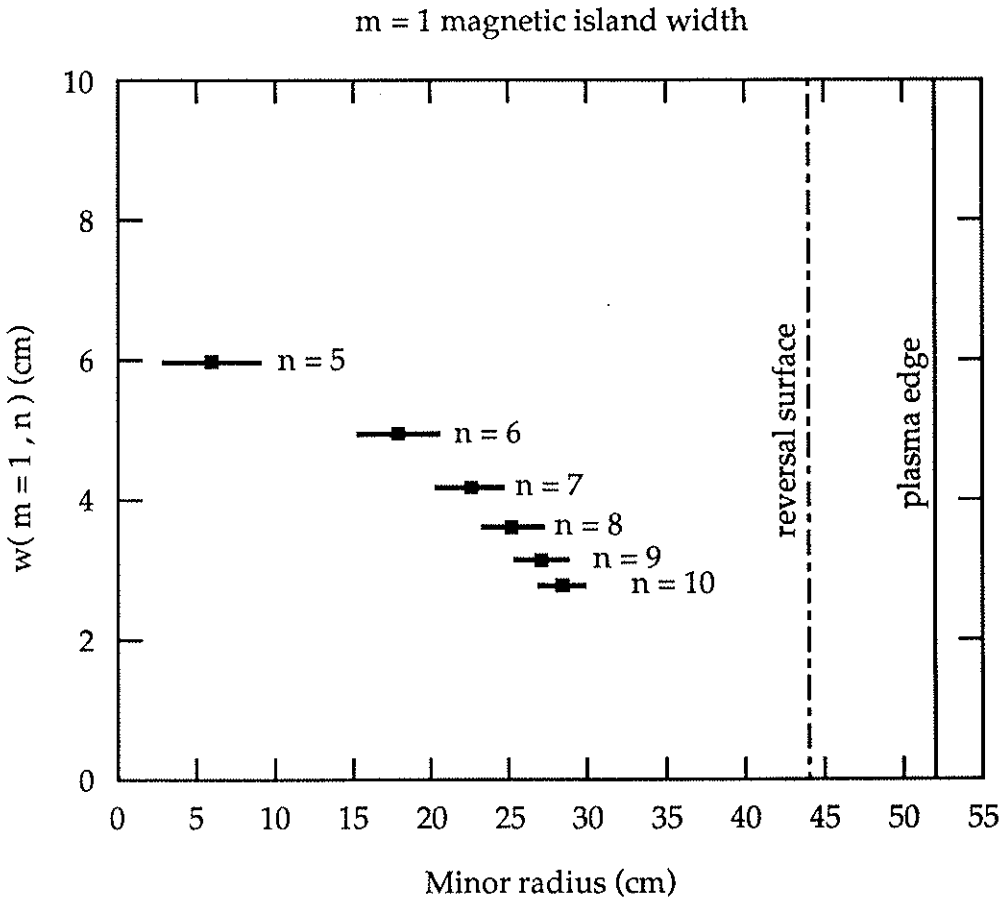

Figure 3.46 The m = 1 magnetic island widths for the locked discharge. The thick solid bars show the radial extent of each n island. The higher n island show some radial overlap.

REFERENCES

1 V. S. Mukhovatov and V. D. Shafranov, Nucl. Fusion 1, 605 (1971)

2 T. Tamano, W. D. Bard, C. Chu, Y. Kondoh, R. J. La Haye, P. S. Lee, M. T. Saito, M. J. Schaffer, and P. L. Taylor, Phys. Rev. Lett. 59,1444(1987).

3 D. W. Kerst, Several shield, Shell and gap problems-method for rough estimation, Universtry of Wiconsin-Madison, Report PLP # 909(1983).

4 K. L. Sidikman Ph.D. Thesis, University of Wisconsin-Madison (1990).

5 K. Hattori, K. Hirano, Y. Yagi, T. Shimada, Y. Maejima, I. Hirota, K. Ogawa, Plasma Physics and Controlled Fusion 31, 2165 (1989).